FCC Feedstocks/Bio-oils Co-processing:

Towards understanding of phenolic compounds impact on Ni- and V-USY zeolites

Roelof Tide Jacob Gerards

Thesis to obtain the Master of Science Degree in

Petroleum Engineering

Supervisor:	Professora Maria Filipa Gomes Ribeiro
Co-supervisor:	Doutora Inês Sofia Biscaya Semedo Pereira da Graça

Examination Committee

Chairperson:	Professora Maria João Correia Colunas Pereira
Supervisor:	Doutora Inês Sofia Biscaya Semedo Pereira da Graça
Members of the Committee:	Professor José Manuel Félix Madeira Lopes

July 2018

Declaration

I declare that this document is an original work of my own authorship and that it fulfills all the requirements of the Code of Conduct and Good Practices of the Universidade de Lisboa.

Abstract

One option for the upgrading of bio-oils would be the co-feeding of liquefied biomass with conventional feedstock in the FCC process of existing petroleum refineries. The main difference between conventional petroleum feedstock and liquefied biomass is the higher oxygen amount of the latter, which has a deactivating effect on the FCC catalysts. The objective of this work is to understand the influence of oxygenated compounds on the catalytic properties of nickel and vanadium USHY zeolite present in the FCC catalysts.

The transformation of n-heptane with and without guaiacol over USHY zeolite, with and without metal impregnation, was studied as a model reaction. It was seen that nickel has a higher deactivating effect on the catalyst activity, as compared to vanadium and USHY zeolite. This is consistent with a more pronounced increase in coke formation and decrease of Brønsted acid sites concentration upon nickel impregnation, as compared to vanadium.

Guaiacol was less poisonous for nickel and vanadium (USHY > V-USHY > Ni-USHY), due to an increase of Lewis acid sites concentration upon metal impregnation. Guaiacol adsorbs preferentially onto Lewis acid sites, which result in relatively more Brønsted acid sites available for cracking reactions.

Both nickel and vanadium induce an increase in hydrogen transfer and dehydrogenation reactions, which led to some changes in cracking products selectivity during pure n-heptane cracking. During guaiacol poisoning, no additional changes in product distribution were observed.

Keywords: Co-processing, oxygenated compounds, deactivation, HY zeolite, Vanadium and Nickel, FCC Catalyst.

Resumo

Uma opção para a valorização de bio-óleos consiste no co-processamento de biomassa liquefeita com a alimentação convencional da unidade de FCC das refinarias de petróleo. A principal diferença entre a alimentação convencional e a biomassa liquefeita é o elevado conteúdo em oxigénio desta última, que leva à desactivação do catalisador de FCC. O objectivo deste trabalho consiste no estudo da influência de compostos oxigenados nas propriedades catalíticas do zeólito USHY dopado com níquel e vanádio, que faz parte da composição do catalisador de FCC.

A transformação de n-heptano, puro e misturado com de guaiacol, catalisada por zeólito USHY, com ou sem metal impregnado, foi escolhida como reacção modelo. Foi observado que a presença de níquel tem maior efeito desactivante sobre a actividade catalítica, quando comparado com o zeólito com vanádio e USHY. Este efeito é concordante com um aumento da formação de coque e a diminuição da concentração de centros ácidos de Brønsted após a impregnação com níquel comparativamente ao vanádio.

Observou-se que o guaiacol provoca menor desactivação quando os zeólitos têm níquel e vanádio (USHY > V-USHY > Ni-USHY), devido a um aumento da concentração de centros ácidos de Lewis após impregnação. O guaiacol adsorve preferencialmente nos centros ácidos de Lewis, o que resulta numa maior disponibilidade de centros ácidos de Brønsted activos para o cracking.

A introdução tanto de níquel como de vanádio leva a um aumento das reacções de transferência de hidrogénio e desidrogenação, o que modifica a selectividade nos produtos de cracking do n-heptano puro. Com a introdução de guaiacol não se observa alteração na distribuição dos produtos.

Palavras-chave: Co-processamento, compostos oxigenados, desactivação zeólito HY, Vanádio e Níquel, Catalisador FCC.

List of Abbreviations

AFWA	Aqueous Fraction Water Addition
BJH	Barrett, Joyner, and Halenda
CPO	Catalytic Pyrolysis Oil
DRS	Diffuse Reflectance Spectroscopy
ECAT	Equilibrium Catalyst
EFAL	Extra-Framework Aluminum
FCC	Fluid Catalytic Cracking
FID	Flame Ionization Detector
FTIR	Fourier Transform Infrared Spectroscopy
GC	Gas Chromatography
H/C	Hydrogen / Carbon
HCN	Heavy Cracked Naphtha
HDO	Hydrodeoxygenation
HGO	Heavy Gas Oil
HTL	Hydrothermal Liquefaction
IR	Infrared Spectroscopy
IUPAC	International Union of Pure and Applied Chemistry
LAIST	Laboratório de Análisis do IST
LCO	Light Cycle Oil
LPG	Liquefied Petroleum Gas
MON	Motor Octane Number
OFWA	Oil Fraction Water Addition
PCP	Protonated Cyclopropane
RE	Rare Earth
RON	Research Octane Number
RT	Room Temperature
STP	Standard conditions for Temperature and Pressure
TCC	Thermochemical Conversion
TOS	Time On Stream
USHY	Ultra-Stable HY
UV-VIS	Ultraviolet-Visible
VGO	Vacuum Gas Oil
XRD	X-ray Diffraction

Index

Table of Figures

Tables

1. General Introduction

An increasing demand for petroleum by emerging economies, decreasing petroleum resources and political and environmental concerns about fossil fuels are encouraging the search for new sources of liquid fuels. From the renewable energy sources currently available, biomass is the only renewable source of carbon that can be converted into liquid fuels and this is mainly done by pyrolysis and liquefaction. One option for the upgrading to biofuel would be the co-feeding of liquefied biomass with conventional feedstock in the FCC process of existing petroleum refineries. Existing modern facilities are able to handle a broad range of chemical compounds and thus little capital cost investment would be required [1-4].

The FCC process has proven to be a very flexible and robust process, as it can be used to convert a wide range of feedstocks into useful products. It is the most widely used process for the conversion of the heavy fractions of crude, such as heavy gas oil (HGO), vacuum gas oil (VGO) or residue feedstocks, into more valuable products, such as gasoline, middle distillate (LCO) and light olefins. The typical FCC equilibrium catalyst (ECAT) consists of several components, such as an inert matrix, active matrix, binder and dealuminated ultra-stable Y zeolite (US-Y). US-Y zeolite is the main active zeolite in the FCC catalyst for today's conventional FCC process, often in a rare-earth stabilized form. ZSM-5 is being used as additive to the FCC catalyst for the purpose of producing more propylene and olefins. Coke formation has a strong impact on catalyst performance by decreasing the conversion and modifying product selectivity, but it also has an important role in the heat balance of the FCC unit. [2, 5-8]

The main difference between conventional petroleum feedstock and liquefied biomass is the higher oxygen amount of the latter. Residues from biomass usually contain between 35 and 50 wt% oxygen, which is why bio-oils have some inconvenient properties for fuel applications; high corrosiveness, low miscibility with hydrocarbon fuels, higher tendency to form coke, thermal- and chemical instability, low heating value, etc. The major challenge in the conversion of biomass is the efficient removal of oxygen from hydrophilic biomass-derived feedstock to convert it into hydrophobic matter. In fact, because of the above-mentioned undesired properties, the direct addition of bio-oil to established processes like FCC is not straightforward, thus creating the need for a previous HDO upgrading step [1, 2, 5]. Phenolic compounds are very resistant to the HDO upgrading step, as compared to most of the oxygenated compounds. For this reason phenolic compounds are usually present in significant numbers after HDO and for this reason this these compounds are studied in the current work.

The amount of heavy feedstock that is used in refining operations has been increasing worldwide. These heavy feedstocks usually present a high amount of metals that are in part responsible for the FCC catalyst deactivation. The objective of this work is to understand the influence of nickel and vanadium

on the deactivating effect of oxygenated compounds and catalytic properties of the FCC catalyst. Guaiacol, a phenolic compound, was used as representative of hydrotreated bio-oil. The deactivation phenomenon resulting from guaiacol poisoning and its influence on the activity, stability and product selectivity of the Y zeolite was studied in this thesis. A model compound study was conducted with CBV500, an US-Y zeolite, and n-heptane as representative of conventional hydrocarbon feedstock. The zeolite was impregnated with varying amount of nickel and vanadium to resemble the industrial composition of the ECAT mixture. The deactivating effect of guaiacol was studied with and without metal impregnation [5]

A literature review is presented in chapter II. The conversion of biomass to bio-oil, integration of bio-oil in the petroleum refinery, current co-processing efforts in the industry, the FCC process and FCC catalyst, coke formation and previous model compound research on the topic will be covered in the literature review. Chapter III incorporates a brief explanation of the experimental techniques used in the model compound research that is covered in chapter IV. Finally, chapter V presents the main conclusions of this thesis.

References

[1] Graça, Inês, et al. "Bio-oils Upgrading for Second Generation Biofuels." Industrial & Engineering Chemistry Research, vol. 52, no. 1, 2013, pp. 275-287.

[2] Corma, A., et al. "Processing biomass-derived oxygenates in the oil refinery: Catalytic cracking (FCC) reaction pathways and role of catalyst." Journal of Catalysis, vol. 247, no. 2, 2007, pp. 307-327.

[3] Zacher, Alan H., et al. "A review and perspective of recent bio-oil hydrotreating research." Green Chem, vol. 16, no. 2, 2014, pp. 491-515.

[4] Talmadge, Michael S., et al. "A perspective on oxygenated species in the refinery integration of pyrolysis oil." Green Chem, vol. 16, no. 2, 2014, pp. 407-453.

[5] Graça, Inês. "Influence of Oxygenated Compounds on the Properties of FCC Catalysts." 2010. Instituto Superior Técnico, PhD Dissertation.

[6] Vogt, E. T., and B. M. Weckhuysen. "ChemInform Abstract: Fluid Catalytic Cracking: Recent Developments on the Grand Old Lady of Zeolite Catalysis." ChemInform, vol. 46, no. 48, 2015.

[7] Akah, Aaron. "Application of rare earths in fluid catalytic cracking: A review." Journal of Rare Earths, vol. 35, no. 10, 2017, pp. 941-956.

[8] H.S. Cerqueira, G. Caeiro, L. Costa, F. Ramôa Ribeiro. "Deactivation of FCC catalysts." Journal of Molecular Catalysis A: Chemical, vol. 292, 1 July 2008, pp. 1-13.

2. Literature Review

2.1. Biomass

Rapid growth in both global energy demand and carbon dioxide emissions associated with the use of fossil fuels has driven the search for alternative sources which are renewable and have a lower environmental impact [1]. Biofuel is recognized as an important renewable and sustainable energy source to substitute fossil fuel. Biofuel releases exhaust gases that contain less carbon monoxide (CO), nitrogen oxide (NO_x), sulfur oxide (SO_x), unburnt hydrocarbon and particulate matters (PM) then petroleum fuel combustion. The content of those pollutants is too insignificant to induce environmental and health risk as compared with petroleum fuel. At the moment biofuel has evolved from first to fourth generation and these generations are mainly different in feedstock and production technology [2].

The three main types of first generation biofuels that were used commercially are biodiesel (bio-esters), ethanol, and biogas. The fuels are substitutes of diesel, gasoline and slightly adapted gasoline in gasoline cars, respectively. Biodiesel, bioethanol and biogas are produced from commodities that are also used for food [3]. The use of food-crop related biomass for 1st generation biofuel can be considered unsustainable and awakens a 'food versus fuel' discussion in society [1].

Since lignocellulosic biomass are mainly derived from biomass which does not require usage of agricultural land, 2nd generation biofuels are not involved in the 'food versus fuel' issue. The feedstock for second generation biofuel include herbaceous and woody plants, agricultural and forestry residues, municipal and industrial solid wastes, process wastes, organic waste, etc. These feedstocks are mainly obtained from agriculture waste/residue that consist of cellulose, hemicellulose and lignin. Note that all the above mentioned feedstock are largely available compared to food crops or energy crops [2].

Recently, third generation biofuel has also been introduced by the research communities. Third generation biofuel is mainly derived from algae, which are also known as oilgae. Algae appear to be one of the most photosynthetically efficient plants as compared to other feedstock. It converts solar energy into chemical energy and stores it in the form of oils, carbohydrates and proteins. Therefore, algae are identified as potential feedstock for biofuel production. Algae have high energy efficiency, rapid growing rate and high oil production volume among other advantages [2].

2.1.1. Conversion Processes

As lignocellulosic biomass appears in diverse physical characteristics and chemical compositions, it needs to be pre-treated before further conversion into biofuel [2]. Biomass conversion technologies can

be broadly categorized in two categories: biochemical and thermochemical conversion. The biochemical processes use enzymes and micro-organisms to convert biomass into desirable energy products. Thermochemical conversions (TCC) make use of heat energy and chemical catalysts for decomposition of biomass into high value energy products [4]. The higher temperature and the use of appropriate catalysts in the TCC process makes it in general much more rapid compared to biochemical conversion techniques [5]. For the purpose of this thesis, only the thermochemical conversion will be looked at in more depth.

The TCC technology is not a new production pathway, as is has been widely studied since 1788 for biomass conversion to bio crude products. Due to low petroleum prices, the TCC technology has been abandoned for a long time. Recently it has been revisited due to growing energy demands and environmental concerns [6]. TCC conversions generally imply the upgrading of biomass by heating it under pressure and in an oxygen deprived environment [5]. The main biomass TCC technologies are gasification, direct combustion, supercritical fluid extraction, hydrothermal liquefaction and pyrolysis [6].

Gasification converts biomass into synthetic gas and can be used for the production of bio-fuels and electricity. The primary product of direct combustion is thermal energy and it is therefore a widely applied process for electricity production [4]. Supercritical fluid extraction separates two components by using the supercritical fluids as the extracting solvent. Due to the need for high pressures, this process infers high operational- and capital costs. Biomass pyrolysis and hydrothermal liquefaction are comparable technologies. In both technologies the products are bio-based intermediates, often called oils or bio crude [6].

2.1.1.1. Hydrothermal Liquefaction (HTL)

The HTL process is synonym for hydrous pyrolysis, with the main difference being the lower temperatures and lower heating rates used. In the HTL process, biomass is converted to liquid fuels by processing it in a hot, pressurized water environment. With sufficient time, the solid bio-polymeric structure is broken down to mainly liquid components. Typical conditions in the hydrothermal process are a temperature between 523-647 K and pressures between 4-22 MPa [5].

A wide variety of bio-based and waste feedstocks have been researched for the HTL process, including woody biomass, industrial wasted, food wastes, swine manure, algae, wastes from forest industry etc. It has been concluded that the HTL process is very flexible as far as the feedstock is concerned [6]. Dry feedstock, with main components being cellulose, hemicellulose and lignin, and wet feedstock, with main components being lipids and proteins, can be distinguished [5].

The pathway of the HTL process comprises three major steps; depolymerisation followed by decomposition and recombination. In the first depolymerisation step the decisive parameters temperature and pressure changes the structure of the long chain polymers to shorter chain

hydrocarbons. The decomposition step involves the loss of water (dehydration), CO_2 (decarboxylation and amino acid content (deamination). The dehydration and decarboxylation steps facilitate the removal of oxygen from the biomass. The last recombination and repolymerisation step involves the recombination of the earlier produced fragments to form high molecular weight char components. This repolymerisation is made possible by the unavailability of hydrogen, causing a high concentration of fragments with uncapped free radicals [5]. Temperature, use of catalyst, residence time, solvents used and biomass-to-solvent ratio are parameters that have been extensively researched and that have a high influence on the yield and product distribution of the HTL process [6].

2.1.1.2. Pyrolysis

Pyrolysis is an indirect conversion method and can be described as a thermal decomposition of biomass in absence of oxygen to solid, liquid and gaseous products. The products can be generalized as biochar, bio-oil and pyrolytic gas [4]. Depending on the heating rate and residence time, the process has three main variations: slow, fast and flash pyrolysis. The processes are characterized by different yields of bio-oil, biochar and pyrolytic gas [7]. Slow pyrolysis, with main product being charcoal, has been utilized for centuries, while over the past 30 years the focus has been on the fast pyrolysis process to produce pyrolysis oils, chemicals and fuels [8]. Two main benefits of pyrolysis is the relative low temperature (673-973 K) necessary compared to gasification (>973 K) and combustion (>1173 K) and the low pressure requirement in the process (0.1-0.2 MPa) compared to hydrothermal liquefaction of biomass (4-22 MPa) [4].

The mechanism of biomass pyrolysis is very complex, due to the difference in decomposition of the biomass components with varying reaction mechanisms and reaction rates, which depend on the thermal conditions and reactor designs. Also the interaction between the components of the biomass (cellulose, hemicellulose and lignin) and the influence of these interactions on the product distribution makes it hard to predict the product- and reaction characteristics solely based on thermal behavior [7].

Three main stages can be distinguished: (i) initial evaporation of free moisture, (ii) primary decomposition, (iii) oil cracking and repolymerisation. It can be seen during the primary decomposition step that the main components of the biomass have different thermal stabilities. Hemicellulose, cellulose and lignin show decomposition at 250-350°C, 325-400°C and 300-550°C, respectively. The primary decomposition, oil cracking and repolymerisation steps are composed of a large number of reactions, including dehydration, depolymerisation, isomerization, aromatization, decarboxylation and charring [7].

Various process parameters and characteristics of the feedstock have influence on the biomass conversion time and therefore the product distribution and quality. Type of feedstock and its physico-chemical properties, such as thermal conductivity, permeability, density, specific heat capacity, particle shrinkage, moisture content and external heat transfer coefficient are important parameters concerning the biomass feedstock. Reactor configuration, heating rate, heating temperature and volatiles residence

time and pressure are process parameters of interest [4].

2.1.2. Biocrude

2.1.2.1. Yield

Determining the yields of char, gas and liquid products is very important for assessing the viability of different feedstocks for production of bio-oil [8]. In the literature two interesting theories can be found. One suggestion states that the yields of the different components of the bio-oil can be estimated through the biopolymer content of the biomass [9]. During the experiments the product yields from the individual biopolymers were measured (table 1) and this data was used to predict the formation of products from biomass pyrolysis based on the measured biopolymer content. A second theory suggests a direct relation between the amount of ash in the feedstock and the organic liquid yield [10]. This is a very plausible suggestion, since alkali metals present in the ash are known to increase the yields of gases, water and char during pyrolysis and therefore decreases the yield of liquid organic compounds [8].

Table 1 - Products from fast pyrolysis of select biopolymers at 500 °C [9]

Yields	Cellulose	Hemicellulose	Lignin
Gas	20%	26%	13%
Char	18%	23%	47%
Liquid	62%	50%	40%

These theories are of interest, since several studies show that woody feedstock typically have lower ash, extractives and hemicellulose, but more lignin content then the herbaceous feedstocks, which influences the yields of gas, liquid and char. Although these theories show correlation between important parameters, doing good estimations is still very complex. Extractives have a major influence on the properties of pyrolysis oil and the pretreatment of the biomass can affect the extractives, which results in a change in bio-oil composition. Inorganic constituents in small quantities also affect the yield and composition of the observed products in pyrolysis oil [8].

2.1.2.2. Oxygen Content

Decomposition of cellulose, hemicellulose and lignin is the main reason for the significant amount of oxygen in the oil, which can add up to 30-60 wt%. Cellulose and hemicellulose contain anhydrosugers with mainly hexoses and pentoses that have atomic formulas $C_6H_{10}O_5$ and $C_5H_8O_4$ respectively. Lignin is a complex polymer of propylaromatic subunits constructed from lignol monomers. The main constituents of lignin are the lignols p-coumaryl, coniferyl and sinapyl alcohol that have atomic formulas $C_9H_{10}O_2$, $C_{10}H_{12}O_3$ and $C_{11}H_{14}O_4$, respectively. Lignins have fewer contribution to the oxygen content of the pyrolysis oil, due to its lower oxygen to carbon ratio [8]. The decomposition of cellulose, hemicellulose and lignin is illustrated in figure 1 of annex 1.

2.2. Integration of Bio-Oil in FCC

The advantages of using bio-oil in refineries are significant [8, 11]:

- The co-processing of bio-oil into existing refinery infrastructure is very cost-efficient, since it leverages existing capital and does not require independent and new infrastructure for the pyrolysis, HDO or process route to the production of finished transportation fuel.

- The products of the conversion process from biomass to transportation fuels are destined for an industry that already has specific characteristics. Therefore a reduction of time consuming and expensive engine- and acceptance testing could be achieved, since the co-processing of the bio-oil with conventional feedstock could produce fuels that are to a high degree indistinguishable from the existing fuels.

- Fast pyrolysis of biomass produces a broad range of chemical compounds that can be handled by the modern refineries, since they have been optimized to use complex and varying feedstocks to produce fuels at a profit.

Several attempts to do direct feeding of bio-oil without any pretreatment resulted in significant amounts of char, coke and water as main products. Also the immiscibility of the bio-oil with hydrocarbons has been given as a reason for the difficulty of direct introduction of bio-oil in the FCC reactor [12]. Some authors have suggested a pre-treatment hydrodeoxygenation (HDO) step before introduction into the FCC process [11]. Another approach would be the replacement of the silica sand by catalysts in the pyrolysis process to produce bio-oils called catalytic pyrolysis oils (CPO) that have better quality and contain less oxygen.

Current research on co-processing of bio-oil and integration into the refinery addresses the negative qualities of bio-oil, such as acid content, water- and oxygen content and coke formation tendency. The goal of current research is to determine the minimal amount of bio-oil pretreatment that is required to produce bio-oil that can be successfully processed in the existing refinery infrastructure. To achieve successful co-processing, a thorough understanding of the broad spectrum of oils between pyrolysis and finished hydrotreated oil and how they react in the existing infrastructure is important [11].

2.2.1. Hydrodeoxygenation (HDO)

It is reported that HDO has the ability to remove up to 99.5% of the oxygen during the deoxygenation of oxygenated compounds. High pressure and temperature is necessary to perform HDO to such extent. Even though a wide variety of oxygenated compounds can be deoxygenated with HDO, phenolic compounds have proven to be very resistant to the treatment. It is relevant to balance the compatibility requirements of the bio-oil for the insertion at the refinery with the severity of the HDO, since a higher degree in deoxygenation results in higher processing costs. This optimization extends from almost complete deoxygenation, which can result in finished fuel blend stocks, to less severe deoxygenation that produces bio-oil suitable for early insertion in a petroleum refinery [11].

2.2.1.1. Physical and Chemical Modifications

In the conversion of biomass into liquid fuels through pyrolysis and HDO, the complexity of the process increases as the whole conversion process progresses towards the final transportation fuel product. The overall process costs and the load on expensive unit operations later in the conversion process could be reduced by addressing negative properties of bio-oil early in the conversion process. Physical modifications steps are of importance, due to the negative impact on equipment and process stability of physical contaminants. These contaminants include for example alkali metals, water content or solids that can cause corrosion, increased viscosity or have a negative impact on the used catalyst in HDO [11].

Bio-oil qualities impact deoxygenation steps in the same way as it does refinery insertion. Chemical modifications can address some of the negative qualities, such as excessive water content, oxygen content, corrosivity or thermal instability. The chemical modifications focus on removing the unwanted compounds without decreasing the carbon yields or increasing process costs. Previous research efforts suggested several methods which are shown to be effective in improving the bio-oil quality, but limited potential is reported due to the cost of reagents and the relative small improvement in bio-oil quality after modification. Since the HDO technology for processing bio-oil is expensive, there is room for including chemical modifications with the goal to decrease the overall process costs of the complete conversion of bio-oil to liquid fuels [11].

2.2.1.2. The Process

Similarities can be seen with the hydroprocessing found in petroleum refineries. The aim in both processes is to remove heteroatoms under high H_2 pressure and elevated temperatures. In the petroleum refinery the goal is usually to remove sulfur, nitrogen and metals through hydrodesulfurization, hydrodenitrogenation and hydrodemetallation reactions. The primary aim of hydrotreating bio-oil is the removal of oxygen by hydrodeoxygenation processes. Some bio-oil feedstocks, primarily those derived from algae, can contain increased amounts of nitrogen and sulfur. In the product streams after hydroprocessing, increased amounts of ammonia and hydrogen sulfide can be detected [11].

It can be found in the literature that up to 99.5% of the oxygen in bio-oil can be removed as water, CO_2 and CO through decarbonylation, decarboxylation and HDO reactions. Most of the reactions that occur during HDO processing are shown in figure 1. Oxygen that is removed from the bio-oil through CO_2 and CO causes a decrease in the carbon yield. For this reason, the removal of oxygen through water is preferred and improvements in this distribution of reactions can lead to a cost reduction in the production of transportation fuels from bio-oil [11].

It is important to improve the H_2 efficiency, since the costs that incur with using H_2 as a reagent should be balanced. H_2 is consumed in different reactions in the process of upgrading hydrocarbons, such as cracking reactions and the saturation of double bonds. The H_2 used in hydroprocessing is also involved in hydrocracking reactions at higher temperatures, in which larger bio-oil compounds are cracked into smaller bio-oil fragments [13].

Hydrotreated bio-oil can be integrated at different points in the upgrading process of hydrocarbon liquids to transportation fuels. This *integrative* approach includes the co-processing of intermediate hydrotreated bio-oil products with comparable petroleum intermediate product streams [14]. For simplicity, the different severities of the hydrotreating process can be roughly grouped into mild HDO and finished HDO. The requirements for oxygen content differs with the severity of HDO treatment. Mild HDO oxygen requirements depend on the place of integration in the refinery. Successful co-processing of bio-oil intermediate products and petroleum streams is an area that is still under investigation [11, 15].

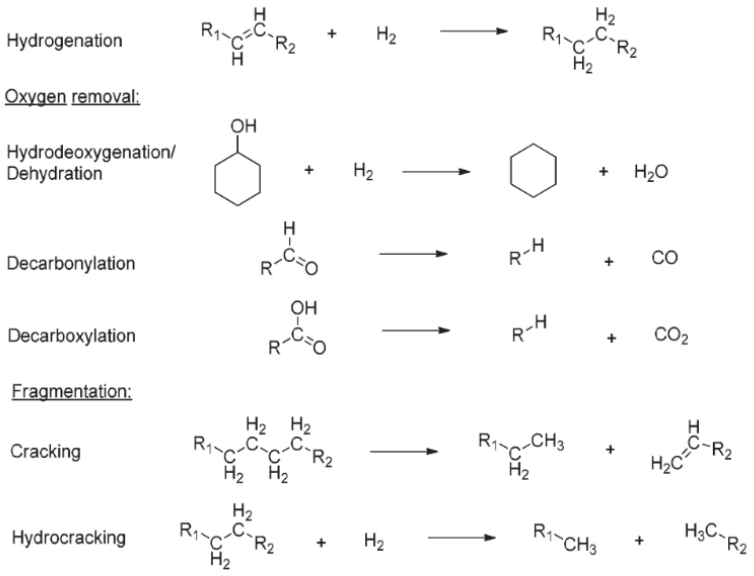

Figure 1 - Major reactions that occur during bio-oil HDO [11]

2.2.1.3. Co-processing HDO Research Efforts

Notable FCC co-processing efforts in which HDO was performed have been summarized in table 2. Research done by CPERI show very early efforts for co-processing bio-oil within the FCC process in the refinery. In 1998, the heavy cut of a mild non-catalytic hydrotreated bio-oil was co-processed with LCO (15/85) in the FCC reactor, which resulted in higher gasoline and coke yield and the product gasoline had a RON of 96. In 2009 the same heavy cut of the non-catalytic hydrotreated oil was co-processed with LCO and VGO (2/13/85), which resulted in an increased gasoline and LCO selectivity and an increased coke yield. The product gasoline had a higher amount of aromatics when processed with 2% hydrotreated oil [11].

Research done by IRCELYON focused on the co-processing of VGO with mild HDO oil that contains 21% oxygen after treatment in simulated FCC conditions. The co-processing of mild HDO with VGO in 20/80 distribution resulted in comparable LCO yields and slightly higher dry gas and coke yield and a small decrease in HCO, gasoline and LPG yield (table 2). ^{14}C analysis showed that the carbon from the mild HDO bio-oil has a preference to form coke and gas over the gasoline fraction. The differences in the observed product yields are explained by the restricted access of the oxygenated molecules into the pores of the zeolite, which in combination with coke formation on the outer surface leads to pore blocking. The observed effects of the co-processing of HDO with VGO on the product quality can be explained by the competition between the cracking route and the deoxygenation at the zeolite acid sites [16].

Table 2 - FCC co-processing efforts with HDO as pre-treatment [11]

Org	CPERI				IRCELYON		Twente		
Year	1998		2009		2010–11		2010–11		
Reactor	MAT, batch		Pilot, Circ.		MAT, batch		MAT, batch		
Co-feed	LCO	LCO	LCO/VGO		VGO		Long res.		none
Wt% HDO Bio-oil	0%	15%	0%	2%	0%	20%	0%	20%	100%
FCC conversion %			57–74%	63–73%	75%	75%	60	60	60
T (°C)	550	550	520	520	500	500	520	520	520
Catalyst/oil (g g^{-1})	2–6	2–6			1–6	1–6	3.1	3–4	12–20
Dry gas (C1, C2) (wt%)					1.5	2	1.5	1.9–2.5	6–11
LPG (C3, C4) (wt%)					24	20	8.5	9–11	10–12
Gasoline (C5) <221 °C (wt%)	17–22	20–25	38–46	42–47	46	44	44	44–45	22–36
LCO 221–370 °C (wt%)			17–22	18–21	20	20	25.2	23–25	11–19
HCO >370 °C (wt%)					4	3	14.8	12–13	7–8
Coke (wt%)	2–3	3–5	2–5.5	3.7–5.7	3.2	4.6	5.9	5.5–7.8	22–38

Pre-fractionation of pyrolysis oil before HDO

In research done by the University of Twente (table 3) various HDO oils were co-processed in simulated FCC units with long residue feedstock delivered by Shell. By mixing pyrolysis oil with water, an oil- and water fraction was obtained (OFWA and AFWA, respectively). Both fractions and the whole pyrolysis oil were treated under HDO conditions at various temperatures (220°C, 270°C and 310°C). It was observed that quality parameters, such as coking tendency and H/C ratio, differed significantly for

the obtained HDO oils, with the highest quality for the HDO oil obtained from the aqueous fractions. The products of HDO treatment of the aqueous AFWA fraction consisted not only of an aqueous phase, but also an oil phase. After co-processing the HDO oils (20/80), it was observed that a comparable product yield distribution was obtained for the different HDO oils, from which it can be concluded that the origin of the oil, i.e. OFWA or AFWA, is not of significant relevance for the product distribution (table 3) [17].

Table 3 - Product yields (wt% - normalized by the amount of produced water) after catalytic cracking of the oil fractions of HDO processed AFWA and OFWA with Long Residue (20/80) at 520°C. Values in parentheses are yields including produced water [17].

	Long Residue reference	20% HDO oil from OFWA (310 °C)		20% HDO oil from AFWA (310 °C)	
Cat/oil ratio	3.2	3.2		3.5	
LPG yield	8.8	9.8	(9.4)	10.0	(9.6)
Gasoline yield	44.6	45.4	(43.6)	44.9	(43.2)
LCO yield	25.5	25.2	(24.2)	25.1	(24.1)
Dry gas yield	1.5	2	(1.9)	2.1	(2.0)
Coke yield	5.0	5.3	(5.1)	5.4	(5.2)
Other (HCO, slurry oil, CO and CO_2)	14.6	12.3	(12.0)	12.5	(12.0)
Water[a]	—	—	(3.8)	—	(3.9)

Separate HDO of AFWA and OFWA is suggested as a feasible process option. The resulting HDO oils can be inserted at different units in the refinery, taking into account their difference in quality. The quality of the oil fraction of AFWA after HDO is high, but it is accompanied by high hydrogen consumption and the low organic concentration of the feed will increase process costs. A significant part of the hydrogen consumption is related to low value gaseous product production, which can be reduced by removing some light components, such as acids, from the whole pyrolysis oil or from the aqueous fraction (AFWA) alone.

A second option the authors suggested is to perform HDO only to the oil fraction (OFWA) of pyrolysis oil, after which this fraction can undergo co-processing. The AFWA fraction can be used for the recovery of chemicals or the production of hydrogen. This concept results in less hydrogen consumption then in the case of performing HDO on the whole pyrolysis oil. A negative consequence is the total carbon yield after HDO of only 35 wt%, compared to 78 wt% when processing the whole pyrolysis oil. Also as stated earlier, the quality of the oil fraction of OFWA is lower than the oil fraction of AFWA [17].

2.3. Current Activity in the Industry

2.3.1. Activity in Patent Applications

To examine the viability of co-processing bio-oil together with conventional feedstock, it is very interesting to observe the efforts related to the subject that have been done or that are currently done in the industry. Multiple oil companies are working on the subject and Petrobras has shown that it is able

to do co-processing of bio-oil with conventional feedstock without pre-treatment of the bio-oil [18] and in another study it was shown that co-processing was possible when the bio-oil was first pre-treated by fast pyrolysis [19]. Both efforts will be summarized in this chapter.

Another interesting thing to look at when evaluating the activity of the petroleum industry in co-processing, is the patents that are currently under review or recently granted. Shell oil company was granted a patent called *Methods and systems for processing cellulosic biomass* in 2017 [20]. In the patent it is described how the cellulosic biomass would be processed in the refinery and what would be the pathway for the released lignin. It describes the methods and systems for conversion, separation and recycling reaction products containing lignin-derived products. Hydrotreatment plays an important role in the described process.

A patent application titled *Crude bio oil pretreatment and upgrading* was done by ExxonMobil and is currently pending acceptance [21]. The patent describes systems and methods for the pre-treatment and upgrading of crude bio-oils for further processing to usable fuel products. The methods included in the application are flash fractionation and thermal cracking for generation suitable fractions that can be further processed, for example by hydroprocessing. The described system reduces metals contents to suitable levels for refinery processing, which can be an advantage in the further processing steps.

A patent was granted to Honeywell UOP in 2017 with the title *Methods and fuel processing apparatuses for upgrading a pyrolysis oil stream and a hydrocarbon stream* [22]. This patent describes the separate introduction of pyrolysis oil, of which the temperature is maintained at maximum 100°C before introduction, and hydrocarbon oil into the reaction zone. The mixture of both oils is catalytically cracked in the presence of a particulate cracking catalyst.

2.3.2. Research Activity with Co-processing

An assessment of the potential of direct co-feeding of bio-oil with conventional feedstock in a FCC reactor has been done by A.R. Pinho et al. from Petrobras [12]. For this research a demonstration-scale FCC unit, with a catalyst inventory of 450 kg and a feed rate of the reactants at 150 kg per hour, was used. Vacuum gasoil (VGO) and bio-oil were introduced into the reactor at temperatures of 50°C and 220-280°C, respectively. In these VGO tests, this heating of the feedstock was done to decrease its viscosity and to improve the feed dispersion. The reactions were controlled at 540°C and 560°C and at 10/90 and 20/80 rates of bio-oil/VGO feed, to see the differences in product characteristics at different conditions [12]. Two years later, starting at 2015, another experiment concerning co-processing is done by A.R. Pinho et al. from Petrobras [19]. In this second experiment raw bio-oil from pine woodchips was co-processed with a standard Brazilian VGO in a 200 kg per hour demonstration scale FCC unit using two commercial FCC equilibrium catalysts. Two different ratios for bio-oil/VGO were used, i.e. 5/95 and 10/90. It was assumed that up to 5 percent of bio-oil addition to the VGO feedstock for co-processing would be a

reasonable starting point for a typical commercial FCC unit. The FCC unit running the experiment at 540°C reached a cumulative operation time of 400h over more or less 18 months. The temperatures that were used are those currently used in the commercial FCC operations at Petrobras.

Bio-oil and regular petroleum streams are immiscible, due to the high polarity of bio-oil. For this reason, at both experiments, the bio-oil and VGO were introduced at two different axial positions in the FCC reactor riser. Bio-oil should not be heated above 50°C, since this accelerates polymerization reactions and coke formation. This separate introduction of the bio-oil and VGO into the riser made it possible to maintain optimal temperatures for both feeds.

Both experiments gave similar trends in the results concerning the main product yields. For this reason only the results from the earlier experiment [18] is discussed. Figure 2 in annex 1 shows the main product groups dry gas, LPG, gasoline, LCO, bottom products, coke, CO_2 and H_2O. In the dry gas- and LPG range, four products are of interest, therefore methane, ethene, propene and hydrogen can be seen in separate figure 3 in annex 1. First it was seen that CO, CO_2 and H_2O formation is much higher when co-feeding bio-oil, as opposed to using 100% VGO. This mainly can be contributed to the fact that bio-oil contains high amounts of oxygen and therefore produces oxygenated compounds during the cracking reaction. From the higher amount of CO compared to CO_2 it can be concluded that there exist a preference of decarbonylation reactions over decarboxylation reactions. Different authors have suggested dehydration- or aldol-condensation reactions as the reason of higher water formation during research of model compounds over zeolite catalysts [12]. A decrease can be seen for the gasoline yield when the reaction is co-fed with 20% bio-oil, but this can be explained by the dilution of the products by H_2O that showed an increased yield. LCO yields also show a decrease for 20% bio-oil, while the bottom products yield shows a small increase. Hydrogen, methane, ethene and propene selectivity was reduced when the reaction is co-fed with bio-oil [12, 19].

In the past, it has been frequently reported that coke production in the FCC units is excessively high when untreated 'raw' bio-oil is used for co-processing. It was seen in experiments done on laboratory- or pilot scale, that co-feeding very small amounts of hydrogenated bio-oils could cause a significant increase in coke yield, leading to operational instability and plugging [23]. The differences in yields obtained in these Petrobras studies, in which much larger scale units are used, could be explained by the characteristics inherent to smaller-scale units used in other research efforts.

To evaluate the difference in gasoline quality after feeding VGO to the reactor and co-feeding bio-oil with VGO, the researchers analyzed the aromatic concentration and benzene content in the gasoline fraction (figure 2) and the properties of the heavy cracked naphtha (HCN) cut, which consist of liquid effluents with boiling point range between 80°C and 220°C (table 4). In figure 2 it can be seen that at the same conversion level, benzene content and aromatics concentration is lower when pure VGO is fed to the reactor. At similar reaction temperatures the conversion is higher when co-feeding bio-oil to the reactor. From table 4 can be concluded that the HCN cut from the product of 20% co-fed bio-oil contains

higher aromatics content and higher MON- and RON numbers. Also phenol is present in higher quantities when bio-oil was co-fed, which does not have to be disastrous for the gasoline quality. Phenolic compounds are believed to stabilize the cracked product in the gasoline range [12, 19]. It has been proposed before to use a combination of a phenol and an ether to acquire gasoline with a higher octane number and increased stability [24].

Table 4 - FCC product properties after processing at 540°C (LCN & HCN fractions)

	VGO	VGO	20% bio-oil	20% bio-oil
	LCN	HCN	LCN	HCN
wt.%	27.1	72.9	25.1	74.9
Density (g/cm^3, 20 °C)	0.6950	0.8053	0.6965	0.8160
Olefins SFC (wt.%)	n.a	28.8	n.a	24.5
Aromatics SFC (wt.%)	n.a	50.0	n.a	53.8
Dienes (g I_2/100 g)	n.a	0.5	n.a	< 0.4
Sulfur (ppm)	< 50	1097	< 50	1050
Phenols (ppm)	<200	3162	<200.0	19,326.
MON ASTM D2700	n.a	83.3	n.a	84.4000
RON ASTM D2699	n.a	95.8	n.a	96.5

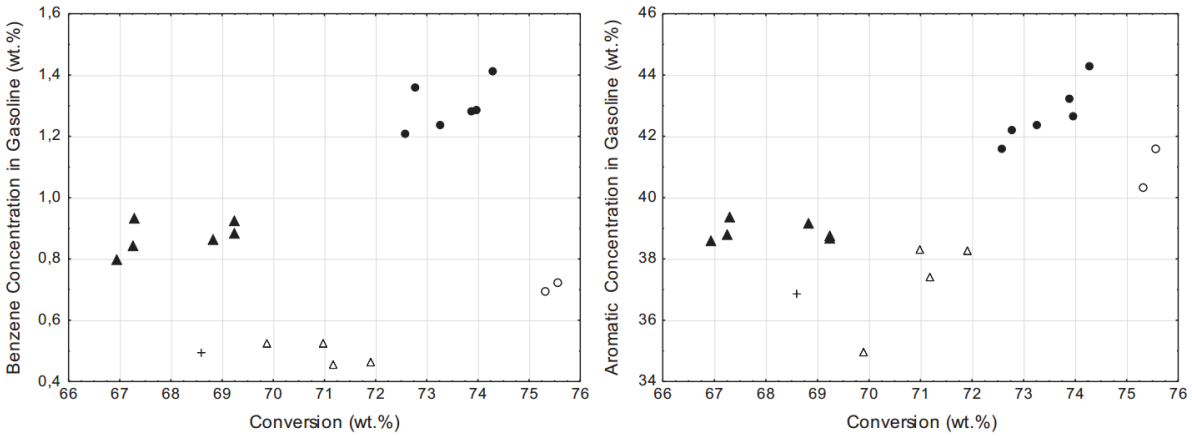

Figure 2 - Benzene and total aromatics concentration in gasoline at different conversion levels: VGO cracking at 540 °C (▲),VGO cracking at 560 °C (●), VGO/bio-oil cracking 90/10 at 540 °C (+), VGO/bio-oil 80/20 at 540 °C (Δ), VGO/bio-oil 80/20 at 560°C (○) [12]

The renewable carbon content of the acquired liquid fractions after the process has been investigated by ^{14}C analysis. Determining the amount of renewable carbon content in liquid fractions after the FCC processing step is desirable. Within the petroleum industry, ^{13}C analyses have been the standard for determining the content of carbon from fossil fuels in products, but it is not useful for measuring renewable carbon concentrations. ^{14}C is more suitable for this purpose due to its half-life of 5730 years, which makes it trace level predictable in any living substance that can be used for the production of bio-oil and therefor (partly) bio-fuels. The ^{14}C analysis can distinguish a renewable carbon from a fossil carbon, since fossil substances do not contain ^{14}C carbon due to its age. The technique can be used to measure the renewable content of a transportation fuel after blending with renewable source derived fuels. Since it is desirable to have a high concentration of renewable carbons in the most valuable streams,

the ^{14}C analysis is used to analyze the characteristics of naphtha- and light cycle oil yields [12].

When 20% bio-oil is co-fed to the reactor, the renewable carbon content is between 3-5% for the gasoline cuts of the liquid fraction. For 5% and 10% bio-oil this percentage of renewable carbon in the gasoline cut is circa 1% and 2%, respectively. For the heavier LCO- and bottom cuts the renewable carbon content is 5% and 6%, respectively. When considering the carbon content of the bio-oil used for these experiments, it can be concluded that ca. 30% of the renewable carbon from the bio-oil is present in the liquid products of the co-fed FCC process [12, 19].

From the research efforts done by Petrobras, it can be concluded that it is technically feasible to co-process raw bio-oil with the fossil feedstock VGO in the FCC process. It is shown that the oxygen in the bio-oil is almost completely removed in the cracking process, mostly as CO, CO_2 and water. The oxygenated compounds concentrations did increase in the obtained gasoline and diesel cuts, but this is not to an extent that causes problems for the fuel quality. Since it is successfully demonstrated that it is possible to co-process raw bio-oil with circa 50 wt% oxygen, the authors suggest that it must also be possible to process partially upgraded bio-oils. An optimal hand-off point must be found between the bio refinery and the petroleum refinery [18, 19]. A possible refining scheme for the co-processing of bio-oil with conventional feedstock is proposed and can be seen in figure 4 of annex 1 [19].

Another things that the authors noted was the fact that oxygenated compounds could interfere with the final sulfur removal step, which is usually carried out as post-treatment step for gasoline in refineries. It is therefore or high importance to investigate the interference of oxygenated compounds in cracked gasoline, with or without co-feeding in the process, with the widely used catalysts for hydrodesulfurization, for example cobalt-molybdenum [18].

2.4. FCC Process

Fluid catalytic cracking (FCC) involves the conversion of heavy hydrocarbon feedstock, such as VGO or residue, through acidic catalysis into a wide range of products that range from light gases to heavy fractions and coke. The more valuable product are constituents of the gasoline pool, with an average yield of 50 wt%, making this process the major gasoline-producing process in the refinery. The gasoline mixture produced by the FCC process consists of aromatics and C_5-C_{11} alkanes and alkenes with a high octane number (RON) of 90-94. Aromatics and branched alkenes contribute most to this high octane number [25-27].

2.4.1. FCC Unit

The actual reactor of a FCC unit is the riser, in which feed that is preheated to ca. 300°C is contacted with fluidized catalyst with a temperature of more than 650°C at a pressure of ca. 2-3 bar.

Catalyst-to-oil ratios are often in the range of 6-9 on a mass basis. Due to expansion of the feed after vaporization, the mixture is driven to the top of the riser. The endothermic reactions cause the temperature in the top of the riser to be lower than the temperature at the bottom. The stripper is designed to minimize subsequent contact between the products and catalyst, thus reducing secondary cracking reactions. To reverse the deactivation of the catalyst due to coke formation, the catalyst is fed to the regenerator after stripping and coke is burned off at temperatures of ca. 700°C. Coke, with the characteristic of having a low H/C ratio, allows the products of the cracking reactions to have a higher H/C ratio then the feed, which is referred to as *upgrading by carbon rejection* [27].

Coke formation plays an essential role in the so called *heat balance* of the FCC process. The combustion of coke in the regenerator provides the heat that is needed for the endothermic cracking reactions in the riser and is the source of heat needed to vaporize the feed in the FCC reactor. This heat is stored in the catalyst that will be fed to the riser after the regeneration [26-28].

The amount of deposited coke is of relevance, since a lower coke deposit can be insufficient to maintain the regeneration reaction, leading to carbon remaining on the regenerated catalyst. Too high coke content can lead to overheating of the catalyst, which in turn can cause hydrothermal processes and permanent deactivation of the catalyst. Coke formation is therefor of relevance and should be carefully considered in the co-processing operation, in which bio-oil is co-fed to the FCC reactor [29]. More detailed information on coke formation and deposition in co-processing conditions can be found in section 6 of this literature review.

2.4.2. Reactions in FCC Reactor

2.4.2.1. Alkoxy Species and Carbocations

Carbocation species, such as carbenium- and carbonium ions, can be created from hydrocarbons under the influence of Brønsted acid sites. Covalent bonding between a carbocation and anionic framework oxygen of the zeolitic catalyst can occur and the created adsorbates are therefore often described as alkoxy species. In their excited state, these alkoxy species are carbocation-like in chemical behavior and can be seen as intermediates in the conversion reactions of hydrocarbons through zeolitic catalysts [30].

The relative stabilities of carbocation species is of high importance and influences the product distribution from the conversion of hydrocarbons. Figure 3 illustrates the relative stabilities of alkyl carbenium ions and it can be seen that stability increases from primary to tertiary carbenium ions, which explains why the formation of, for example, methane and ethane is highly unfavorable in the catalytic cracking process [30].

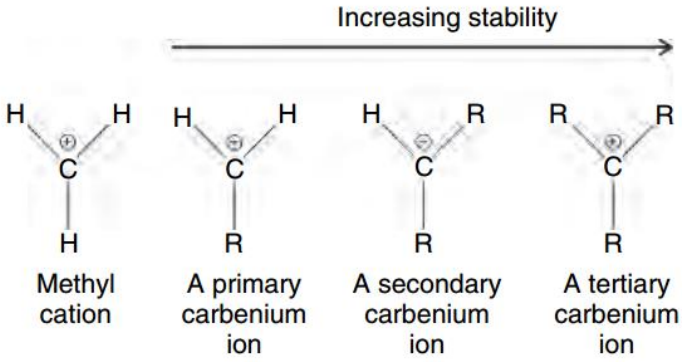

Figure 3 - Relative stability of alkyl carbenium ions, with R being the alkyl group [30]

2.4.2.2. Isomerization

The terms type A and type B are used to distinguish between different isomerization reactions. Type A isomerization describes reactions in which the number of branchings remains constant, but the position changes. In type B reactions the number of branchings increases or decreases and this type of reaction is usually slower than the type A reactions. A simplified mechanism for type A reactions, in which anionic framework oxygen is involved, is shown in figure 4. An intramolecular shift of a hydride ion, followed by an intramolecular shift of the alkyl group creates the intermediate carbocation that will result in the isomerization product after a last intermolecular hydride transfer with a new reactant molecule [30].

B type reactions are believed to have mechanistic models that do not involve primary carbenium ions due to their instability. One widely accepted pathway involves protonated cycloalkylcarbonium ions that possess three-ring protonated cyclopropanes (PCPs). Through the equilibrium that exists between edge- and corner protonated PCPs the reactant molecule can be isomerized as exemplified in figure 5 [30].

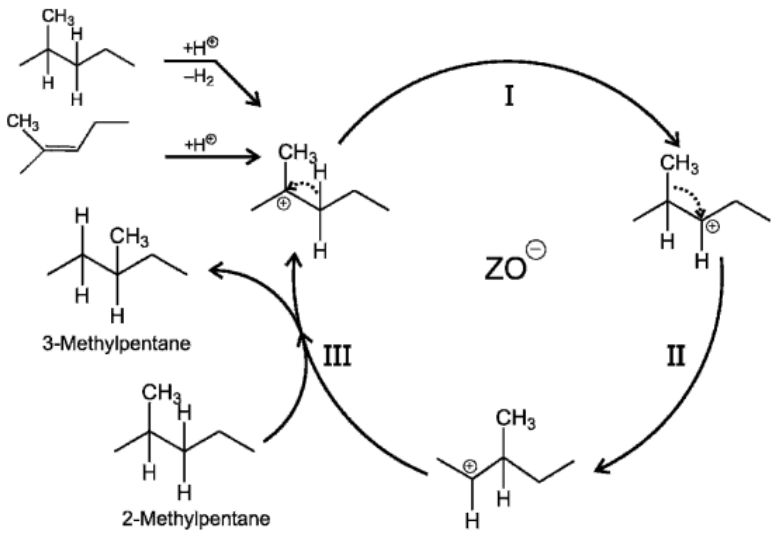

Figure 4 - A simplified mechanism for type A reactions, in which anionic framework oxygen is involved [30]

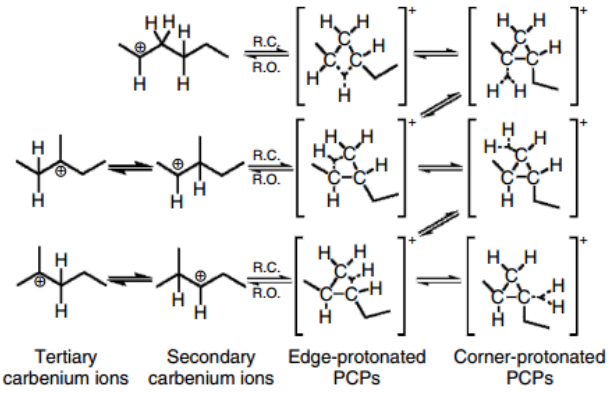

Figure 5 - Catalytic cycle including three-ring protonated cyclopropanes (PCPs). ZO¬- is symbol for an anionic framework oxygen of the zeolite [30]

2.4.2.3. β-Scission Cracking

β-scission stands for the carbon-carbon bond cleavage of the second carbon-carbon bond relative to a positively charged carbon atom. Several types of β-scission, from type A to type D, have been identified and they differ in the classification of alkylcarbenium ion reactants and products (i.e. primary, secondary or tertiary) (figure 6) [31].

The rate of β-scission reactions decreases rapidly from type A to type D, which is why type A reactions are fast and likely to proceed on acidic zeolites even at temperatures as low as 100°C, while type D reactions are unlikely to be found in the cracking process. The reaction rates for the different types of β-scission explain why almost no methane and ethane hydrocarbons are formed during the cracking reaction. The restriction on the number of carbon atoms on alkylcarbenium ions, i.e. 8^+ for type A reactions or 6^+ for type C reactions, are the reason why the cracking reaction comes to a stop for hydrocarbons with five carbon atoms or less. Due to the bulky precursors for type A and type B reactions, these β-scission reaction types are likely to occur in large-pore zeolites, while type C and type D reactions are more likely to occur in medium-pore zeolites [30, 31].

β-scission reactions involving carbon-carbon bonds that are part of naphthenic rings are less favorable and reaction rates are very slow. Brouwer et al. [32] suggested that differences in overlap of the p-orbital and the breaking β-bond are the cause of this reluctance of cyclic carbenium ions to undergo the β-scission reactions.

2.4.2.4. Mono- and Bimolecular Cracking

On the left side of figure 7 the monomolecular cracking reaction can be seen. It is proposed that this mechanism is relevant in acid-cracking reactions where the pores are small enough to inhibit the classical bimolecular cracking reactions. Indeed it is pointed out that the relative importance of the monomolecular cracking mechanism increases with decreasing pore size, increasing reaction temperature and low alkene partial pressure [33].

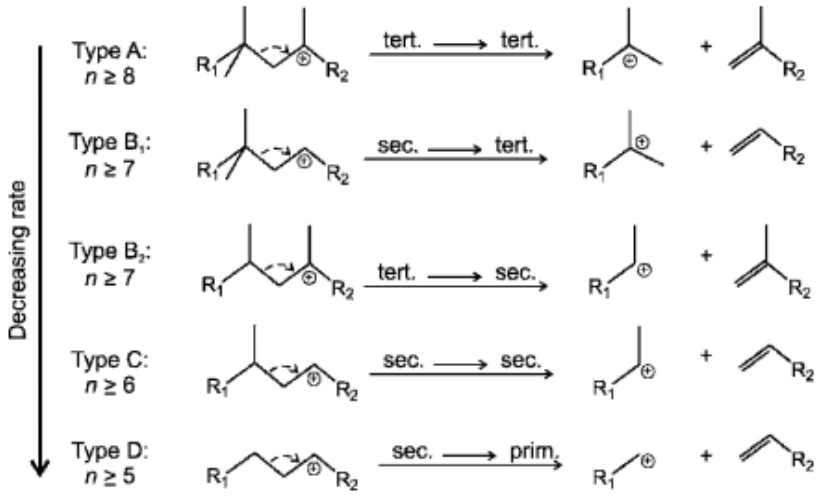

Figure 6 - Classification of B-scissions of alkylcarbenium ions; n is the number of carbon atoms of alkylcarbenium ions that can undergo the type of B-scission [31]

A simple bimolecular cracking mechanism can be seen at the right side of figure 7. A carbenium atom is created by direct protonation or from alkene impurity, followed by a type B branching rearrangement (isomerization). After an intramolecular hydride shift followed by β-scission the products are an alkene molecule and a smaller carbocation. This carbocation undergoes an intermolecular hydride transfer with another alkane, which closes the catalytic cycle. The 4th step in the mechanism shown on the right side is a reaction between two molecules, thus giving this mechanism the name 'bimolecular', and this step is believed to be rate controlling in the cracking mechanism [30].

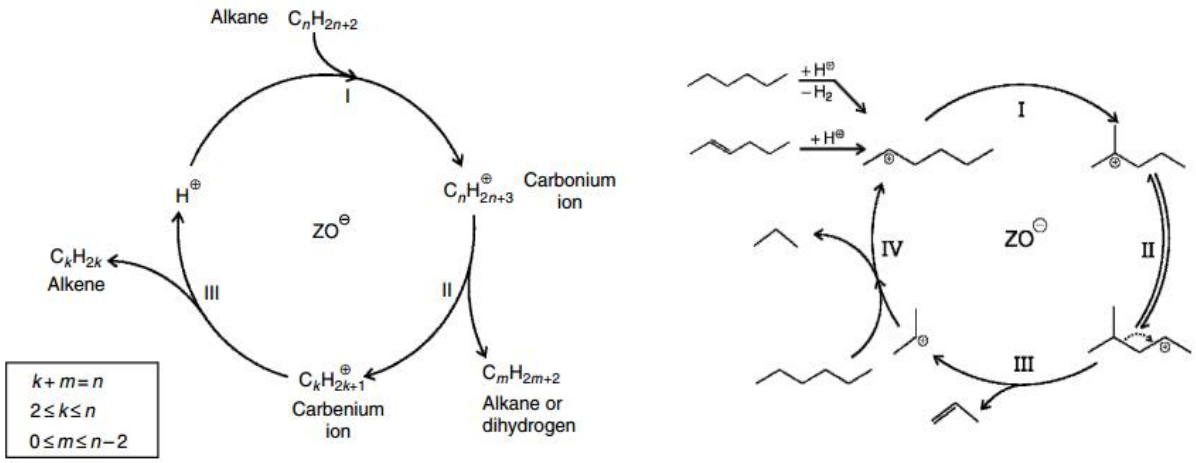

Figure 7 - Acid-catalyzed cracking of an alkane through a monomolecular mechanism (left) and a simple bimolecular cracking mechanism (right). ZO^- stands for an anionic zeolitic framework oxygen [30].

As can be seen in the acid catalyzed cracking mechanisms, the main difference is the type of carbocation produced in the first step and the deprotonation that concludes the monomolecular mechanism, as opposed to the hydride transfer that concludes the bimolecular cracking mechanism.

2.4.2.5. Hydrogen Transfer Reactions

In FCC the main focus in regard to hydrogen transfer reactions is on intermolecular hydrogen transfer that can occur between any two hydrocarbon molecules as long as one of them is unsaturated. One of the most relevant hydrogen transfer reactions is the transformation of three alkenes and one naphthene into three alkanes and an aromatic. One of the most accepted mechanisms for this reaction is illustrated in figure 8.

1. Deprotonation of a cyclic carbenium-like ion, thus producing a cycloalkene.
2. Hydride transfer reaction between a second carbenium-like ion and the cycloalkene to form an adsorbed alkene.
3. A cyclodiene is formed through deprotonation of the adsorbed alkene, which regenerates a Brønsted acid site.
4. A hydride transfer occurs between the cyclodiene and a third carbenium-like ion.
5. The protonated cyclodiene resorbs from the surface, producing an aromatic and regenerating an acid site.

It has been questioned why the reaction exchanges hydride ions between cycloalkenes and cyclodienes and does not make use of Brønsted acid sites. Research from Corma et al. suggests that hydride transfer is easier for cycloalkenes than for naphthenes, because the unsaturated carbenium-like ion is very stable [26, 34].

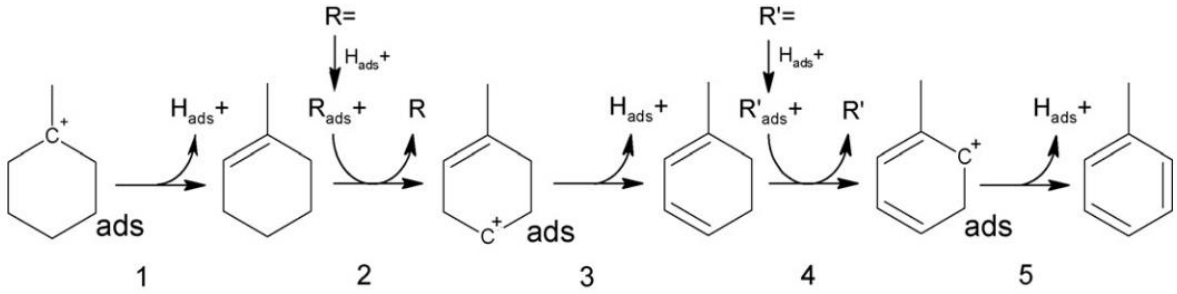

Figure 8 - Hydrogen transfer mechanism for the transformation of three alkenes and one naphthene into three alkanes and an aromatic [26]

2.5. FCC Catalysts

Catalysts used in the FCC process can be permanently or reversibly deactivated through several mechanisms. Coking and metal poisoning due to impurities in the feedstock are examples of reversible deactivation. Dealumination by steam generated during the regeneration process and mechanical degradation of particles cause permanent degradation. To maintain catalyst activity, fresh catalyst

addition is frequently needed. The catalyst mixture that participates in the cracking reaction therefore has an age distribution. The mixture of catalyst from an industrial FCC unit contains old (high metal concentration and low activity) and young (low metal concentration and high activity) particles and goes by the name equilibrium catalyst (ECAT) [26, 27].

The typical FCC ECAT is a mixture of several components [26]:

- Inert matrix (kaolin)
- Active matrix (alumina)
- Binder (silica or silica-alumina)
- Y zeolite

The reaction between hydroxyl groups from the zeolite and steam at elevated temperatures results in dealumination and consequently the loss of acid sites. This dealumination makes the catalyst less acidic, but increases the thermal- and hydrothermal stability of the zeolite. For this reason, the Y zeolites are usually treated with steam in optimized conditions before being used in the catalytic process and the resulting catalyst is the so-called ultra-stabilized Y-zeolite (US-Y). US-Y zeolite is the main active zeolite in the FCC catalyst for today's conventional FCC process, often in a rare-earth stabilized form. The stability of US-Y zeolite is affected by the presence of Na and steam. ZSM-5 is being used as additive to the FCC catalyst for the purpose of producing more propylene and olefins [26, 30, 35].

2.5.1. FCC Catalyst Deactivation

Many factors need to be considered when FCC catalysts are evaluated, with deactivation being the most decisive parameter in the catalytic testing. Deactivation of catalysts in heterogeneous catalysis can have a physical- or chemical cause. Physical phenomena are usually not the main cause for deactivation, since zeolites used in industrial applications should withstand the process operation conditions and are designed to do so. Chemical causes are the main problem of deactivation and include two important concepts: Chemical degradation and poisoning. The first explains the loss of reactivity, caused by a reaction of a chemical compound with the catalyst and the latter expresses the reduction of activity caused by irreversible adsorption of unwanted compounds on the catalyst active sites. It is certain that FCC catalyst deactivation is a complex phenomenon, in which the different variables of the process (feed composition, catalyst composition and process operation) are all inter-related [26, 35, 36].

One type of classification for the deactivation of FCC catalyst is based on the possibility of restoring the catalyst activity by regeneration. The deactivation processes can therefore be grouped by those that could be reversed by combustion (reversible) and those that lead to the replacement of the catalyst after a limited time in the process (irreversible) [26].

2.5.1.1. Coke

The deactivation of zeolite catalysts by coking can be caused by pore blockage or by poisoning of the acid sites [98]. Several types of coke, the impact of coke on the catalysts, the impact of catalysts on coke formation, the impact of bio-oil or oxygenated compounds on coke formation and the characterization of coke are subject of section 6.

2.5.1.2. Heteroatoms

FCC feedstocks contain small amounts of oxygen, sulfur and nitrogen, besides the hydrocarbon components. Sulfur does not have a deactivating effect on the catalysts used in the FCC process if their presence is below a certain limit, but has to be treated in the process due to environmental regulations imposed by the European Union. Since this is out of scope for this thesis, only nitrogen and oxygen will be analyzed.

2.5.1.2.1. Nitrogen

VGO and recently increasing amounts of vacuum residue are the main components of the feedstock for the FCC process and contain approximately 25-30% and 70-75% of the nitrogen present in crude oil, respectively. Non-basic nitrogen compounds are usually found in high molecular weight molecules that also contain sulfur and oxygen atoms, while the basic nitrogen compounds are found more in lighter fractions of crude oil. The nitrogen bases deactivate catalysts in the FCC process by interaction with acid sites, thus decreasing activity [26]. Several research efforts have demonstrated that the deactivating power of the nitrogen base increases with increasing proton affinity [37, 38]. Lewis acid sites of the active matrix present in FCC catalysts show adsorption of the nitrogen compounds. Therefore, catalysts are less affected by basic molecules, like nitrogen containing compounds, in presence of high acidity matrices [39]. To conclude, the poisoning effect of a nitrogen compound is determined mainly by its size and basicity.

2.5.1.2.2. Oxygen

Biomass derived feedstock contains more oxygenated compounds than conventional feedstock like VGO. Efficiently removing oxygen from the hydrophilic feedstock and converting it into hydrophobic compounds with preferential properties has been the major challenge in biomass conversion strategies. FCC catalysts are proven to be effective at removing this oxygen as CO, CO_2 and H_2O in the conversion reaction. Previous studies show that the conversion of carbohydrates over ZSM-5 catalysts produces CO, CO_2, hydrocarbons and coke as main products [40]. Work carried out with oxygenated model compounds will be discussed in section 7 of this literature review.

2.5.1.3. (Hydro)-Thermal Dealumination

FCC catalysts have to possess high thermal- and hydrothermal stability, since they are exposed to very high temperatures during the reaction and regeneration steps of the FCC process and this can easily lead to dealumination of the catalyst structure [35, 41]. Zeolites undergo various structural changes due

to thermal treatments, such as cell volume contraction, transformation into a more metastable phase, structural collapse, amorphization and negative thermal expansion. Dealumination can be reduced by applying a regeneration treatment in two steps, in which the first reaction temperature (600-700°C) is lower than the second (700-800°C) [26].

Dehydroxylation reactions on the Brønsted acid sites are responsible for the dealumination and thus for the decrease in catalytic activity of the zeolites. After dehydroxylation, the Al atom can be easily removed from the zeolite framework. These removed Al atoms form the extra-framework Al (EFAL) compounds and then act as Lewis acid sites. This conversion from Brønsted to Lewis acid site can be seen in figure 9. The second step is made possible by the NNN Al atoms that cause instability of the leaving aluminum framework atom. This also explains why in ZSM-5, which has a higher Si/Al ratio, the second step is less favored [35, 41]. It has been proposed that Lewis acid sites have a decisive role in initiating cracking reactions over zeolite catalysts [26]. Extra-framework Lewis acid sites can exist in different forms, such as Al^{3+}, AlO(OH), $Al(OH)_2^+$, $(OH)_3$, AlO^+ or $\equiv Si^+$. M. Elanany et al. concluded that the AlO^+ and $\equiv Si^+$ contribute to super acidity in dealuminated zeolites [42].

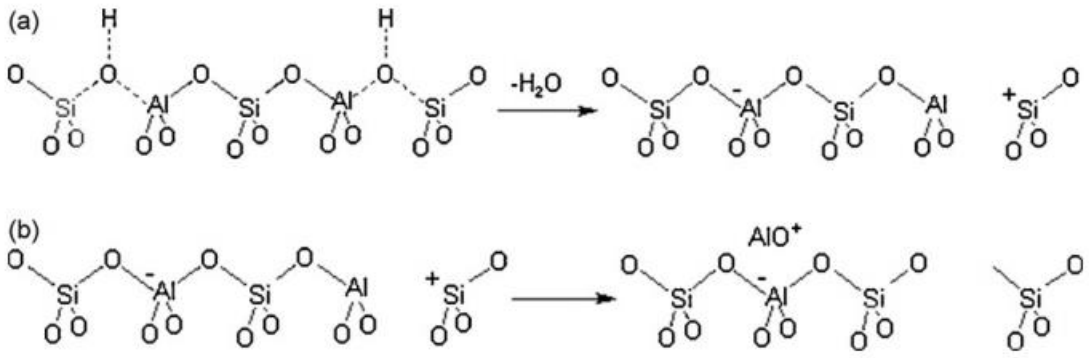

Figure 9 - Two step mechanism for the production of EFAL species. Dehydroxylation (a) and Al segregation (b) [44]

2.5.1.4. Metal Poisoning

Metals such as Iron (Fe), Sodium (Na), Nickel (Ni) and Vanadium (V) act as poisons for the catalysts of the FCC process, including US-Y zeolite [45]. These metals can temporarily poison the catalyst by favoring dehydrogenation reactions, which increase coke yield and decrease gasoline yield [45, 46]. Macropore accessibility is limited with increasing metal concentrations. Blocking these highways of the structural catalyst network prevents hydrocarbon molecules from reaching the catalytically active domains, which results in a reduction of conversion with time on stream [35].

2.5.1.4.1. Sodium (Na) and Iron (Fe)

Sodium increases the hydrothermal instability of zeolites and has a synergetic effect on the action of vanadium [45]. It reduces the catalytic cracking activity by Brønsted acid site neutralization and decreases the quality of the obtained gasoline fraction after processing [47]. Fe contaminants, which are

known to be present at relative high concentrations in shale oil, affect the morphology of the catalysts used in FCC due to *nodulation*, which reduces the accessibility of the catalyst pores and thus its activity [26, 35, 45]. Paramagnetic iron can be exploited to selectively discard older e-cat with higher iron content, which increases the activity of the equilibrium catalyst and lowers the metal content [26].

2.5.1.4.2. Vanadium (V) and Nickel (Ni)

Of all metal species, vanadium presents the most deleterious effect, since it is mobile and can easily move in between older and newer catalyst particles. Coke can be produced on vanadium, regardless of its oxidation state. The vanadium species can deactivate the Y zeolite reversibly and irreversibly. In the first case, the vanadium compounds are adsorbed on the acid sites of the catalyst. In the latter the deactivation is coherent with the formation of vanadic acid in the presence of steam and high temperatures. The zeolite crystalline structure can collapse by the hydrolysis of the silica-alumina framework of the zeolite, with a decrease in surface area as a result. Vanadic acid is a strong acid (pKa = 0.05) and it is responsible for the mobility and consequent attack of the zeolite structure of vanadium. A two-step reaction mechanism in which vanadium reacts with oxygen to produce vanadium(V)oxide, followed by a reaction with water to produce vanadic acid is proposed by Wormsbecher et al. Although it is certain that vanadium plays the role of a catalyst in the destruction of zeolite structure, the exact mechanism is still subject to discussion [35, 45, 47].

The presence of vanadium increases the amount of dehydrogenation reactions and decreases the amount of hydrogen transfer reactions. This results in an increase in coke formation and gasoline quality (RON), while decreasing the gasoline yield [48].

$$4V + 5O_2 \rightarrow 2V_2O_5 \qquad \text{(Eq. 1)}$$

$$V_2O_5 + 3H_2O \rightarrow 2H_3VO_4 \qquad \text{(Eq. 2)}$$

Nickel is highly deleterious, because it changes the main reaction pathway after deposition on the catalyst surface. It establishes parallel reaction pathways such as dehydrogenation and carbonization that cause a shift in catalyst selectivity, thereby reducing the selectivity of the desired cracked products from the FCC process. Although nickel does not contribute to the destruction of the zeolite structure, it has a higher dehydrogenation activity than vanadium due to its catalytic activity towards this reaction. This hydrogenation results in excessive coke and hydrogen production and a shift away from the desired cracking products. Nickel predominantly increases coke formation through its reduced state [35, 45].

Metals can have a synergetic effect when present together with zeolite catalysts, as has been proposed by various authors [45, 46, 47]. A synergetic effect exists between Ni and V species over US-Y zeolite. Bimetallic catalysts containing Ni and V show a decrease in coke formation, compared to the

monometallic ones [60 28]. Addition of Fe or Ca to this bimetallic catalyst even reduced the formation of coke by 70%. This increase in coke formation, in the presence of metallic species, is caused by an increase of acid sites, which enhance olefin conversion and therefore coke formation. This is also the reason that olefin / paraffin ratio is increased when metals are included in the catalysts for the FCC process. Rare earth elements (RE) integration in bimetallic catalysts results in decreased coke formation on vanadium sites, while promoting the formation of coke on nickel sites [45].

2.5.2. Rare Earth Influence on FCC Catalysts

2.5.2.1. Metal Trap

When dealing with high metal contamination, adding more fresh catalyst alone may be an ineffective catalyst management strategy, since this will not reduce the impact of the metal content. It is therefore important to trap these metal contaminants through reactions that form stable and catalytically inactive compounds. This process, also known as metal passivation, reduces the harmful effect of metals without removing the metals from the reaction unit [35].

Rare metals can be used to trap vanadium and nickel, thus reducing the deleterious effect of vanadium that acts as a catalyst for hydrolysis of the zeolite framework. Rare earth oxides, in general form RE_2O_3, are basic in nature and have the ability to neutralize vanadic acid in a reaction that produces vanadates (equation 3). The viability of this metal passivation is determined by the stability of the initial metal oxides and the stability of the metal vanadate product. In general the stability of rare earth vanadates is even preserved at high temperatures during the FCC regenerator [35, 49].

$$RE_2O_3 + 2H_3VO_4 \rightarrow 2REVO_4 + 3H_2O \qquad \text{(Eq. 3)}$$

Yang et al. showed that the inhibiting effect of nickel to the deleterious properties of vanadium is also present in rare earth exchanged Y zeolite. The unit cell size, a measure for the dealumination of the zeolite structure, has the following order: RE-Y > Ni-RE-Y > Ni-V-RE-Y > V-RE-Y. Also the loss of Lewis acid sites by vanadium is reduced when introducing nickel together with vanadium, thus reducing metal poisoning and increasing aluminum framework retention [50].

The method of introduction of RE species can have significant effect on the magnitude of vanadium tolerance for the zeolite catalyst. Research done by Moreira et al. shows that cerium introduced by incipient wetness impregnation is more effective in increasing the vanadium tolerance than cerium introduced by precipitation or ionic exchange. This difference could be related to the higher mobility of vanadium in the latter two methods [51].

2.5.2.2. Hydrothermal Stability

Rare earths can improve hydrothermal stability of FCC catalyst, thus mitigating the problem of irreversible catalyst deactivation and increasing the preservation of acid sites. Indeed, research shows that ion-exchange by lanthanum or cerium in HY zeolite improves the thermal stability, probably owing to the interaction of RE cations with lattice oxygen to form stable oxygen complexes [35, 52, 53].

Although lanthanum and cerium are the main rare earth metals used in FCC catalysis, more hydrothermal stability could be achieved by using RE species with smaller ionic radius. Several authors [53, 54] have concluded that the stability and activity of RE-Y zeolites increase with decreasing ionic radius of the RE elements [53].

Du et al. proposed a mechanism for the transfer or RE ions into zeolite Y [54]:

(I) RE ions exist in aqueous solution as $RE(H_2O)_n^{3+}$. The complexes in supercages yield $RE(OH)^{2+}$ through dehydration during hydrothermal treatments and calcination.

$$RE(H_2O)_n^{3+} \rightarrow RE(OH)^{2+} + H^+ + H_2O$$

(II) The $RE(OH)^{2+}$ cation has a smaller diameter then the opening of the sodalite cage (0.23 nm and 0.66 nm, respectively), which allows the movement of the cation from the supercage into the sodalite cage.

$$RE(OH)^{2+}\ (supercage) \rightarrow RE(OH)^{2+}(sodalite\ cage)$$

(III) At the same time as (II), the RE cations form RE oxides in a reaction with oxygen, which spread to the zeolite surface instead of moving to the sodalite cages.

$$2RE(OH)^{2+} + O_2 \rightarrow RE_2O_3 + H_2O$$

2.6. Coke Formation

Coke formation can have a strong impact on catalyst performance by modifying the conversion and product selectivity. In the FCC unit it also plays an essential role in the heat balance [26].

Multiple types of coke can be found when processing hydrocarbons in the FCC reactor. Five main coke types can be identified [26, 29]:

- *Catalytic coke* can be burned at ca. 500°C, is less hydrogenated and accounts for almost 70% of total coke production in the FCC process. It is formed when hydrocarbons are cracked via acid catalysis as a byproduct of undesirable dehydrogenation and condensation reactions.
- *Catalyst-to-oil coke* is easily burned at 300°C and can be seen as some kind of hydrogenated coke precursors.

- *Thermal coke* is produced by a free radical mechanism, which is favored at high temperatures. Due to the conditions in the FCC process, which do not promote thermal cracking, this type of coke is produced to a lesser extent.
- *Additive coke* is produced from the heavy hydrocarbons present and is related to Conradson carbon residue.
- *Contaminant coke* is created as a by-product from dehydrogenation reactions catalyzed by metals Cu, Ni, V and Fe.

The different types of coke have different influence on the activity of the catalysts in catalytic cracking. This difference in activity depends on the timescale of the deposition for the different types of coke, which determines the type of deactivation. This deactivation can be active site deactivation or pore blockage [26].

2.6.1. Influence on Coke Formation

2.6.1.1. Catalyst and Reactants

After analyzing the loss of mass when regenerating spent catalysts after processing of VGO oil at FCC conditions, it was found that coke deposits on spent catalysts after processing were accumulated in or around the US Y zeolites, while the FCC matrix had much smaller deposits [29]. For the most relevant family, i.e. catalytic coke, coke formation is influenced by several factors [26, 45, 55-57]:

- *Reactants* – The nature of reactants are highly determinant in coke formation. For example, olefins and aromatics show faster rates of coking then alkanes and naphthenes.

- *Operating conditions* – Temperature, pressure and the concentration and nature of the reactants are of relevance. The H/C ratio decreases with temperature and at lower temperatures (<250ºC), the H/C ratio of formed coke molecules is highly similar to that of the reactants. At lower temperatures, the coke formation involves mainly condensation and rearrangement steps. With increasing temperature (>350ºC), the coke components are polyaromatic and formed mainly by hydrogen transfer, dehydrogenation, condensation and rearrangement steps. High reactant partial pressures favor coke formation reactions, due to their bimolecular nature.

- *Zeolite acidity* – The chemical structure of the acid sites of the zeolites, the acid strength and acid site density are of interest for coke formation. Increasing acid site density and strength result in faster coke formation, with increasing catalyst deactivation.
- *Zeolite porous structure* – Acid sites are located in cavities or channel intersections of the zeolite structure. Therefore these can be considered as micro reactors and the size and shape of these cavities influence the rate and nature of the coke formation. The difference in size of cages for

coke production and the size of pore openings is very relevant. Deactivation of catalytic activity is induced by stereochemical blockage when large coke molecules cannot leave the zeolite structure through smaller pore openings.

2.6.1.2. Bio-Oil and Oxygenated Compounds

Gueudré et al. processed VGO and CPO over US-Y zeolite and the average H/C ratio obtained after analyzing the spent catalyst was 0.54 and 0.14, respectively. From the data it can be concluded that most of the hydrogen present in the feedstock is used in the cracking of bio-oils, which leads to highly dehydrogenated coke deposits. Hydrogen content of the spent catalyst after VGO processing (0.98 wt%) was more than the hydrogen content after CPO processing (0.79 wt%), which indicates that there were still hydrogenated compounds present on the spent catalyst [29].

2.7. Model Compound Research

In the recent past a lot of research has been done to co-processing bio-oil with conventional feedstock in the FCC process, by using model compounds to mimic the feedstock and bio-oil conversion over HY zeolite [35, 58]. Many factors, of which deactivation is considered the most decisive, need to be considered when evaluating the catalysts used in the FCC process. The prediction of the behavior of the commercial catalysts is one of the most fundamental research activities, which is why the challenge is to simulate the deactivation of FCC catalysts in the laboratory [35].

2.7.1. Influence Oxygenated Compounds on the Cracking Reaction

The influence of oxygenated compounds phenol and guaiacol on the activity, stability, selectivity and deactivation of the HY zeolite is investigated by I. Graca [58]. This is done by comparing conversion, carbon content and products distribution in the presence and absence of an oxygenated compound.

It can be observed that phenol and guaiacol induce higher deactivation since the beginning of the reaction (figure 10). Increasing the oxygenated compounds from 1.2 wt% to 4.0 wt% does not increase the deactivating effect, which suggests that a maximum deactivating effect by the poisons is already achieved at 1.2 wt% injection. A relation can be seen between the pronounced deactivation of the catalyst in presence of oxygenated compounds and the increase of carbonaceous materials deposited inside the zeolite pores (figure 11). By comparing the evolution of n-heptane conversion as a function of carbon content, it was observed that the toxicity of the carbon deposits is equal for the carbon deposited in the case of pure n-heptane and in presence of 1.2 wt%- and 4.0 wt% oxygenated compound at 450°C. It can be concluded that the deactivation of the HY zeolite is related to the amount of carbon deposited and not to the origin of the carbon [58].

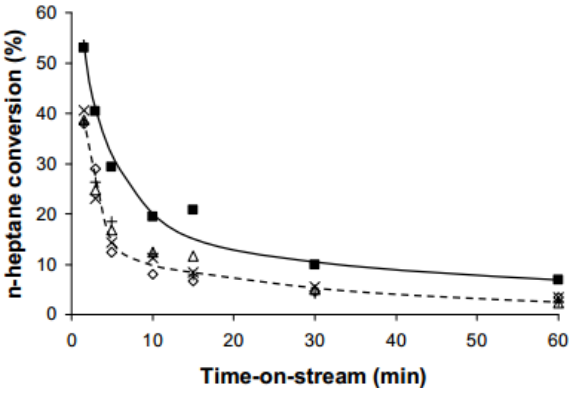

Figure 10 - n-heptane conversion vs. TOS for a contact time of 4 min during the transformation of pure n-heptane (■), n-heptane + 1.2 wt.% phenol (◊), n-heptane + 4.0 wt.% phenol (Δ), n-heptane + 1.2 wt% guaiacol (x) and n-heptane + 4.0 wt% guaiacol (+) at 450ºC [58]

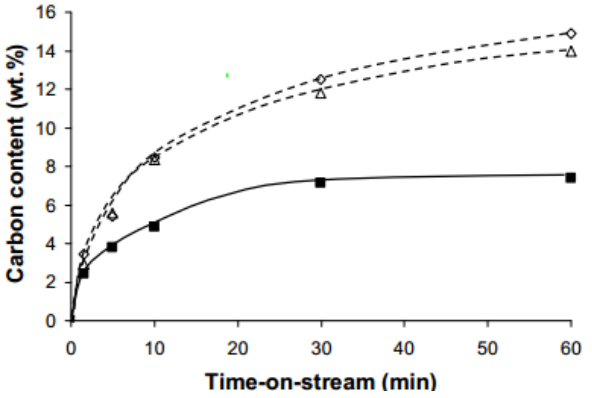

Figure 11 - Carbon content vs. TOS for a contact time of 4 min during the transformation of pure n-heptane (■), n-heptane + 4.0 wt% phenol (Δ) and n-heptane + 4.0 wt% guaiacol (◊) at 450ºC [58]

After analyzing the IR spectra of the coked zeolite samples after pure n-heptane cracking and cracking of n-heptane in presence of oxygenated compounds, it was concluded that the increase of the carbon content that is observed in the presence of phenol and guaiacol should mostly result from the adsorption of the oxygenated compounds on the acid sites of the zeolite, together with the polyaromatic compounds that are produced through n-heptane transformation. Through the IR spectra an increase of the branching of the carbon content could be detected, in the case of cracking n-heptane in presence of phenol or guaiacol [58].

2.7.1.1. Product Distribution

No differences between cracking pure n-heptane and n-heptane with oxygenated compound could be detected in the selectivity of cracking products, aromatics and n-heptane isomers, although the overall conversion is lower in presence of phenol and guaiacol. This was the case for fresh catalyst (1.5 min TOS) and deactivated catalyst (15-60 min TOS). The small amounts of phenol and guaiacol deposited on the HY zeolite after 1.5 min TOS are not sufficient to alter the different product selectivity [58].

When comparing the paraffins/olefins molar ratio of the cracking products, it can be seen that n-heptane cracking in presence of oxygenated compounds leads to an increased paraffins/olefins ratio (figure 12). The selectivity for C_3 and C_4 paraffins is the same for pure n-heptane cracking and in presence of phenol and guaiacol, so it can be concluded that this increase in ratio is the result of a decrease in C_3 and C_4 olefins, which was detected on the effluent of the reaction. A possible explanation for this phenomenon is the occurrence of alkylation of the oxygenated compounds by olefins [58].

An increase of iso/n-paraffins ratio could be detected when cracking of n-heptane was done in presence of oxygenated compound, compared to pure n-heptane cracking (figure 13). It was concluded that this increase is the result of a decrease of steric constraints from highly substituted aromatics on the acid sites of the zeolite. High open spaces between coke molecules can be created, when oxygenated

compounds like guaiacol or phenol are adsorbed on an acid site instead of a polyaromatic (a>4) compound, which allows easy diffusion of branched species [58].

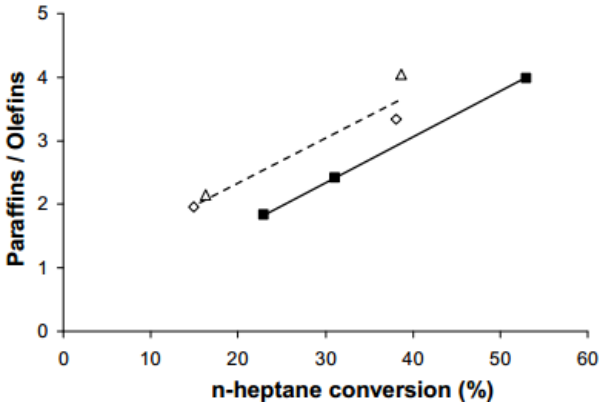

Figure 12 - Paraffins/olefins molar ratio as a function of the n-heptane conversion for the pure n-heptane (■), n-heptane + 4.0 wt% phenol (Δ) and n-heptane + 4.0 wt% guaiacol (◊) at 450ºC, for fresh catalysts (1.5 min TOS) at different contact times [58]

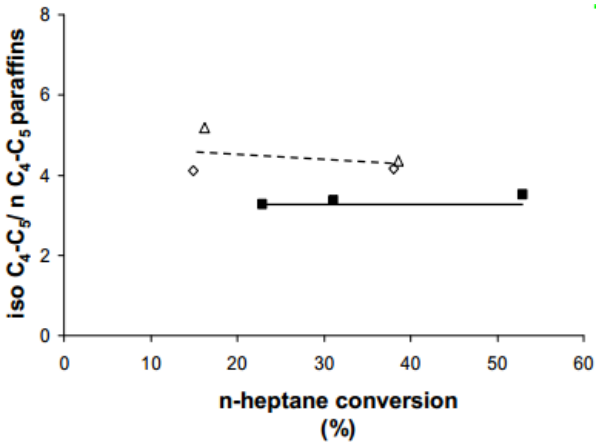

Figure 13 - (iC_4+iC_5)/ (nC_4+nC_5) molar ratio as a function of the n-heptane conversion for the pure n-heptane (■), n-heptane + 4.0 wt% phenol (Δ) and n-heptane + 4.0 wt% guaiacol (◊) at 450ºC, for fresh catalysts (1.5 min TOS) at different contact times [58]

2.7.2. Influence of Oxygenated Compounds on Acid Sites and Porosity

Through analyzing the IR spectra before and after pyridine adsorption experiments it can be seen that the band corresponding to the strongest HY protonic acid sites disappears from the start of the reaction (1.5 min TOS). This reveals a preferential interaction of the guaiacol compound with the stronger acid sites. After 60 min TOS, all protonic acid sites seem to be covered by coke molecules. From the data is was possible to conclude that guaiacol molecules use both oxygen functions for interacting with protonic acid sites, which could lead to the disappearance of two acid sites per guaiacol molecule. From the IR spectra before and after pyridine adsorption the evolution of the number of Brønsted and Lewis acid sites with TOS could be determined for pure n-heptane and in presence of oxygenated compounds (figure 14). It can be concluded that phenol and guaiacol molecules adsorb on both Brønsted and Lewis acid sites, while coke molecules only adsorb on the Brønsted acid sites [58].

An almost complete reduction of microporous volume and a 40% decrease of mesoporous volume was observed when the cracking of n-heptane was done in presence of guaiacol. The same was not observed for pure n-heptane cracking, which resulted in a ca. 20% decrease in microporous volume and no significant decrease in mesoporous volume. When comparing the estimates of guaiacol and phenol accumulated on the HY zeolite determined by carbon content and nitrogen adsorption experiment, a higher value was observed in the estimates from the adsorption experiments for all TOS. From this it can

be concluded that the deactivation of the HY zeolite due to guaiacol proceeds simultaneously by active sites poisoning and pore blocking [58].

From the external surface measurements it was seen that guaiacol molecules, as opposed to phenol molecules, are also adsorbed at the zeolite pores, even if the pore apertures are large enough to allow diffusion of the molecules to the inside of the zeolite structure. It was concluded that this adsorption of the oxygenated compounds on the external surface of the zeolite has a negative effect on the diffusion of molecules to the interior of the zeolite and therefore contributes in part to the pore blocking that is observed [58].

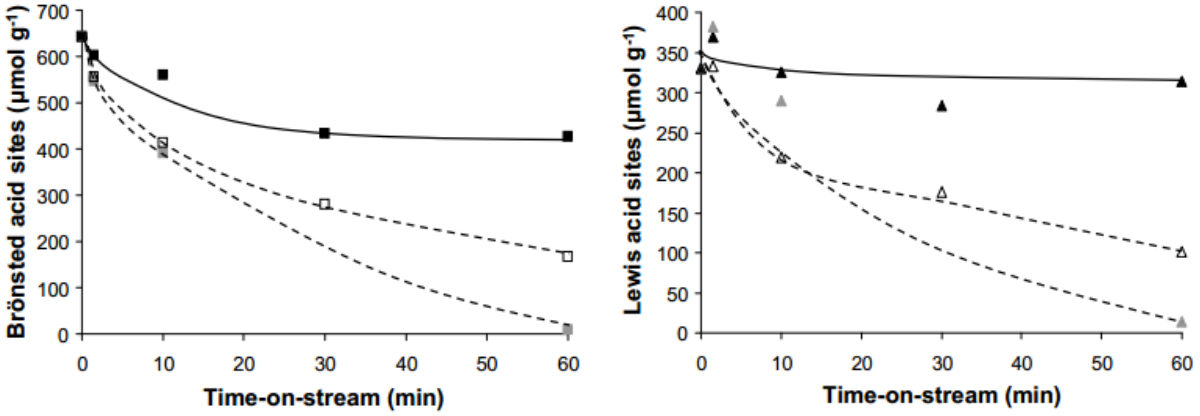

Figure 14 - Evolution of the number of Brønsted (■) and Lewis (▲) acid sites along with time-on-stream for the pure n-heptane (closed symbols), n-heptane + 4.0 wt% phenol (black open symbols) and n-heptane + 4.0 wt% guaiacol (grey closed symbols) transformations, at 450ºC [58]

2.7.3. Similar Research Efforts

Similar research was done on the deactivating effect of oxygenated compounds on the transformation of naphthenes over HY zeolites [59]. The addition of oxygenated compound on the reaction mixture induced an additional deactivation of the HY zeolite, with main difference being the time from which the deactivation was observed (from 5 min of TOS). Other research efforts discussed the deactivating effect of oxygenated compounds on the ECAT additive ZSM-5 catalyst [60] or on the mixture of HY zeolite with ZSM-5 [61]. In all catalysts the deactivation was mostly due to a strong adsorption of oxygenated molecules on the acid sites of the zeolites, while for ZSM-5 also pore blocking has a role in the deactivating effect.

2.8. References

[1] Ho, Dang P., et al. "A mini review on renewable sources for biofuel." Bioresource Technology, vol. 169, 2014, pp. 742-749.

[2] Liew, Weng H., et al. "Review of evolution, technology and sustainability assessments of biofuel production." Journal of Cleaner Production, vol. 71, 2014, pp. 11-29.

[3] Naik, S.N., et al. "Production of first and second generation biofuels: A comprehensive review." Renewable and Sustainable Energy Reviews, vol. 14, no. 2, 2010, pp. 578-597.

[4] Sharma, Abhishek, et al. "Biomass pyrolysis—A review of modelling, process parameters and catalytic studies." Renewable and Sustainable Energy Reviews, vol. 50, 2015, pp. 1081-1096.

[5] Gollakota, A.R.K., et al. "A review on hydrothermal liquefaction of biomass." Renewable and Sustainable Energy Reviews, 2017.

[6] Dimitriadis, Athanasios, and Stella Bezergianni. "Hydrothermal liquefaction of various biomass and waste feedstocks for biocrude production: A state of the art review." Renewable and Sustainable Energy Reviews, vol. 68, 2017, pp. 113-125.

[7] Kan, Tao, et al. "Lignocellulosic biomass pyrolysis: A review of product properties and effects of pyrolysis parameters." Renewable and Sustainable Energy Reviews, vol. 57, 2016, pp. 1126-1140.

[8] Talmadge, Michael S., et al. "A perspective on oxygenated species in the refinery integration of pyrolysis oil." Green Chem, vol. 16, no. 2, 2014, pp. 407-453.

[9] Qu, Tingting, et al. "Experimental Study of Biomass Pyrolysis Based on Three Major Components: Hemicellulose, Cellulose, and Lignin." Industrial & Engineering Chemistry Research, vol. 50, no. 18, 2011, pp. 10424-10433.

[10] Oasmaa, Anja, et al. "Fast Pyrolysis Bio-Oils from Wood and Agricultural Residues." Energy & Fuels, vol. 24, no. 2, 2010, pp. 1380-1388.

[11] Zacher, Alan H., et al. "A review and perspective of recent bio-oil hydrotreating research." Green Chem, vol. 16, no. 2, 2014, pp. 491-515.

[12] Pinho, Andrea D., et al. "Co-processing raw bio-oil and gasoil in an FCC Unit." Fuel Processing Technology, vol. 131, 2015, pp. 159-166.

[13] Elliott, Douglas C., et al. "Catalytic hydroprocessing of biomass fast pyrolysis bio-oil to produce hydrocarbon products." Environmental Progress & Sustainable Energy, vol. 28, no. 3, 2009, pp. 441-449.

[14] De Miguel Mercader, F., et al. "Production of advanced biofuels: Co-processing of upgraded pyrolysis oil in standard refinery units." Applied Catalysis B: Environmental, vol. 96, no. 1-2, 2010, pp. 57-66.

[15] Venderbosch, R.H., et al. "Stabilization of biomass-derived pyrolysis oils." Journal of Chemical Technology & Biotechnology, vol. 85, no. 5, 2010, pp. 674-686.

[16] Fogassy, Gabriella, et al. "From biomass to bio-gasoline by FCC co-processing: effect of feed composition and catalyst structure on product quality." Energy & Environmental Science, vol. 4, no. 12, 2011, p. 5068.

[17] De Miguel Mercader, Ferran, et al. "Hydrodeoxygenation of pyrolysis oil fractions: process understanding and quality assessment through co-processing in refinery units." Energy & Environmental Science, vol. 4, no. 3, 2011, p. 985.

[18] Pinho, Andrea D., et al. "Co-processing raw bio-oil and gasoil in an FCC Unit." Fuel Processing Technology, vol. 131, 2015, pp. 159-166.

[19] Pinho, Andrea D., et al. "Fast pyrolysis oil from pinewood chips co-processing with vacuum gas oil in an FCC unit for second generation fuel production." Fuel, vol. 188, 2017, pp. 462-473.

[20] Shell Oil Co, Powell, Joseph B, et al. Methods and systems for processing cellulosic biomass. US 9783740 B2, United States Patent and Trademark Office, 1 Oct 2014.

[21] ExxonMobil Research and Engineering Co, Reiner, Virginia M, et al. Crude bio oil pretreatment and upgrading. US 20170158967 A1, United States Patent and Trademark Office, 4 Dec 2015.
[22] Honeywell UOP LLC, Baird, Lance A, et al. Methods and fuel processing apparatuses for upgrading a pyrolysis oil stream and a hydrocarbon stream. US 9663729 B2, United States Patent and Trademark Office, 30 May 2017.
[23] Marker, T.L. "Opportunities for Biorenewables in Oil Refineries." 2005.
[24] Oinonen, M., et al. "Biofuel proportions in fuels by AMS radiocarbon method." Nuclear Instruments and Methods in Physics Research Section B: Beam Interactions with Materials and Atoms, vol. 268, no. 7 8, 2010, pp. 1117-1119.
[25] Cruz, Pedro L., et al. "Modelling of co-processing of HDO-oil with VGO in a FCC unit." Fuel, vol. 196, 2017, pp. 362-370.
[26] H.S. Cerqueira a,1, G. Caeiro b, L. Costa c, F. Ramôa Ribeiro. "Deactivation of FCC catalysts." Journal of Molecular Catalysis A: Chemical, vol. 292, 1 July 2008, pp. 1-13.
[27] Marcello S. Rigutto, Rob van Veen and Laurent Huve "Zeolites in Hydrocarbon Processing" Introduction to Zeolite Science and Practice (3rd edition), Elsevier, 2007, pp. 855-914
[28] Wilson, Joseph W. Fluid Catalytic Cracking Technology and Operations. PennWell Books, 1997.
[29] Gueudré, Laurent, et al. "Coke chemistry under vacuum gasoil/bio-oil FCC co-processing conditions." Catalysis Today, vol. 257, 2015, pp. 200-212.
[30] Weitkamp, J., Hunger, M. "Acid and Base Catalysis on Zeolites" Introduction to Zeolite Science and Practice (3rd edition), Elsevier, 2007, pp. 787-804
[31] Weitkamp, Jens, et al. "Isomerization and hydrocracking of C9 through C16 n-alkanes on Pt/HZSM-5 zeolite." Applied Catalysis, vol. 8, no. 1, 1983, pp. 123-141.
[32] Brouwer, D. M., and H. Hogeveen. "The importance of orbital orientation as a rate-controlling factor in intramolecular reactions of carbonium ions." Recueil des Travaux Chimiques des Pays-Bas, vol. 89, no. 2, 2010, pp. 211-224.
[33] Krannila, H., et al. "ChemInform Abstract: Monomolecular and Bimolecular Mechanisms of Paraffin Cracking: n- Butane Cracking Catalyzed by HZSM-5." ChemInform, vol. 23, no. 32, 2010, pp. no-no.
[34] Corma, Avelino, et al. "Methylcyclohexane and methylcyclohexene cracking over zeolite Y catalysts." Applied Catalysis, vol. 67, no. 1, 1990, pp. 307-324.
[35] Akah, Aaron. "Application of rare earths in fluid catalytic cracking: A review." Journal of Rare Earths, vol. 35, no. 10, 2017, pp. 941-956.
[36] O'Connor, P., and A.C. Pouwels. "FCC Catalyst Deactivation: A Review and Directions for further Research." Catalyst Deactivation 1994, Proceedings of the 6th International Symposium, 1994, pp. 129-144.
[37] Fu, Chia M., and Arnold M. Schaffer. "Effect of nitrogen compounds on cracking catalysts." Industrial & Engineering Chemistry Product Research and Development, vol. 24, no. 1, 1985, pp. 68-75.
[38] Ho, Teh C., et al. "Effect of nitrogen compounds on cracking catalysts." Industrial & Engineering Chemistry Research, vol. 31, no. 7, 1992, pp. 1589-1597.
[39] Corma, A., and F.A. Mocholí. "New silica-alumina-magnesia FCC active matrix and its possibilities as a basic nitrogen passivating compound." Applied Catalysis A: General, vol. 84, no. 1, 1992, pp. 31-46.
[40] Corma, A., et al. "Processing biomass-derived oxygenates in the oil refinery: Catalytic cracking (FCC) reaction pathways and role of catalyst." Journal of Catalysis, vol. 247, no. 2, 2007, pp. 307-327.
[41] Chen, Tiehong, et al. "Lewis acid sites on dehydroxylated zeolite HZSM-5 studied by NMR and EPR." Catalysis Today, vol. 30, no. 1-3, 1996, pp. 189-192.
[42] Elanany, Mohamed, et al. "Periodic density functional investigation of Lewis acid sites in zeolites:

relative strength order as revealed from NH3 adsorption." Applied Surface Science, vol. 246, no. 1-3, 2005, pp. 96-101.

[43] Babitz, Scott M., et al. "Role of Lewis Acidity in the Deactivation of USY Zeolites during 2-Methylpentane Cracking." Industrial & Engineering Chemistry Research, vol. 36, no. 8, 1997, pp. 3027-3031.

[44] Kühl, G.H. "The coordination of aluminum and silicon in zeolites as studied by x-ray spectrometry." Journal of Physics and Chemistry of Solids, vol. 38, no. 11, 1977, pp. 1259-1263.

[45] Escobar, Alyne S., et al. "Effect of iron and calcium over USY coke formation." Applied Catalysis A: General, vol. 339, no. 1, 2008, pp. 61-67.

[46] Vasileios Komvokis , Lynne Xin Lin Tan , Melissa Clough , Shuyang Shaun Pan , and Bilge Yilmaz. "Zeolites in Fluid Catalytic Cracking (FCC)." Zeolites in Sustainable Chemistry: Synthesis, Characterization and Catalytic Applications, Springer, 2016, pp. 271-298.

[47] Xu, Mingting, et al. "Pathways for Y Zeolite Destruction: The Role of Sodium and Vanadium." Journal of Catalysis, vol. 207, no. 2, 2002, pp. 237-246.

[48] Myrstad, Trond. "Effect of vanadium on octane numbers in FCC-naphtha." Applied Catalysis A: General, vol. 155, no. 1, 1997, pp. 87-98.

[49] Baugis, Guintar L., et al. "The luminescent behavior of the steamed EuY zeolite incorporated with vanadium and rare earth passivators." Microporous and Mesoporous Materials, vol. 49, no. 1-3, 2001, pp. 179-187.

[50] Yang, S.-J., et al. "ChemInform Abstract: Vanadium-Nickel Interaction in REY Zeolite." ChemInform, vol. 26, no. 1, 2010

[51] Moreira, Carla R., et al. "Evidence of multi-component interaction in a V–Ce–HUSY catalyst: Is the cerium–EFAL interaction the key of vanadium trapping?" Microporous and Mesoporous Materials, vol. 115, no. 3, 2008, pp. 253-260.

[52] Lemos, F., et al. "Influence of lanthanum content of LaHY catalysts on their physico-chemical and catalytic properties." Applied Catalysis, vol. 39, 1988, pp. 227-237.

[53] Shu, Yuying, et al. "Effect of Ionic Radius of Rare Earth on USY Zeolite in Fluid Catalytic Cracking: Fundamentals and Commercial Application." Topics in Catalysis, vol. 58, no. 4-6, 2015, pp. 334-342.

[54] Du, Xiaohui, et al. "Effect of cation location on the hydrothermal stability of rare earth-exchanged Y zeolites." Catalysis Communications, vol. 35, 2013, pp. 17-22.

[55] Guisnet, M., et al. "Roles of acidity and pore structure in the deactivation of zeolites by carbonaceous deposits." Catalyst Deactivation, Proceedings of the 7th International Symposium, 1997, pp. 1-19.

[56] Guisnet, M., and P. Magnoux. "Organic chemistry of coke formation." Applied Catalysis A: General, vol. 212, no. 1-2, 2001, pp. 83-96.

[57] Cerqueira, Henrique S., et al. "Coke formation and coke profiles during the transformation of various reactants at 450°C over a USHY zeolite." Applied Catalysis A: General, vol. 208, no. 1-2, 2001, pp. 359-367.

[58] Graça, Inês. "Influence of Oxygenated Compounds on the Properties of FCC Catalysts." 2010. Instituto Superior Técnico, PhD Dissertation.

[59] Graça, Inês, et al. "Effect of phenol adsorption on HY zeolite for n-heptane cracking: Comparison with methylcyclohexane." Applied Catalysis A: General, vol. 385, no. 1-2, 2010, pp. 178-189.

[60] Graça, Inês, et al. "Influence of Phenol Addition on the H-ZSM-5 Zeolite Catalytic Properties during Methylcyclohexane Transformation." Energy & Fuels, vol. 23, no. 9, 2009, pp. 4224-4230.

[61] Graça, Inês, et al. "n-Heptane cracking over mixtures of HY and HZSM-5 zeolites: Influence of the presence of phenol." Fuel, vol. 94, 2012, pp. 571-577.

3. Experimental Techniques

3.1. Catalyst Preparation

The parent zeolite, ultra-stable Y zeolite *CBV500*, was impregnated with 0.5%, 1% and 2% nickel and vanadium to resemble the industrial composition of the ECAT mixture. Nickel and vanadium were introduced in the zeolite using dry impregnation, while cerium was introduced by an ion-exchange procedure. CBV500 was delivered by *Zeolyst* in the ammonium form, which makes it very suitable for post-synthesis modifications.

3.1.1. Dry (Incipient Wetness) Impregnation

One of the ways to introduce metal species in the zeolitic structure is the incipient wetness impregnation. The zeolite support is contacted with a solution that contains the metal salt of the metal that needs to be included in the zeolite. The impregnation is called 'incipient wetness' when the solution volume does not exceed the pore volume of the zeolite support. During calcination the counter ions of the used salt are decoupled [1].

The amount of H_2O in the zeolite CBV500, which is relevant for the calculation, has been determined by thermogravimetry. The amount of H_2O that is needed to fully fill the pores per gram of sample can be determined by saturating the sample drop by drop until it is visible that the pores are completely filled.

For both nickel and vanadium three samples were prepared (0.5wt%, 1wt% and 2wt% metal in CBV500). Knowing the molecular weights of the metal salts $Ni(NO_3)_2 \cdot 6H_2O$ (nickel(II)nitrate hexahydrate) and NH_4VO_3 (ammonium vanadate) used for the procedure, it was possible to calculate the amount of salt needed for the impregnation. The metal salts were dissolved in an amount of H_2O that would fill the pores of the zeolite completely (0.95 mL/gr). For the ammonium vanadate it was necessary to heat up the solution to 50°C while stirring for the salt to dissolve. The solution with metal salt was dropped on the sample drop by drop, while stirring the sample manually with a glass rod. The saturated sample was aged (1h) before it was dried at 100°C (24h). The dried sample was calcined under the usual conditions used in this thesis (see *CALCINATION*).

3.1.2. Calcination

Calcination is the heating of a substance to high temperatures in the presence of air or oxygen, according to IUPAC. The calcination treatment can be seen as a post-synthesis treatment, just like ion exchange, dealumination or sorption [4, 5]. The Y zeolite used in this research (CBV500) was supplied in the NH4-Y (ammonium) form. Calcination is needed to obtain the protonated form (HY) that will have desirable catalytic properties and therefore will be suitable for use in the present work.

Another reason to perform calcination is desorption or decomposition of unwanted species in the sample. With respect to the impregnation- and ion-exchange steps that are performed in this work, the calcination is used to decompose or burn the counter-ions of the metals to be precipated. For this reason it is preferable to use nitrates, since they easily decompose under the conditions used in calcination [1].

The calcination was performed using the temperature profile shown below. First the sample was heated to 200°C (2°C/min). This step was used to let the water evaporate out of the zeolite structure, which could cause dealumination in a later stage at higher temperature. After a plateau at 200°C (1h) the sample was heated to 500°C (5°C/min) and the treatment was finished with a plateau at 500°C (6h). The procedure was performed under a steady air flow (60 mL/min/gr).

$$RT \xrightarrow{2^0C/min} 200^0C \xrightarrow{5^0C/min} 500^0C$$

3.2. Characterization of Catalyst

For the structural analysis of the fresh samples, X-ray diffraction (XRD) was performed on fresh CBV500 samples with and without impregnated metal, while UV-vis spectroscopy was only performed on fresh samples impregnated with nickel and vanadium. Fourier transform infrared spectrometry (FTIR) and nitrogen adsorption experiments were performed on all fresh and coked samples, as compared to elemental analysis, for determining carbon content in the zeolite, which was only performed with coked samples.

3.2.1. X-ray Diffraction (XRD)

XRD measurements were performed to investigate the structure, phase composition and thermostability of the fresh catalyst samples with and without metal impregnation [6].

The structural characterization of all CBV500 samples was carried out with a D8 Advance diffractometer from Bruker (Bragg-Brentano geometry), using copper radiation (filtered with Ni slit) and equipped with a linear Lynxeye detector (192 silicon strip sensors). The powder XRD patterns were obtained from 5° to 70° (2θ), with a step size of 0.02° and a time per step of 2s.

3.2.2. UV-vis Spectroscopy

UV-vis diffuse reflectance spectroscopy (DRS UV-Vis) was performed to determine the electronic states of the present nickel and vanadium species [6]. Diffuse reflectance is light that is redirected over a certain range of angles after contacting the sample and is a focus of spectral measurements. The Kubelka-Munk function (equation 4) was used and presents a linear relation between analyte concentration and reflectance for this type of UV-Vis spectroscopy. R_∞ is the reflectance after scattering throughout the non-absorbing matrix of infinite depth [7].

$$f(R_\infty) = \frac{(1 - R_\infty)^2}{2R_\infty}$$

(Eq. 4)

DRS UV–Vis spectra of powder samples were collected on a Varian Cary 5000 UV–Vis–NIR spectrophotometer, in the range 200-800 nm, with the following spectroscopic parameters (spectral bandwidth of 4 nm, data interval of 1 nm and scan rate of 600 nm.min^{-1}). A Praying Mantis integration sphere accessory was used for this purpose. For all the samples, parent sample (starting zeolite, CBV500 material) was used as baseline reference. The UV-Vis DRS spectra obtained were then converted into F(R) (Kubelka-Munk function) spectra.

3.2.3. FTIR Spectroscopy

The Fourier Transform Infrared Spectrometric technique allows the analysis of fresh and coked zeolite acidity, which can be characterized by two methodologies:

- The hydroxyl (OH group) stretching vibration bands can be seen in the 3500 – 3800 cm^{-1} region of the spectrum. By analyzing these bands, it is possible to obtain information concerning Brønsted acid sites.
- The interaction of pyridine as probe molecule with the acid sites of the zeolite can be studied. For both Lewis and Brønsted acid sites this gives valuable information regarding the nature, concentration and strength of the acid sites.

Interaction of pyridine with the acid sites of the zeolites results in the appearance of some bands in the 1300 – 1700 cm^{-1} region that are characteristic for pyridine adsorbed on Lewis and Brønsted acid sites. The concentration of both Lewis and Brønsted acid sites can be determined through a modified Lambert-Beer law (equation 5) [8], by integrating the absorbance of the bands at 1455 and 1540 cm^{-1}, respectively.

$$\int_{\bar{\nu}_i}^{\bar{\nu}_f} A_i(\bar{\nu})\,d\bar{\nu} = \varepsilon_i \ell \left(\frac{n_i}{S\ell}\right) \Leftrightarrow C_i = \frac{\int_{\bar{\nu}_i}^{\bar{\nu}_f} A_i(\bar{\nu})\,d\bar{\nu} \times S}{\varepsilon_i\, m} \qquad \text{(Eq. 5)}$$

The extinction coefficients used for the Lewis and Brønsted acid site concentration were previously reported by M. Guisnet et al. [9]: 1.28 cm/µmol for the PyH^+ (pyridinium ions) and 1.15 cm/µmol for the PyL (pyridine coordinated to Lewis acids).

3.2.4. FTIR Apparatus

The acid properties were measured by Fourier-transform Infrared spectroscopy (FT-IR) of adsorbed pyridine, using a Nexus Thermo Nicolet apparatus (64 scans and resolution of 4 cm^{-1}) equipped with a home-made vacuum cell, and using self-supported discs (5-10 mg cm^{-1}) and pyridine as the base probe molecule. After in-situ outgassing at 450ºC (fresh samples) or 200ºC (coked samples) for 3h under high vacuum (10^{-5} Torr), pyridine (99.99 %) was contacted with the sample at 150ºC for 10 min and then evacuated at 150 ºC (all the samples) and 250ºC, 350ºC and 450ºC (fresh samples) for 30 min under high vacuum (10^{-5} Torr).

3.2.5. Nitrogen Adsorption Measurements

3.2.5.1. Pre-Treatment: Degassing

All physically adsorbed fluid should be removed from the zeolite surface to ensure a reproducible initial state and to obtain correct data. Degassing under vacuum is preferential, since the volumetric adsorption experiments that follows usually starts at relative pressures as low as 10^{-7} Pa. Usually the physisorbed water in nonporous or mesoporous zeolites will be lost at relatively low temperatures (<200ºC), while higher temperatures together with long outgassing periods can be required for desorption of physisorbed water in narrow micropores. To avoid structural damage of the zeolite due to surface tension and steaming effects, a special heating profile is usually needed [10].

According to methodology by I. Graça [8], the fresh zeolite samples can be outgassed at 90ºC (1h) followed by 350ºC (3h) under vacuum. Coked zeolites are degassed at 110ºC (1h) under vacuum. The

pre-treatment of coked zeolite will be less severe, since removal of coke molecules that are deposited on the zeolite surface should be prevented [8].

3.2.5.2. Nitrogen Adsorption

Nitrogen adsorption measurements were carried out at -196°C on a Micrometrics ASAP 2010 apparatus. The low temperature favors the adsorption reaction and is therefore chosen on the boiling point of nitrogen [11]. Through analysis of the isotherm, t-plot and BJH adsorption and desorption, the type of pores (micro, meso), the volume of the micropores (V_{micro}) and the external surface area (S_{ext}) can be calculated.

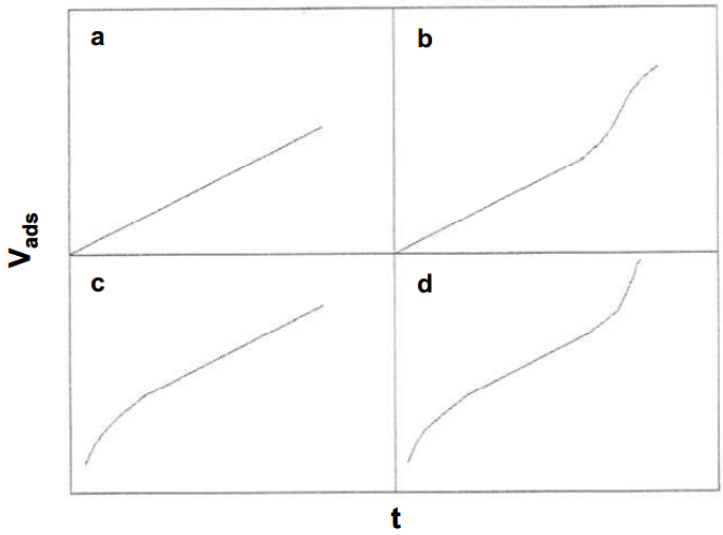

Figure 15 - t-plot obtained after adsorption of non-porous (a), mesoporous (b), microporous (c) and composite micro- and mesoporous (d) solids [8]

3.2.5.3. T-Plot

The t-plot method, as proposed by Lippens and de Boer [12], compares the adsorption isotherm of a microporous material with the adsorption isotherm of a nonporous material with the same surface characteristics. The method allows the determination of micropore volume, surface area and to obtain information about the average pore size. Differences between the shape of the reference isotherm and the experimental isotherm result in regions of the t-plot that are non-linear. These deviations from the reference isotherm can be used to obtain information about the existence of micro- and/or mesopores as can be seen in figure 15.

The film thickness on pore walls is assumed to be uniform, which makes it possible to obtain the statistical thickness (t) from the gas adsorption isotherms and a thickness equation can be constructed. In this experiment the thickness equation formula constructed by Harkins and Jura will be used (equation 6). This equation represents nitrogen sorption at -196°C on nonporous adsorbents that contain oxidic surfaces, thus being representable for zeolitic materials:

$$t(\text{Å}) = \left[\frac{13.99}{0.034 - \log\left(\frac{P_0}{P}\right)}\right]^{\frac{1}{2}}$$

(Eq. 6)

The experimental adsorption isotherm data is reconstructed as a t-curve through the conversion of p_0/p to statistical thickness by the thickness equation formula given above.

The adsorbed volume (V_{ads}) can be calculated with the use of the liquid nitrogen density inside the pores. Equation 7 [13] gives the adsorbed volume, in which V_f is the volume of the nitrogen in gaseous form (cm^3/g), 22414 is the molar volume (cm^3/mol, STP), M is the molar mass of the adsorbed nitrogen (g/mol) and ρ is the density of the liquid nitrogen (g/cm^3):

$$V_{ads} = \left(\frac{V_f * M}{22414 * \rho}\right)$$

(Eq. 7)

In the case of solids that contain micropores, after complete filling of the micropores volume by nitrogen at relative low pressures (low p_0/p and t values), a linear region can be seen in the t-plot. The slope of this linear portion of the plot is directly proportional to the external surface area and the micropores volume (V_{micro}) is obtained by interpolation and interception of the slope at t=0 as demonstrated in figure 16 and 17 [8, 13, 14].

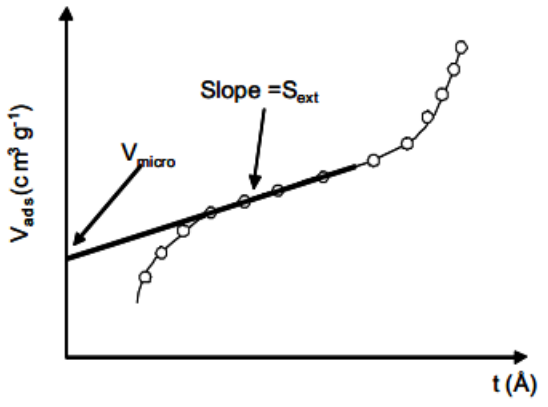

Figure 16 - Micropores volume and external surface determination using the t-plot method [8]

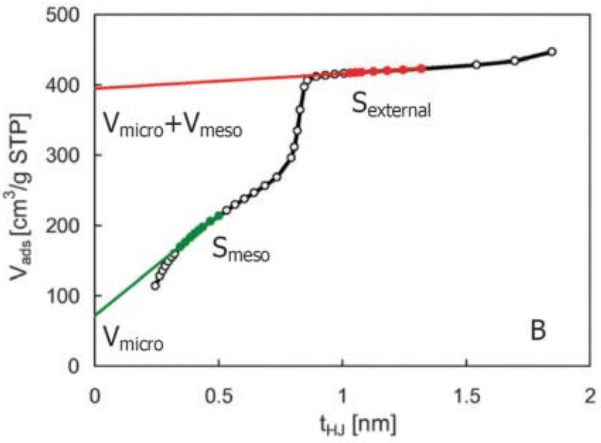

Figure 17 - Micro- and mesopores volume and external surface determination using the t-plot method [14]

3.2.6. Elemental Analysis

The carbon content on the zeolite was analyzed by LAIST (Laboratório de Análysis do IST) by using methodology M.M. 8.6 (A.E.)(2009-05-06). This analysis was done for all coked catalytic samples at 1.5 and 60min of TOS.

3.3. Catalytic Tests

The methodology for catalytic testing of zeolites in the cracking reactions of model molecules n-heptane will be based on the methodology used by I. Graça [8] on the research to the influence of oxygenated compounds on the properties of FCC catalysts. Based on the equipment available and the experiments carried out by I. Graça, the experimental description for the catalytic testing is summarized below.

The catalysts should have a calcination pretreatment, which starts with heating up to 200ºC (5ºC/min), followed by a plateau at this temperature (1h). The next step is heating to 450ºC (5ºC/min), followed by a plateau at 450ºC (6h). The pretreatment is carried out under constant N_2 flow (60 cm^3/min) at atmospheric pressure. The fixed bed reactor is heated to the reaction temperature in a vertical oven. To know the real reaction temperature, a thermocouple Cr/Ni will be placed close to the catalytic bed of the reactor to know the reaction temperature with high precision.

The reactor feed will be composed of 10 mol% n-heptane and 90 mol% N_2. Different amounts of guaiacol will be injected together with the n-heptane in the poisoning tests. The N_2 flow is controlled (120cm^3/min) at atmospheric pressure and room temperature by a BROOK Instruments controller.

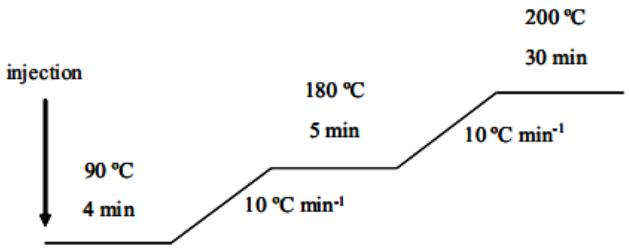

Figure 18 - GC column temperature profile for n-heptane [8]

A conversion profile can be obtained by taking samples for different TOS (time-on-stream) values from 1.5 to 60 minutes, the first value being the time to get a stable reactant pressure in the reactor. A 10-position valve is used to capture these samples, before being analyzed through a GC chromatograph (SHIMADZU GC-14B) with a Plot Al_2O_3/KCl fused silica capillary column (50m). Nitrogen will be used as carrier gas and for detection a flame ionization detector will be used. At the detector the flowrate for hydrogen and air are 40 cm^3/min and 500 cm^3/min, respectively. In figure 18 the temperature profile of the GC column is illustrated and the schematics of the catalytic testing equipment can be seen in figure 19. The data acquisition will be carried out by software that is commercialized by Shimadzu under the name Class VP. The same software is used to control the GC and the positioning of the 10-position valve.

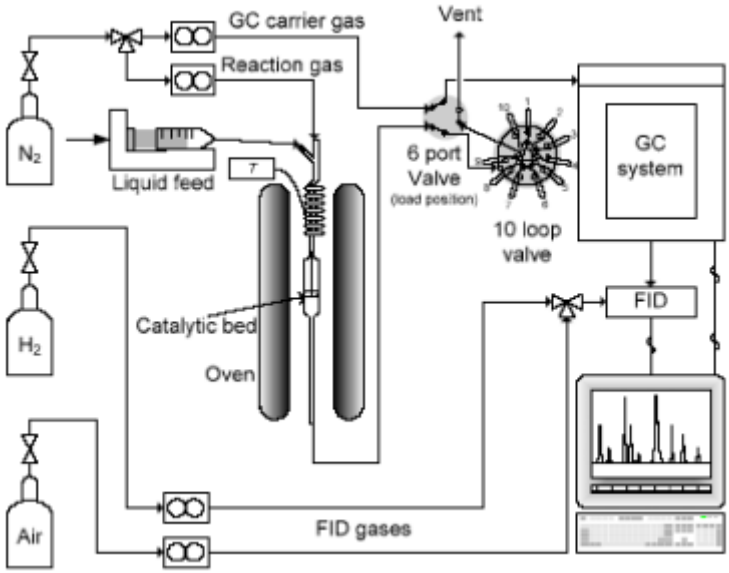

Figure 19 - Schematics of the catalytic testing equipment at IST [8]

3.4. Evaluation of the Catalyst Performance

3.4.1. Conversion, Yield and Selectivity

From the results obtained from the GC with the flame ionization detector (FID), several performance metrics of the catalyst can be calculated. Since the FID is mass sensitive, the peak areas (A) from the GC are proportional to the mass concentration of the compounds in the product mixture and therefore also to the number of carbon atoms. Since the sensibility of the detector is dependent on the type of compounds that are analyzed, a response factor (F_R) should be given to each type of compound to obtain a corrected area (A_c). The response factor for n-heptane is close to 1, which makes it relatively simple to calculate the conversion, yield and selectivity of the n-heptane conversion [8].

Conversion on desorbed products (X (%)), yield (Y_i (wt%)) and selectivity (S_i (wt%)) for each product *i* can be calculated from the GC peak areas, as can be seen in equation 8-10. Coke is not accounted for in the peak areas, since coke molecules are trapped in the pores of the zeolite. This results in a smaller A_{total} in the calculations and therefor an underestimation for the conversion and overestimation for the yield and selectivity.

$$X\ (\%) = (\ 1 - \frac{A_{reactant}}{A_{total}}\ ) * 100$$

(Eq. 8)

$$Y_i\ (wt\%) = \frac{A_i}{A_{total}} * 100$$

(Eq. 9)

$$S_i\ (wt\%) = \frac{A_i}{A_{total} - A_{reactant}} * 100 = \frac{Y_i}{X} * 100$$

(Eq. 10)

3.5. References

[1] Pinho, Andrea D., et al. "Co-processing raw bio-oil and gasoil in an FCC Unit." Fuel Processing Technology, vol. 131, 2015, pp. 159-166.

[2] Vogt, E. T., and B. M. Weckhuysen. "Fluid catalytic cracking: recent developments on the grand old lady of zeolite catalysis." Chemical Society Reviews, vol. 44, no. 20, 2015, pp. 7342-7370.

[3] Lemos, F., et al. "Influence of the cerium content of CeHY catalysts on their physicochemical and catalytic properties." Applied Catalysis, vol. 29, no. 1, 1987, pp. 43-54.

[4] McCusker, L.B., Baerlocher, C. "Zeolite Structures" Introduction to Zeolite Science and Practice (3rd edition), Elsevier, 2007, pp. 13-38.

[5] http://goldbook.iupac.org/html/C/C00773.html

[6] Petranovskii, V., et al. "Formation of catalytically active copper and nickel nanoparticles in natural zeolites." Zeolites and related materials: Trends, targets and challenges, Proceedings of the 4th International FEZA Conference, 2008, pp. 513-516.

[7] Steward, Genevieve C. "Diffuse Reflectance Spectroscopy for the Characterization of Calcareous Glacial Till Soils from North Central Montana." 2006. Montana State U, MS thesis.

[8] Graça, Inês. "Influence of Oxygenated Compounds on the Properties of FCC Catalysts." 2010. Instituto Superior Técnico, PhD Dissertation.

[9] Morin, S., et al. "Influence of the framework composition of commerical HFAU zeolites on their activity and selectivity in m-xylene transformation." Applied Catalysis A: General, vol. 166, no. 2, 1998, pp. 281-292.

[10] Thommes, Matthias. "Textural Characterization of Zeolites and Ordered Mesoporous Materials by Physical Adsorption." Introduction to Zeolite Science and Practice, 2007, pp. 495-523.

[11] Trunschke, Annette. "Surface area and pore size determination." Modern Methods in Heterogeneous Catalysis Research, 1 Nov. 2013, Presentation.

[12] De Boer J. H. Lippens B.C, Linsen B.G., Broeckhoff J.C.P., van den Heuvel A., and Onsinga T.V., (1966), J. Colloid Interf. Sci. 21

[13] Leofanti, G., et al. "Surface area and pore texture of catalysts." Catalysis Today, vol. 41, no. 1-3, 1998, pp. 207-219.

[14] Roth, Wieslaw J., et al. "ChemInform Abstract: Layer Like Porous Materials with Hierarchical Structure." ChemInform, vol. 47, no. 31, 2016.

4. Results & Discussion

4.1. n-Heptane cracking scheme

Figure 20 represents the pathways for n-heptane cracking that correspond to the classical β-scission mechanism. N-heptyl ions ($C_7H_{15}^+$) can be created from n-heptane by a hydrogen transfer reaction or through a protolytic cracking mechanism (step 1). In the latter the linear alkane is cracked into hydrogen, methane, propane, butanes or pentanes and the corresponding carbenium ions (C_2^+ - C_6^+). These carbenium ions can desorb as alkenes or can have a hydride transfer reaction with n-heptane molecules and desorb as an alkane, which changes the n-heptane molecule into an n-heptyl carbenium ion. Protolytic cracking through this so-called Haag and Dessau's mechanism is favored by zeolitic catalysts with medium sized pores that allow the monomolecular reaction and restricts the bimolecular reaction seen in classical cracking due to steric hindrance in the zeolite pore system [1, 2].

Different C_7^+ species can be formed through structural isomerization of the n-heptyl ions, as can be seen in the cracking scheme. These C_7^+ species can undergo β-scission cracking (steps 2-7), from which mainly C_3 and C_4 are formed due to the very unstable primary carbenium ions involved in the creation of methane and ethane. Also the reaction in step 2 is very unlikely to occur, since it also involves the creation of primary carbenium ions. From the reactions shown in steps 3-7, the ones that involve a tertiary carbenium ion (step 5 and 7) are the most likely to occur. A hydride transfer reaction of the carbenium ion formed in the β-scission with a reactant n-heptane molecule creates an alkane and a new n-heptyl ion [2].

Since the reactions in step 5 and step 7 are more likely to occur, a relative high formation of propane, propene, isobutane and isobutene can be expected when the bimolecular cracking mechanism is the dominant mechanism. The occurrence of protolytic cracking can be detected by analyzing the amount of hydrogen, methane, ethane and linear C_5-C_7 alkenes in the reaction products [2].

4.2. CBV500 (reference)

4.2.1. Fresh catalyst characterization

Characteristics of the fresh Y zeolite (CBV500), the global Si/Al ratio, framework Si/Al ratio, unit cell size and Na content are reported in previous work [2] or obtained from *Zeolyst*, the manufacturer of the zeolite [3]. Since CBV500 is an ultra-stable Y zeolite, which means it has suffered dealumination, the global Si/Al ratio and framework Si/Al are not the same due to the presence of extra framework aluminum

species (EFAL). Elemental analysis was used to determine global Si/Al ratio and Na content, while the framework Si/Al ratio was estimated from the unit cell size through the Breck-Flanigen equation [2, 4]. The chemical composition, unit cell size and unit cell formula are presented in table 5.

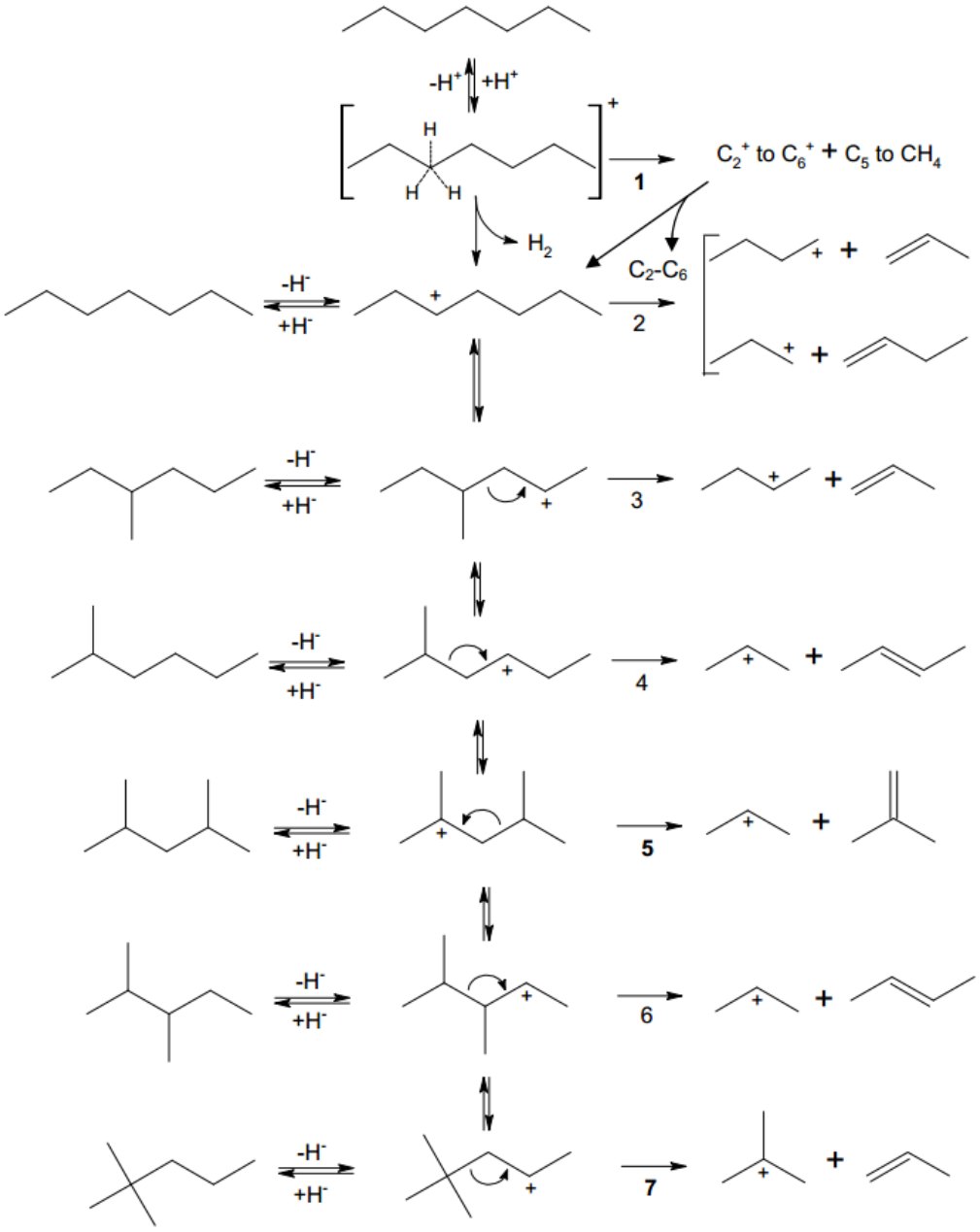

Figure 20 - β-scission cracking mechanism of n-heptane [2]

Table 5 - Chemical composition, unit cell size and formula of CBV500

Unit Cell Formula	*Unit Cell Size (Å)*	*Si/Al $_{global}$*	*Si/Al $_{framework}$*	*Na_2O (%)*
$Na_{0.6}H_{31.6}Al_{32.2}Si_{142.7}O_{384}$ (17 EFAL)	24.53	2.9	4.4	0.2

Microporous volume, mesoporous volume, total volume and external surface area were obtained by performing nitrogen adsorption experiments. Figure 21 presents the nitrogen adsorption and desorption isotherm for the CBV500 sample at 77 K, which can be classified as type I in accordance with the classification of IUPAC. Primary adsorption can be seen below 0.1 p/p^0, which indicates the presence of highly porous material and the possibility of a narrow pore size distribution. The presence of mesopores is indicated by a small degree of hysteresis [5, 6]. According to the procedure described in the experimental techniques, the total volume and the volume for the various pores were obtained using the t-plot method. Table 6 summarizes the textural properties of the HY zeolite.

Table 6 - Textural properties, such as total-, microporous- and mesoporous volume and external surface area for CBV500

V_{total} (cm^3/gr)	V_{micro} (cm^3/gr)	V_{meso} (cm^3/gr)	S_{ext} (m^2/gr)
0.380	0.302	0.078	53

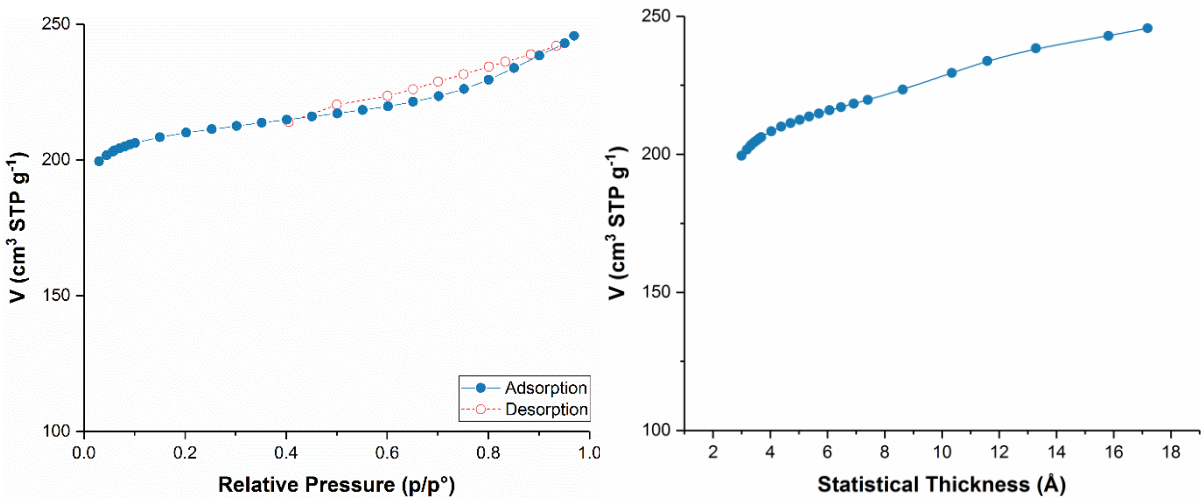

Figure 21 – Nitrogen adsorption and desorption isotherms of CBV500 (left) and the constructed t-plot from the adsorption isotherm (right)

The acidic form of zeolites is important in various catalytic reactions including the cracking of hydrocarbons, isomerization and alkylation. Since catalytic activity is related to acidity, it is of high importance to determine the nature, amount and strength of the acid sites in the characterization of the material [7, 8]. Pyridine adsorption in combination with FTIR spectroscopy is performed to identify and analyze the Brønsted and Lewis acid sites of CBV500.

Different regions can be distinguished in the FTIR spectrum of a zeolite. In the region between 1500 cm^{-1} and 200 cm^{-1} the stretching and bending modes of the T-O-T structural units of the lattice are observed, which is the reason why signal saturation is observed in this region [9].

Desorption of pyridine is performed for different temperatures ranging from 150°C to 450°C. When the spectrum obtained before pyridine absorption is subtracted from the spectrum obtained after pyridine absorption at 150°C, the acidic and accessible Brønsted acid sites can be identified (figure 22). It is possible to evaluate the acidic strength of the Brønsted acid sites by comparing the spectra after desorption of pyridine at different temperatures. It is widely accepted that acid sites that are able to retain pyridine at higher temperature (450°C) are the stronger acid sites. The spectra after pyridine desorption can be seen in figure 23 for different desorption temperatures in the relevant vibration region. The following peaks have been identified for this specific zeolite [2, 10, 11]:

3744 cm^{-1} Silanol groups have low acidity and therefor are non-active to the cracking reactions. These groups have the lowest acidity of the identified acid sites.

3665 cm^{-1} It is suggested in previous work [11] that this band could correspond to partial framework groups that exist in defects originating from the steaming treatment. In strength these groups are higher than the silanol groups and hydroxyl groups in the sodalite- and supercages of the zeolite without interaction with EFAL, but lower than the acid groups in interaction with EFAL species. They are of so called *medium acidity*.

3622 cm^{-1} Bridging hydroxyl groups located in the supercages of the zeolite. Next to silanol groups, these bridging hydroxyls possess very low acidity as can be seen in the disappearance of the peak in the 450°C desorption spectrum.

3598 cm^{-1} Bridging hydroxyl groups located in the supercages of the zeolite, but in interaction with extra framework aluminum (EFAL) species. The hydroxyl groups in interaction with EFAL species are the stronger type of Brønsted acid sites found in this zeolite. Actually through the interactions of the hydroxyls with the Lewis acid sites created by the dealumination process, these Brønsted acid sites have previously been said to be *super acidic* [10].

3552 cm^{-1} Bridging hydroxyl groups located in the sodalite cages of the zeolite. They possess low acidity, which is comparable with the acidity from the hydroxyls located in the supercages.

3527 cm^{-1} Bridging hydroxyl groups in interaction with EFAL species, located in the sodalite cages of the zeolite. The OH groups in interaction with EFAL species are the stronger type of Brønsted acid sites found in this zeolite.

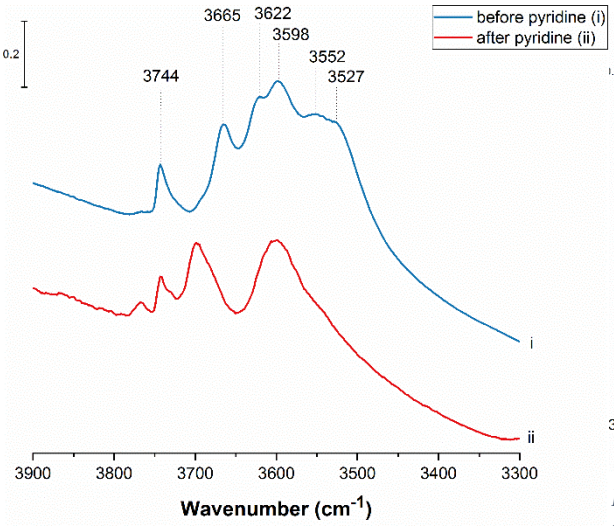

Figure 23 - Hydroxyl region of the FTIR spectra recorded before (i) and after (ii) pyridine adsorption at 150°C

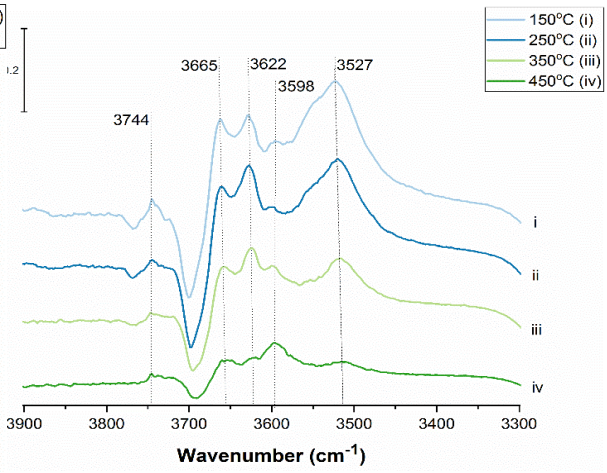

Figure 22 - Difference between the hydroxyl vibration spectrum before pyridine adsorption (150°C) and the spectra recorded after desorption at different desorption temperatures

The region of interest for the determination of Brønsted and Lewis acid site concentration lies between 1700 cm^{-1} and 1400 cm^{-1}. This region is shown on the left side of figure 24 for the FTIR spectra after desorption of pyridine at different temperatures. At 1545 cm^{-1} and 1455 cm^{-1} the adsorption bands from adsorbed pyridinium ion and pyridine can be seen, respectively. Pyridinium ions can be related to pyridine adsorbed onto Brønsted acid sites (1545 cm^{-1}), while the band at 1455 cm^{-1} can be related to the adsorption of pyridine onto Lewis acid sites. The area of these bands are proportional to the concentrations of the corresponding acid sites through the Lambert-Beer law. The band at 1630 cm^{-1} is related to pyridinium ions adsorbed to Brønsted acid sites while the band at 1620 cm^{-1} is related to the adsorption of pyridine to Lewis acid sites. Finally, the band at 1490 cm^{-1} is not related to one specific acid site, but is proportional to both Brønsted and Lewis acid sites [7].

The concentration of Brønsted and Lewis acid sites as a function of desorption temperature is shown on the right side of figure 24. In previous research [2] the concentration of all framework Al atoms was determined for this specific zeolite (2913 µmol/gr) and this value is much higher than the experimentally obtained amount of Brønsted acid sites after pyridine desorption at 150°C (816 µmol/gr). It can be concluded that there exist Al-O-Si groups that do not serve as Brønsted acid sites able to retain pyridine at 150°C. Another explanation could be the change of framework Al species to EFAL species due to dealumination.

The high amount of Lewis acid sites (442 µmol/gr) is related to the fact that CBV500 is an ultra-stable Y zeolite that has undergone steaming and dealumination. The aluminum atoms extracted from the framework during this treatment can stay in the zeolite structure as EFAL species, which makes them potential Lewis type acid sites [12].

Acid sites that are able to retain pyridine at 450°C are considered strong acid sites. From the evolution of acid site concentration for increasing desorption temperature, it can be seen that the Lewis

acid sites are stronger than the Brønsted acid sites. At 450°C only 16.2% (132 µmol/gr) of the Brønsted acid sites were able to retain pyridine, while this is the case for 37.6% (166 µmol/gr) of Lewis acid sites.

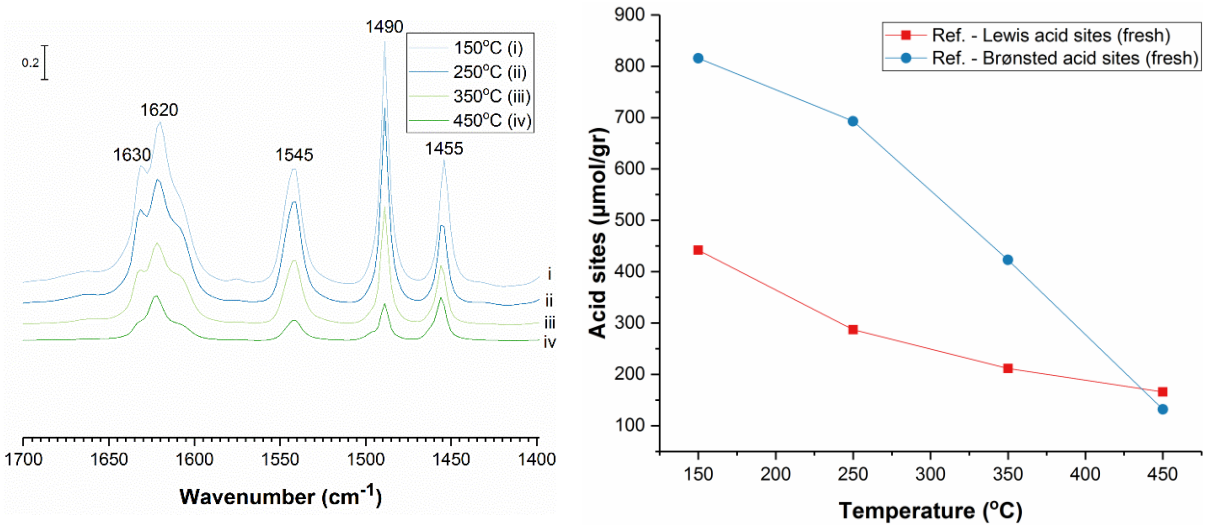

Figure 24 - Difference between the spectrum recorded before pyridine adsorption and spectra recorded after desorption (left) and calculated Brønsted and Lewis acid site concentration for increasing desorption temperatures

4.2.2. n-Heptane conversion

4.2.2.1. Deactivation

Conversion of n-heptane over CBV500 was evaluated at 450°C according to the procedure described in the experimental section. At increasing times on stream (TOS) the effluent was analyzed to evaluate the n-heptane conversion, deactivation of the catalyst and the characteristics of the cracking products obtained. Figure 25 shows the n-heptane conversion as a function of time on stream. For the fresh catalyst (1.5 min of TOS), 53.2% of n-heptane was transformed. This value decreases significantly between 1.5 – 10 min of TOS, with the residual activity being only 48.9% of the initial activity after 10 min of TOS (26.1% n-heptane conversion). This is probably due to a higher rate of coke formation, and therefore a more pronounced decrease in acid site concentration, at the beginning of the reaction. After 10 min of TOS the deactivation continues, but at a slower rate. At 60 min of TOS only 12.4% of n-heptane is transformed, which corresponds to a residual activity of 23.3% compared to the initial activity at 1.5 min of TOS.

The n-heptane cracking reaction is not the only reaction that takes place in the zeolite. Several other secondary reactions that lead to aromatics and coke formation can occur during transformation over acidic zeolites, such as hydrogen transfer, oligomerization and cyclization. In previous research [2], a direct correlation was found between the amount of coke retained inside the zeolite pores and the deactivation of CBV500. The carbon content after pure n-heptane cracking can be seen in table 7 and it

seems that deactivation increases with increasing coke formation. Although in the current work carbon analysis was only done on two samples at 1.5 min of TOS and 60 min of TOS, it can be seen from previous works that the observed trend is valid and the amount of deposited coke inside the zeolite increases with increasing TOS and decreasing activity [2].

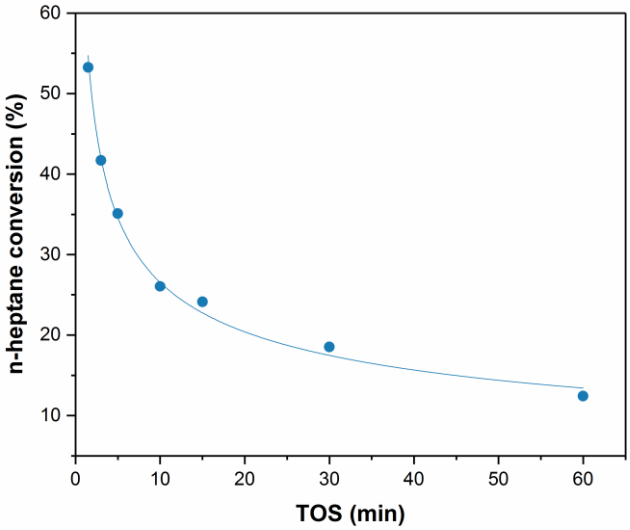

Figure 25 - Conversion of n-heptane over CBV500 as a function of TOS

Table 7 - Carbon content inside the zeolite after pure n-heptane cracking for 1.5 and 60 min of TOS

TOS	
1.5 min	***60 min***
1.7%	9.4%

Lewis and Brønsted acid site concentration in the zeolite after 1.5 min of TOS pure n-heptane cracking reaction can be seen in table 8. Both Lewis and Brønsted acid site concentration decreases with 24% and 18%, respectively, as compared to the concentrations for fresh CBV500. The decrease in both types of acid sites can be related to the increase in carbon content, i.e. an increase in adsorbed coke molecules on acid sites, which was observed after 1.5 min of TOS.

Table 8 - Lewis and Brønsted acid site concentration of CBV500 after 1.5 min of TOS pure n-heptane cracking reaction

	Lewis acid site concentration (µmol/gr)	**Brønsted acid site concentration (µmol/gr)**
	CBV500	*CBV500*
fresh	442	816
pure n-heptane	335	672
	-24%	-18%

The results from nitrogen absorption experiments are shown in figure 26 for fresh CBV500 and CBV500 after 1.5 min of TOS of the pure n-heptane cracking reaction. It can clearly be seen that very soon in the cracking reaction after 1.5 minutes, a significant decrease is observed in microporous volume (12.6%). This is an indication that the coke molecules, that are deposited in the zeolite structure, are poisoning the acid active sites located in the pores of the zeolite. This is probably the most important reason for the more pronounced deactivation with increasing TOS. A small decrease in mesoporous volume and external surface area can also be observed, but this is not significant taking into account the error associated with the measurement. From this it can be concluded that the coke is mostly located in the micropores of the zeolite.

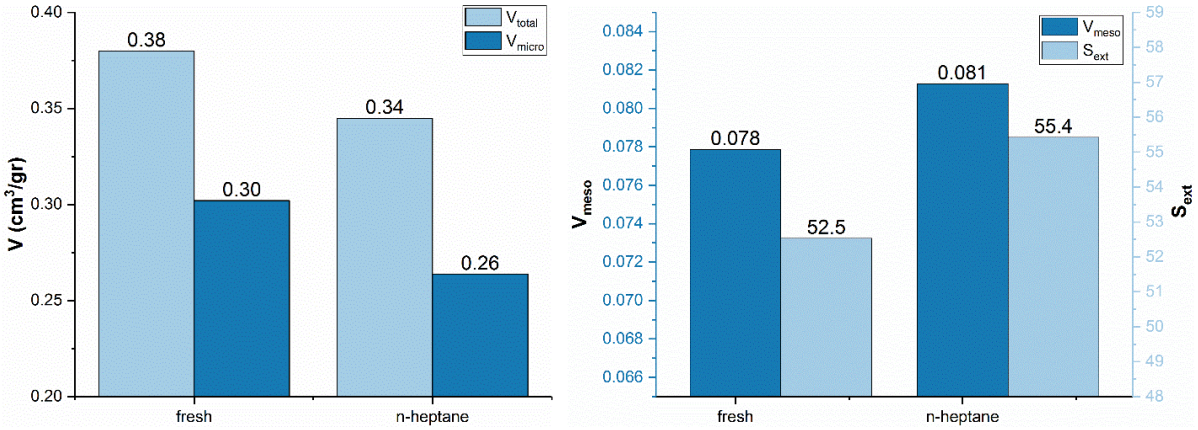

Figure 26 - Total pore volume and microporous volume (left), mesoporous volume and external surface area (right) for fresh CBV500 and CBV500 after 1.5 min of TOS n-heptane cracking

4.2.2.2. Product distribution

For this section and the sections on product distribution yet to come, there will be a distinction between fresh catalyst (1.5 min of TOS) and deactivated catalyst for which the evolution of product distribution with TOS will be discussed. The products from the reaction effluent that were identified can be seen in table 9.

4.2.2.2.1. Fresh catalyst

Catalytic tests with varying contact times have been performed to obtain the product distribution at iso-conversion for the main product groups, i.e. isomers, cracking products and aromatics for the reaction at 1.5 min of TOS. From the trend in this data the selectivity of the different products in the effluent could be interpolated and an n-heptane conversion of 35% is used for all data concerning product distribution. In figure 27 (left) the selectivity of the main product groups are illustrated for fresh CBV500 at 450°C.

Table 9 - Identified products from the main product groups, i.e. cracking products, C_7 isomers and aromatics

Cracking products		C_7-isomers	Aromatics
Paraffins	*Olefins*		
C_1	C_3=	*i-C_7*	*toluene*
C_2	C_4=		*m,p-xylene*
C_3	C_5=		*o-xylene*
i-C_4	C_6=		
n-C_4			
i-C_5			
n-C_5			
C_6			

It can be seen that the main desorbed products are the ones that result from the cracking reaction of n-heptane (96.0%). As discussed in the cracking scheme at the start of this chapter, it can be expected to have some C_7 isomers in the effluent due to the isomerization step preceding the cracking reaction. However, this cannot be seen in the data, in which the C_7 isomers show 0% selectivity. The C_7 isomer selectivity is in agreement with previous research for which the C_7 isomer selectivity was also very low to non-existent [2]. It was suggested that the n-heptane isomers are not easily desorbed and are subject to cracking reactions, since they are more reactive then the reactant n-heptane. The aromatics show a selectivity of 4.0%.

In figure 27 (right) and 28 the cracking products selectivity can be seen in more detail for paraffins and olefins, respectively. The data is also presented in table 1 in annex 2. It can be seen that the selectivity of C_3 and i-C_4 is relatively high, which is an indication of the prevalence towards the classical β-scission cracking mechanism. The relatively low amounts of methane and ethane indicate the minor importance of the protolytic cracking mechanism, which can have different origins: i) less energy is associated with the formation of n-heptyl ions by hydride transfer as a result of the β-scission cracking reaction as compared to the energy needed to initiate protolytic cracking and ii) with increasing pore dimensions the relative contribution of the monomolecular protolytic cracking route decreases as compared to the bimolecular classical route [13]. The transition state complex of the intermediate in the β-scission route is larger than those of the intermediate involved in the protolytic cracking reaction. C_5 and C_6 species can be found in the effluent, but these molecules are not products of the direct cracking reaction. I. Graça [2] suggests an oligocracking mechanism, which is present at a low extent.

The high amounts of iso-paraffin relative to the amount of n-paraffin (for C_4 and C_5) can be explained by the existence of isomerization before the scission reaction. Iso-paraffins are created from a more stable tertiary carbenium ions as compared to n-paraffin, which are formed from a less stable secondary carbenium ion.

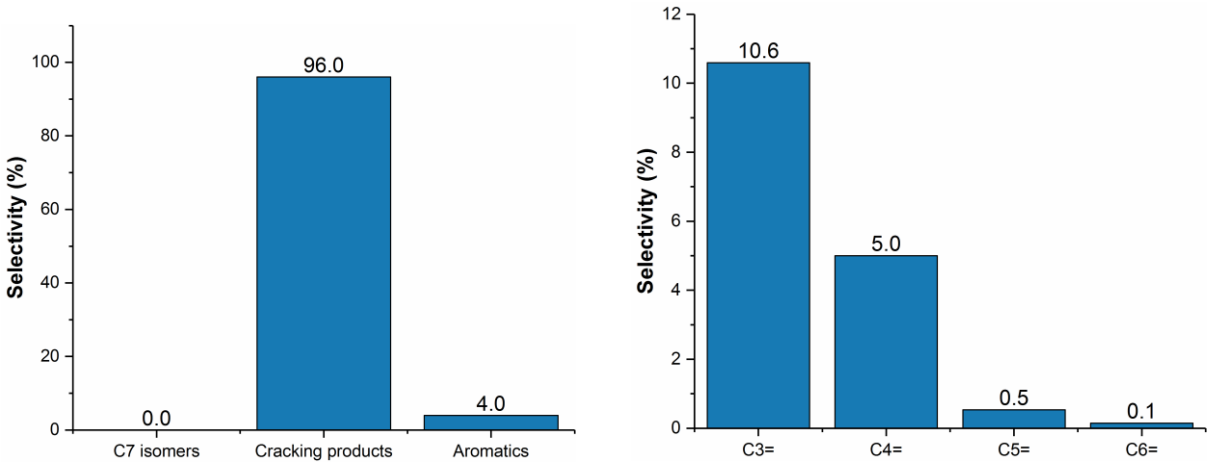

Figure 27 - Product group selectivity (left) and olefin cracking products selectivity (right) at 35% n-heptane conversion over fresh CBV500 (1.5 min of TOS)

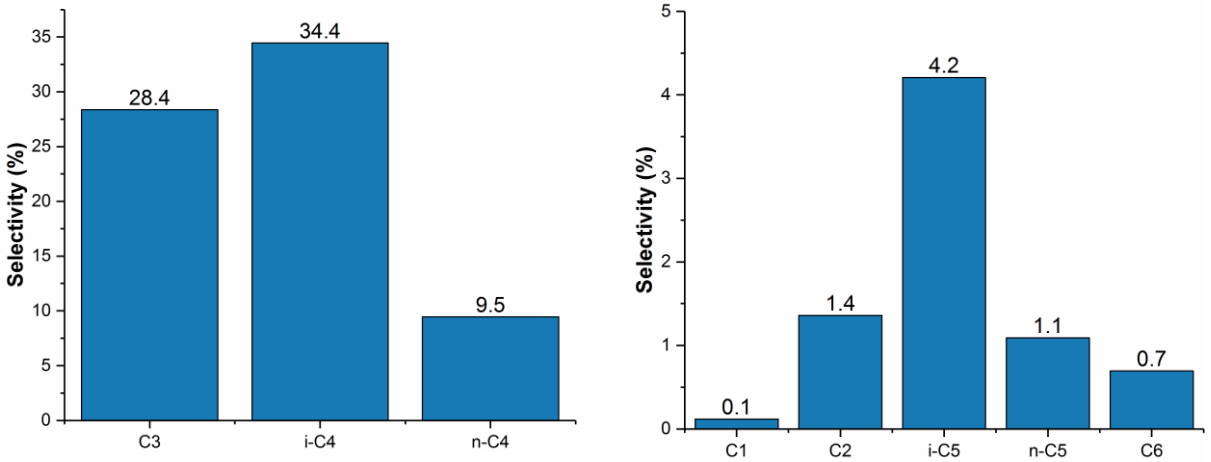

Figure 28 – Paraffin cracking products selectivity at 35% n-heptane conversion over fresh CBV500 (1.5 min of TOS) at 450°C

From the olefin product distribution it can be seen that the amount of paraffin products is much higher than the amount of olefin products. The main reason for this is the existence of secondary processes that consume olefins, such as hydrogen transfer reactions and/or reactions that produce coke. The smaller amount of butene compared to propene is due to the higher reactivity of butene compared to propene. Stable tertiary carbenium ions are associated with butene, while less stable secondary carbenium ions are associated with propene [2].

4.2.2.2.2. Deactivated catalyst

Coke is deposited inside the zeolite structure during the cracking reaction, which results in acid site poisoning and pore blocking. This phenomenon results in a decrease of active acid sites, can influence the mobility of reactants and products and can effect the preponderance of certain reactions. The consequences from the deposition of coke could therefore influence the selectivity of the catalyst. Figure 29 shows the paraffin/olefin ratio and the i-paraffin/n-paraffin ratio of the products from the cracking reaction as a function of time on stream.

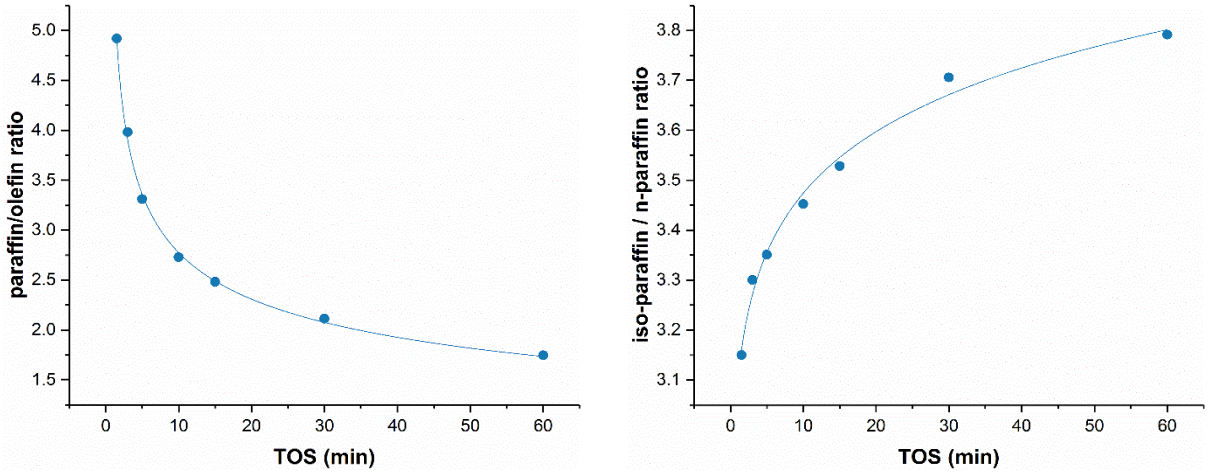

Figure 29 - Paraffin/olefin ratio (left) and iso-paraffin/n-paraffin ratio (right) of the cracking products as a function of TOS for CBV500

A trend can be observed for both the paraffin/olefin ratio and i-paraffin/n-paraffin ratio. The paraffin/olefin ratio shows a high decrease from 1.5 min of TOS until 10 min of TOS, and a more gentle decrease from 10 min of TOS until 60 min of TOS. There seems to be a direct correlation between the amount of coke deposited inside the zeolite, the resulting decrease of acid site concentration the paraffin/olefin ratio. Hydrogen transfer reactions are unfavored by the lowering of the acid site density [2, 14] and this results in a decrease in paraffin/olefin ratio, since olefins act as reactants in this type of reaction.

A direct correlation between iso-paraffin/n-paraffin ratio, coke deposition and acid site concentration also seems to exist. This can be explained by a difference in deactivation effect of coke on the various elementary reaction steps [15]. It was seen that the deactivation effect increases from β-scission reactions where tertiary carbenium ions are involved to β-scission reactions in which secondary carbenium ions are involved, which results in an increased selectivity for iso-paraffins as compared to n-paraffins.

4.2.3. n-Heptane conversion – Influence of guaiacol poisoning

4.2.3.1. Deactivation

In order to evaluate the poisoning effect of the oxygenated compound guaiacol, the cracking of n-heptane over CBV500 was also performed in presence of 1.2wt% guaiacol. In this section the activity and product selectivity of CBV500 will be analyzed with the introduction of guaiacol to the reaction mixture.

n-Heptane conversion as a function of time on stream (TOS) is shown in the left side of figure 30. The residual activity, i.e. the conversion at *t* min of TOS with or without 1.2% guaiacol as compared to the initial conversion for pure n-heptane conversion at 1.5 min of TOS (equation 11), can be seen on the right side of figure 30.

$$Residual\ Activity\ = \frac{X(t)}{X_{nhp}\ (1.5\ \text{min})} * 100$$

(Eq. 11)

X (t) - Conversion of n-heptane with or without guaiacol at t min of TOS

X_{nhp} (1.5 min) - Conversion of pure n-heptane at 1.5 min of TOS

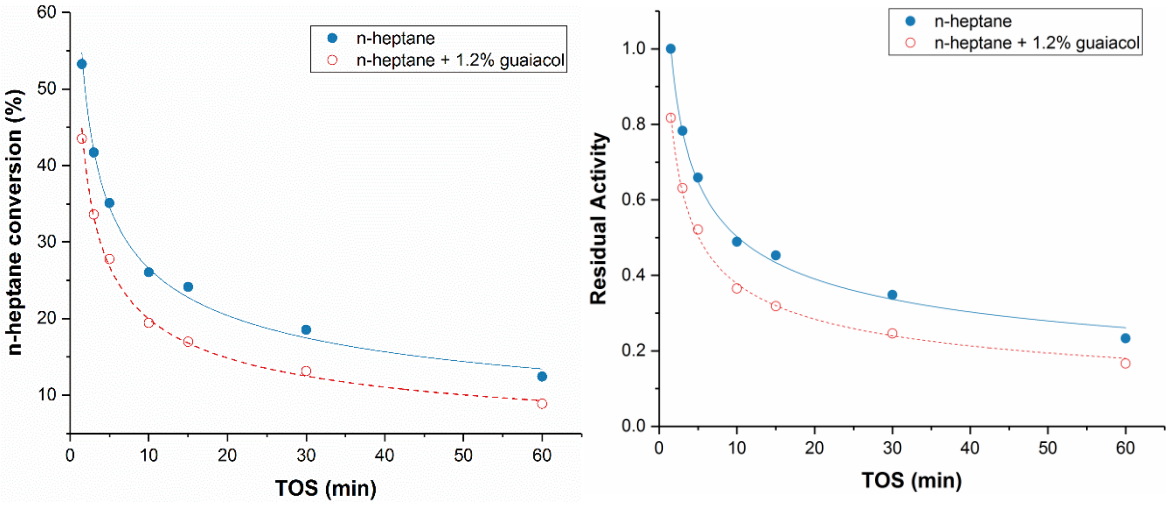

Figure 30 – Conversion of n-heptane (left) and residual activity (right) for n-heptane conversion with and without 1.2% guaiacol added to the reaction mixture

It can be seen that the small amount of 1.2% guaiacol leads to a higher deactivation of the catalyst. Already from the beginning of the reaction (1.5 min of TOS) the deactivation is more pronounced with the introduction of guaiacol, which results in an n-heptane conversion of 43.5% compared to the 53.2% in case of pure n-heptane. The deactivation also goes on to a higher extent as can be seen at 60 min of TOS. Only 16.6% of the initial activity is remained in the case of guaiacol addition, while this is 23.3% in the case of pure n-heptane. Since the deactivation of the catalyst is more pronounced when introducing guaiacol, it can be assumed that this is caused by a reduction in both Lewis and Brønsted acid site concentration. This reduction could be a result of an increase in coke formation and therefore increased poisoning of the active acid sites by adsorbed coke molecules. Another explanation could be poisoning of the acid sites by guaiacol.

The observed deactivation is consistent with the results seen in previous research [2]. It was noticed that for this temperature (450°C), an increase of guaiacol addition from 1.2% to 4% did not contribute to an enhancement of the zeolite deactivation. It was concluded that with 1.2% guaiacol injected, a maximum in the deactivating effect of guaiacol was already achieved. This is due to the saturating effect of guaiacol on the acid sites that is already achieved when injecting 1.2% guaiacol with n-heptane cracking.

Carbon content on CBV500 after n-heptane cracking with and without guaiacol can be seen in table 10 for 1.5 and 60 min of TOS. It can be seen that no increase in coke formation is observed after 1.5 min of TOS when the reaction with and without guaiacol are compared. However, it is believed that this decrease is partly the result of an increase in coke formation. The uncertainty in the experimental technique for determining carbon content can be the reason for the inconsistency. There is a higher decrease in Lewis and Brønsted acid site concentration in presence of guaiacol as compared to the decrease observed for pure n-heptane cracking (figure 31). It seems plausible that the decrease in activity is also partly the result of guaiacol poisoning of the active acid sites of the zeolite.

Table 10 - Carbon content deposited on the zeolite after n-heptane cracking with and without 1.2% guaiacol for 1.5 and 60 min of TOS

	TOS	
	1.5 min	***60 min***
pure n-heptane	1.7%	9.4%
n-heptane + 1.2% guaiacol	1.6%	10.4%

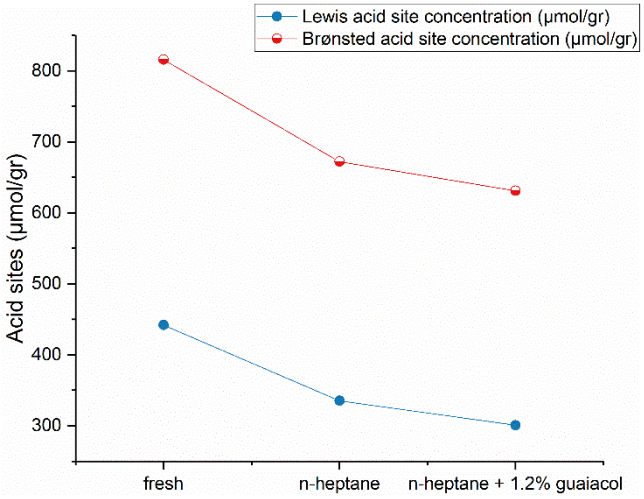

Figure 31 - Lewis and Brønsted acid site concentration after 1.5 min of TOS n-heptane cracking with and without guaiacol

The data obtained by nitrogen absorption is shown in figure 32 for fresh CBV500 and coked samples at 1.5 min of TOS. As noted earlier, a decrease in microporous volume can be seen for the coked sample after 1.5 min of TOS cracking reaction with pure n-heptane. When introducing guaiacol to the reaction mixture, the decrease in microporous volume (left diagram) is similar to the decrease observed for pure n-heptane cracking. This is in accordance with the carbon content of the zeolite after 1.5 min of TOS cracking reaction, for which also no significant change could be seen when comparing the cracking reaction with and without guaiacol. Mesoporous volume and external surface area (right diagram) are also similar for cracking with and without guaiacol in the reaction mixture.

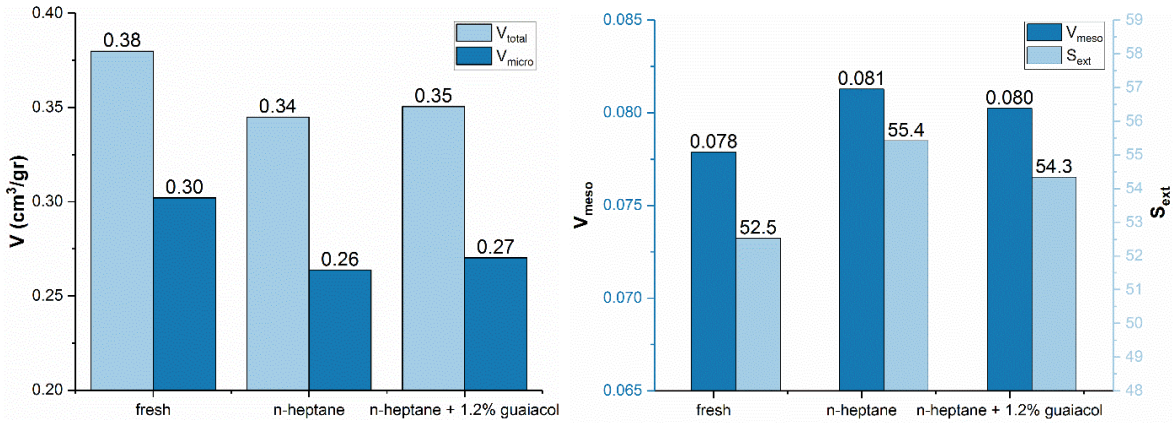

Figure 32 - Total pore volume and microporous volume (left), mesoporous volume and external surface area (right) for fresh CBV500 and coked CBV500 at 1.5 min of TOS

4.2.3.2. Product distribution

4.2.3.2.1. Fresh catalyst

Selectivity of the main product groups can be seen in figure 33 (left), while more detailed paraffin and olefin selectivity is shown in figure 33 (right) and 34, for cracking of n-heptane with and without guaiacol. The data is also presented in table 1 in annex 2. It is interesting to notice that no significant change can be detected in the product distribution and product group selectivity.

Iso-paraffin / n-paraffin ratio and paraffin / olefin ratio at iso-conversion (35% n-heptane conversion) for pure n-heptane cracking and n-heptane cracking in presence of guaiacol can be seen in figure 35. For the fresh catalyst at 1.5 min of TOS, both ratios do not seems to change when guaiacol is added to the reaction mixture.

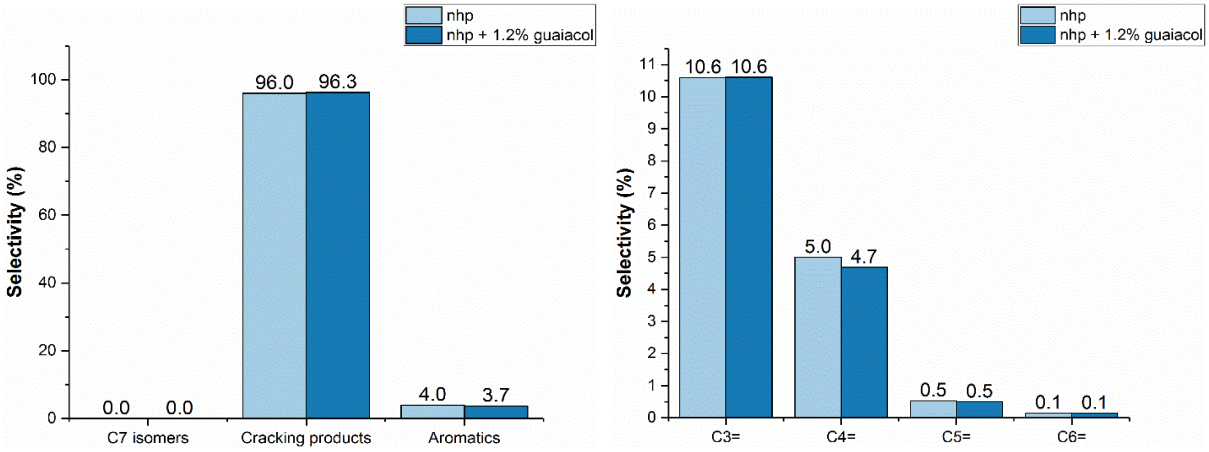

Figure 33 - Product group selectivity (left) and olefin cracking products selectivity (right) at 35% n-heptane conversion for cracking of n-heptane with and without guaiacol at 1.5 min of TOS

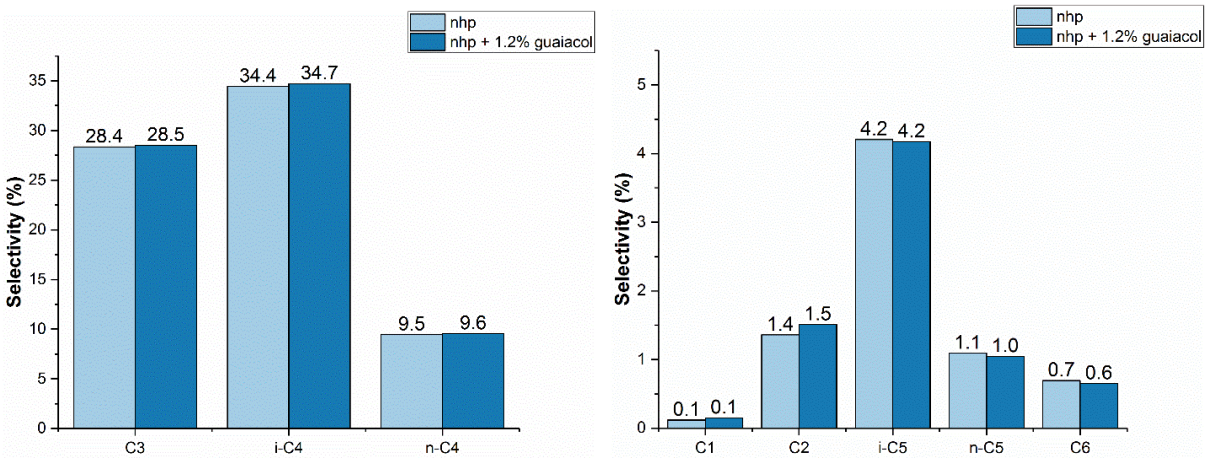

Figure 34 - Paraffin cracking products selectivity at 35% n-heptane conversion for n-heptane conversion with and without guaiacol at 1.5 min of TOS

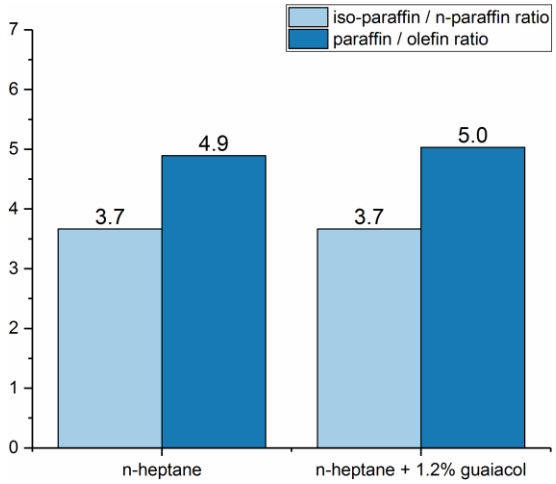

Figure 35 - i-paraffin/n-paraffin ratio and paraffin/olefin ratio at 35% n-heptane conversion over CBV500 (1.5 min of TOS) at 450oC for pure n-heptane conversion and in presence of guaiacol

4.2.3.2.2. Deactivated catalyst

Figure 36 compares the paraffin / olefin ratio (left) and iso-paraffin / n-paraffin ratio (right) as a function of TOS for products from pure n-heptane conversion and those from n-heptane with guaiacol conversion. For the obtained results, an increase can be seen in iso-paraffin / n-paraffin ratio, that is more pronounced with increasing TOS. From the available data, it can be concluded that an increase of the iso-paraffin/n-paraffin ratio is mainly due to an increase of C_4 iso-paraffin selectivity, which is the result of an increase in space available for diffusion. Adsorption of bulky coke molecules onto the acid sites inside the zeolite decreases the available space and induces steric constraints for branched molecules. When

added to the reaction mixture, guaiacol can adsorb to acid sites instead of coke molecules, which will create an open space between coke molecules, allowing easy diffusion for the branched paraffins. This effect can be more pronounced when more bulky coke molecules are formed at longer times on stream. The bulkier the coke that is exchanged by guaiacol, the higher the relative increase in space available for diffusion.

A decrease in olefins, rather than an increase in paraffins, is the reason for the observed increase in paraffin/olefin ratio. A small decrease in propene, butene and pentene selectivity can be seen with the introduction of guaiacol, but the paraffin selectivities don't change significantly. This leads to the conclusion that the increase of this ratio is likely not a result of an improvement in hydrogen transfer reactions.

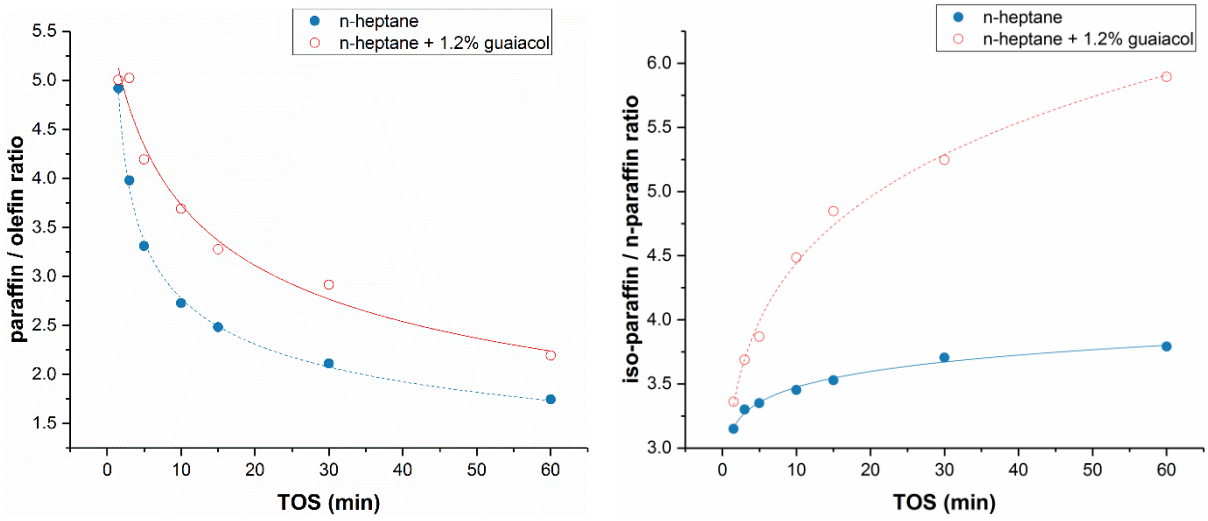

Figure 36 - Paraffin/olefin ratio (left) and iso-paraffin/n-paraffin ratio (right) of the cracking products as a function of TOS for CBV500 in the case of pure n-heptane cracking and in presence of guaiacol

4.3. Nickel and Vanadium impregnated CBV500

4.3.1. Characterization of Ni and V impregnated CBV500

CBV500 was delivered by *Zeolyst* in the ammonium form, which makes it very suitable for post-synthesis modifications like metal impregnation or ion exchange [3].

To determine the type of nickel and vanadium species (metallic, cationic or oxides) after impregnation, UV-vis spectroscopy was performed on the fresh CBV500 and metal impregnated samples. The spectra can be seen in figure 37. For nickel a band at 390nm and a doublet with maxima around 650nm and 720nm can be seen. According to Petranovskii et al. [16], this is a typical spectra of $Ni(H_2O)_6^{2+}$

species. Nickel exist in CBV500 after impregnation partly in a hydrated cationic form. Another peak can also be observed at ca. 250nm, which would correspond to the presence of NiO species. For vanadium the bands are less pronounced and seem to be overlapping. Two bands that increase in intensity with increasing vanadium content can be distinguished at ca. 240nm and 410nm. The band at 240nm can be ascribed to tetrahedral coordinated species that form vanadium monomer and oligomer, while the band at 410nm can be ascribed to octahedral coordinated species that form vanadium oligomers [17]. For both nickel and vanadium the intensity of the bands increase with increasing metal content.

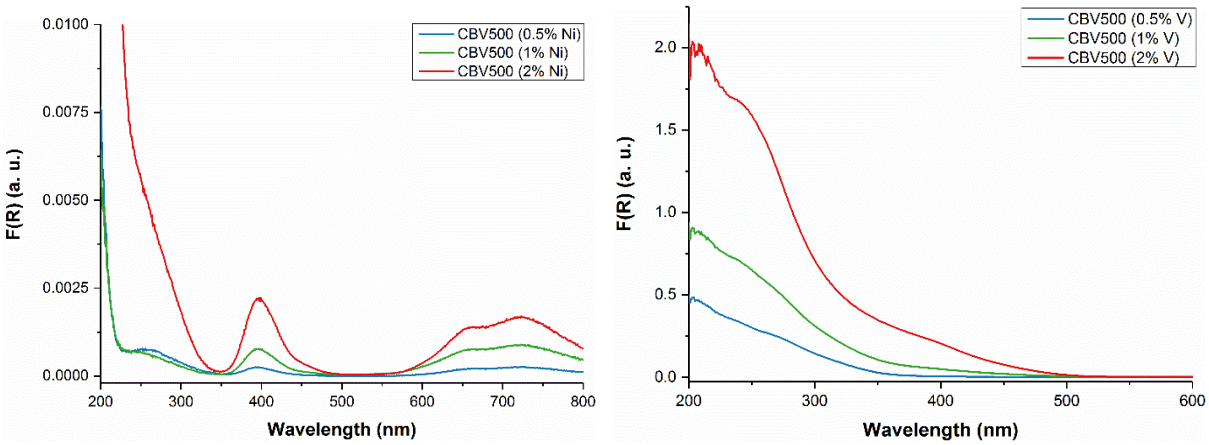

Figure 37 – Diffuse reflectance UV-vis spectra for increasing amounts of nickel (left) and vanadium (right) impregnated samples

The results from XRD measurements of fresh CBV500 and metal impregnated samples can be seen in figure 5 and 6 of annex 3. When looking at the XRD data it is interesting to analyze the difference in intensity between the peaks seen for nickel and vanadium impregnated zeolites as compared to those for the fresh CBV500. A decrease in intensity for peaks at the same 2θ values could indicate a decrease in crystallinity. A decrease in intensity is not observed and crystallinity did not change significantly when impregnating CBV500 with varying amounts of nickel and vanadium.

Microporous volume, mesoporous volume, total volume and external surface area were obtained from nitrogen adsorption experiments and the results can be seen in figure 38. The microporous volume (left diagram) of the CBV500 impregnated with nickel or vanadium is more or less the same compared to the CBV500 without any metal impregnation. A small decrease in the mesoporous volume and external surface area (right diagram) can be seen for nickel and 0.5% vanadium impregnated samples and a more pronounced decrease can be seen for 2% vanadium impregnated samples. This indicates that the metal is enriched on the external surface layer of the zeolite crystallite and to a minor extent in the mesopores of the zeolite. It was suggested that the presence of non-framework metallic cations in the pores of the zeolite, such as EFAL species, can complicate the migration of nickel from the external surface to the internal surface [18]. The higher decrease observed for 2% vanadium samples could be the result of an increasing size of vanadium particle size, as compared to that of nickel particles.

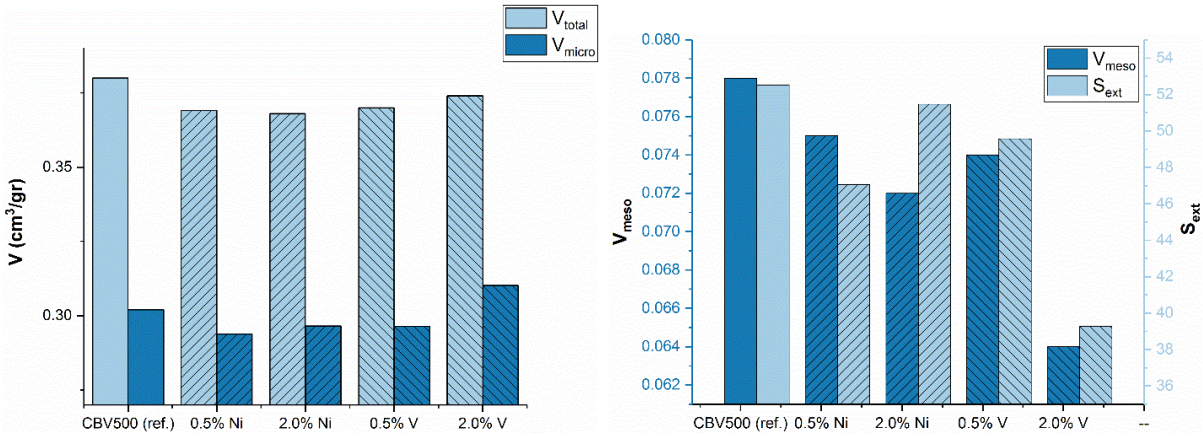

Figure 38 - Total pore volume and microporous volume (left), mesoporous volume and external surface area (right) for fresh CBV500 and fresh CBV500 impregnated with increasing amounts of Ni and V

The hydroxyl vibration region of the FTIR spectrum before pyridine adsorption is shown in figure 39 for nickel and vanadium impregnated samples. All spectra are corrected to 10mg to make sure the comparison is accurate. The intensity of the peaks are very similar, except for the silanol hydroxyl groups (3744cm^{-1}) of vanadium that show a small decrease. This is not very relevant, since the silanol groups possess very low acidity and are therefore have minor relevance in the cracking reaction. Another interesting observation is the new peak that can be observed at 3686cm^{-1} for nickel. Earlier research showed that this band can be assigned to a metal hydroxyl species [19] and therefore it is concluded that this band in the present work can be assigned to hydroxylated nickel species.

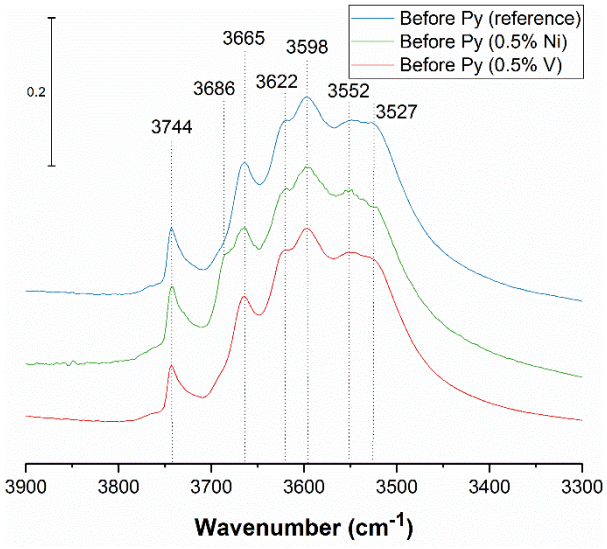

Figure 39 - Hydroxyl vibration spectrum recorded before pyridine adsorption for CBV500 with and without impregnated metal, corrected for 10mg sample weight

Lewis and Brønsted acid site concentration are illustrated in figure 40 for 0.5% nickel and 0.5% vanadium impregnated CBV500, together with the data obtained from the reference sample for comparison. It is interesting to analyze the acid sites concentration and strength for the metal impregnated fresh samples, since the stronger acid sites are important for the initiation step of the cracking mechanism (section 4.1) and all acid sites participate in the cracking reaction. Changes in the acid site distribution, concentration and strength can influence the activity and product selectivity of the catalyst under study.

For 0.5% nickel impregnated CBV500 the number of Lewis acid sites that were able to retain pyridine at 150°C have increased with 54.4% from 441.9 µmol/gr for the reference sample to 682.4 µmol/gr for the nickel impregnated sample. This significant increase is due to the introduced nickel particles that can act as Lewis acid sites [20]. From the evolution of the acid site concentration with increasing temperature, it can be concluded that the strength of these Lewis acid sites is low. At 450°C most of the 'new' Lewis acid sites were not able to retain pyridine and a relative small increase of 9.7% can be seen for the Lewis acid site concentration for the nickel impregnated sample (182.1 µmol/gr) as compared to the reference sample (166.0 µmol/gr).

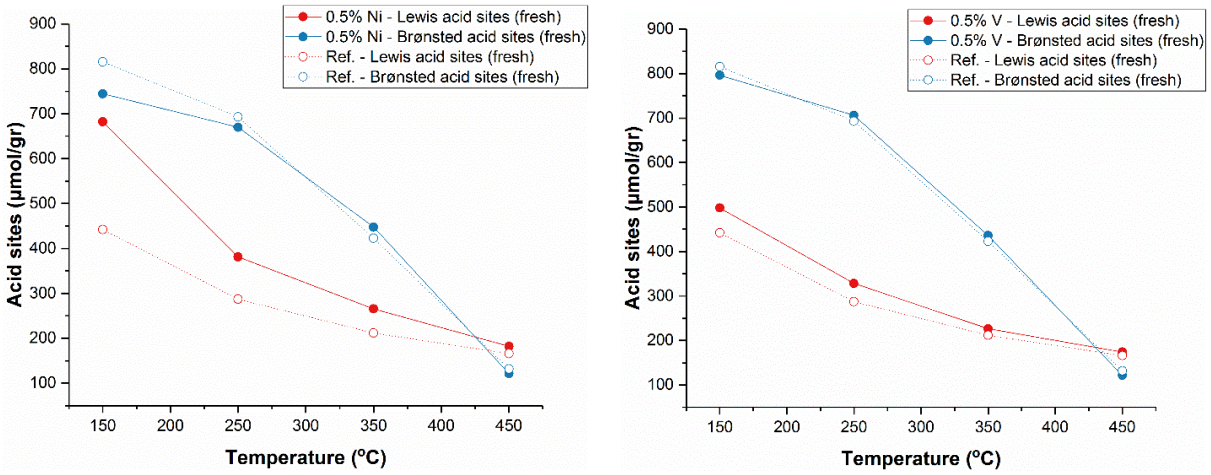

Figure 40 - Lewis and Brønsted acid site concentration for 0.5% nickel (left) and 0.5% vanadium (right) impregnated CBV500

Brønsted acid sites that are able to retain pyridine at 150°C have decreased with 8.7% from 815.6 µmol/gr for the reference sample to 744.3 µmol/gr for the nickel impregnated sample. From the evolution of the Brønsted acid site concentration with increasing temperature, it can be seen that mostly weak Brønsted acid sites are responsible for this decrease. The number of Brønsted acid sites that are able to retain pyridine at 250°C and 350°C are almost the same and at 450°C only a decrease from 131.9 µmol/gr for the reference sample to 121.5 µmol/gr for the nickel impregnated sample could be observed. As could be seen from the UV-vis spectra, the nickel appears after impregnation as hydrated Ni^{2+} species (cationic). Part of the nickel could have existed as the weak basic oxide NiO, before the reaction with a stronger

Brønsted acid site to produce water (equation 12) [37]. One explanation for the observed decrease in strong Brønsted acidity could be the reaction between NiO and stronger Brønsted acid sites. Another plausible explanation would be the replacement of protons by Ni^{2+} by ion exchange, which also reduces the Brønsted acidity.

$$NiO + 2H^+ \rightarrow Ni^{2+} + H_2O \qquad \text{(Eq. 12)}$$

In the case of 0.5% vanadium impregnation the same trend can be seen but to a lesser extent. At 150°C the concentration of Lewis acid sites that are able to retain pyridine is 497.8 µmol/gr, which is an increase of 12.6% compared to the reference sample (441.9 µmol/gr). The amount of strong Lewis acid sites (174.0 µmol/gr), the ones that are able to retain pyridine at 450°C, is very similar to the Lewis acid site concentration of the reference sample (166.0 µmol/gr).

Brønsted acid site concentration for the vanadium impregnated sample is very similar to the concentration of Brønsted acid sites from the reference sample at all desorption temperatures.

4.3.2. n-Heptane conversion

4.3.2.1. Deactivation

Pure n-heptane conversion as a function of time on stream for CBV500 impregnated with 0.5%, 1% and 2% nickel and vanadium can be seen in figure 41. The deactivation data from reference CBV500 is added to the graphs for comparison.

From the data it becomes clear that the activity of the Y-zeolite is decreasing with increasing metal content. This is true for both nickel and vanadium impregnated samples and the result is in agreement with conversion values obtained in previous research [21, 22].

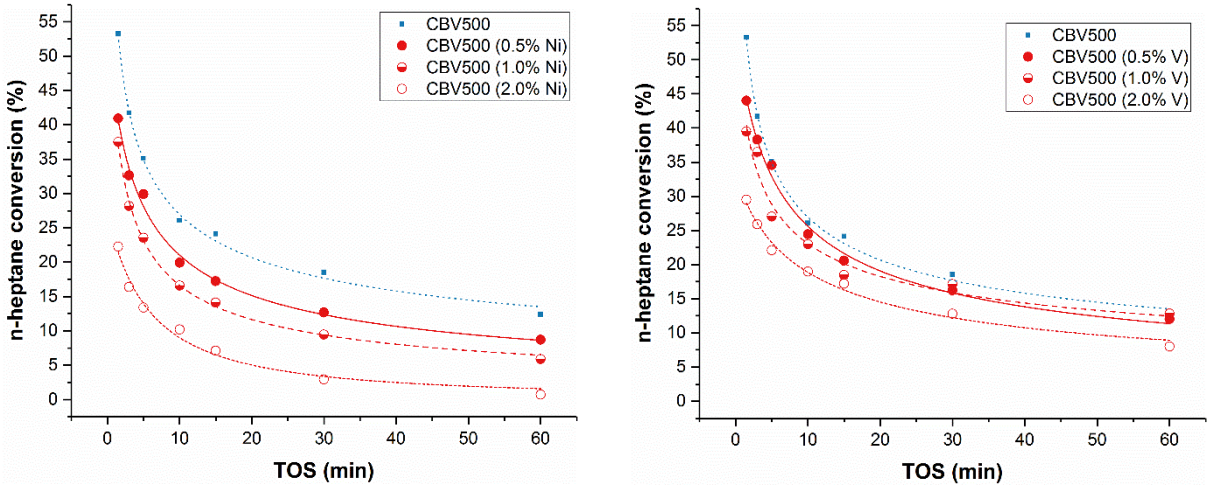

Figure 41 - Conversion of n-heptane for reference CBV500 and 0.5%, 1% and 2% nickel (left) and vanadium (right) impregnated samples as a function of time on stream

For nickel impregnated samples this result is very well illustrated and for every measurement from 1.5 – 60 min of TOS a clear decrease of n-heptane conversion can be seen with increasing nickel content. For vanadium impregnated samples the graph clearly shows a decrease in n-heptane conversion with increasing vanadium content early in the reaction (1.5 – 15 min of TOS). For longer times on stream the n-heptane conversion seems to be very similar for the reference sample and for samples impregnated with 0.5% and 1% vanadium. For 2% vanadium, the decrease in n-heptane conversion is more pronounced.

It would be preferential to rearrange and simplify the data to give a clear view on the correlation between metal content and n-heptane conversion. This is especially the case for the data obtained from the vanadium impregnated samples, since the curves are closer together, thus making it difficult to draw conclusions. In figure 42, the n-heptane conversion can be observed as a function of metal content for 1.5 and 60 min of TOS.

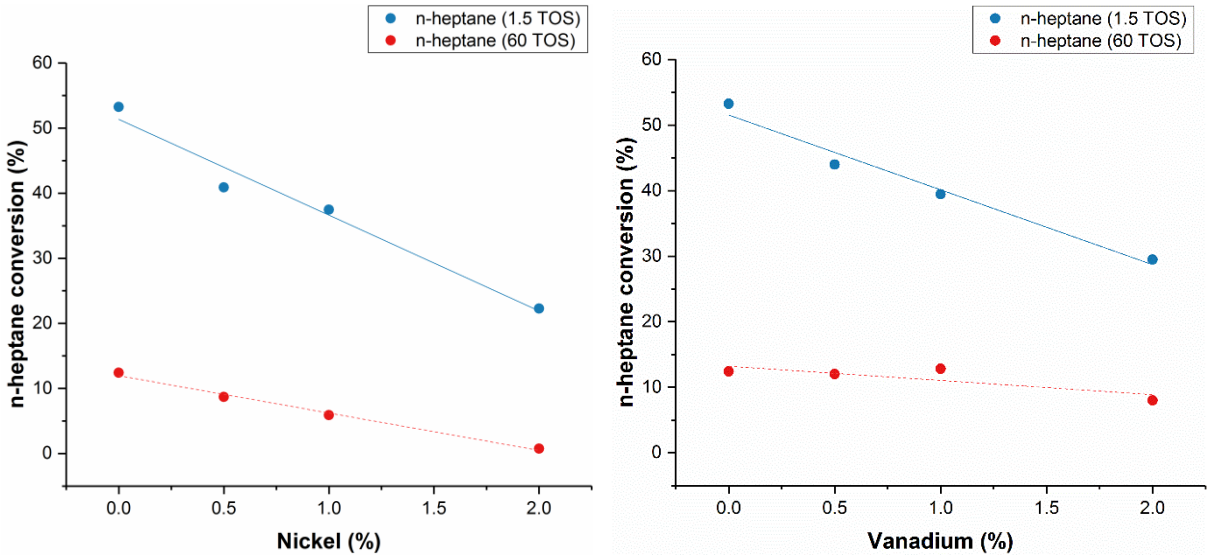

Figure 42 – Pure n-heptane conversion as a function of nickel (left) and vanadium (right) content for 1.5 and 60 min of TOS

In figure 42 it is easy to see the correlation between metal content and initial activity, which decreases for both nickel and vanadium with increasing metal content. When comparing equal metal loading, nickel has a more deactivating effect compared to vanadium. At 1.5 min of TOS and 2% metal loading, the fresh n-heptane conversion values are 29.5% and 22.3% for vanadium and nickel, respectively. The main reason for this would be a difference in the deactivating effect of nickel and vanadium. Nickel has an inductive effect on the dehydrogenation reactions, with an increase in coke, and therefore a decrease in activity as the result. For the deactivated catalyst at 60 min of TOS, n-heptane conversion decreases significant with increasing nickel content and the deactivation of the catalyst proceeds to a greater extent as compared to vanadium. In the case of vanadium impregnated samples,

the n-heptane conversion at 60 min of TOS seems to be very similar and relatively high compared to n-heptane conversion for equal amounts of nickel. The biggest difference between the metals can be seen for 60 min of TOS with 2% metal loading, which have n-heptane conversion values of 8.0% and 0.7% for vanadium and nickel, respectively.

In previous research it was seen that vanadium can have a detrimental effect as soon as its concentration is greater than 0.5% and steaming treatment is performed on the catalyst [22]. Similar results have not been observed in the current research, which signifies that introducing vanadium before steaming treatment induces a complete different result as compared to introducing vanadium in absence of a steaming treatment. The effect of steaming was explained in section 2.5.1 (literature review).

A small part of the deactivating effect of nickel can be the result of its weak acidic nature. Through coverage of original moderate acidic sites possessed by the zeolite, nickel can act as a poison for some acid sites of the zeolite [20, 21].

Table 11 - Carbon content deposited on the zeolite after pure n-heptane cracking over reference sample and CBV500 impregnated with increasing metal content, at 1.5 and 60 min of TOS

	TOS	
	1.5 min	***60 min***
CBV500	1.7%	9.4%
CBV500 (0.5% Ni)	1.8%	10.6%
CBV500 (2.0% Ni)	1.5%	15.7%
CBV500 (0.5% V)	1.8%	8.9%
CBV500 (2.0% V)	1.7%	8.7%

Carbon content after 1.5 and 60 min of TOS for the pure n-heptane cracking reaction and CBV500 with and without impregnated metal can be seen in table 11. It is interesting to notice that the coke deposited on the zeolite seems lower in the case of 2% metal impregnation, as compared to the amount deposited for 0.5% metal impregnation. However, from the acid site concentration it can be seen that there probably is an increase in coke formation with higher metal concentration. The error in the carbon analysis can be the reason for the inconsistency seen in table 11.

At 60 min of TOS the coke deposited on the zeolite is slightly lower in case of vanadium impregnated sample and higher in case of nickel impregnated sample. 2% nickel gives the highest amount of carbon content (15.7%) after 60 min of cracking reaction. Various researchers have found that coke deposited on the Y zeolite is higher in the case of nickel, as compared to vanadium [18, 21, 23]. Although it would be expected that coke deposition would be higher for both metals [21, 23], this cannot be concluded from the current work. Nevertheless, a very significant difference can be seen in sample preparation, which can be the reason for this difference. In the current work the temperature of the

catalyst does not exceed 500°C (calcination), while reduction of the metal species was carried out in the previous work [21]. It was observed before that reduced vanadium has a higher tendency to form coke. Another reason for the relatively low coke deposition for vanadium impregnated samples is an interaction between EFAL species and vanadium that can reduce the accessibility of hydrocarbon molecules to vanadium sites and consequently the coke formation.

For nickel, two explanations can be given for the high increase in coke formation at 60 min of TOS: i) In general, metals favor hydrogen transfer reactions as well as coke formation reactions [24] and ii) after 1.5 min of TOS some nickel is reduced to metallic form. Option i) is plausible, since a decrease in C_3, C_4 and C_5 olefin selectivity can be seen in the case of nickel impregnation. This would be an indication of hydrogen transfer reactions. Option ii) is also plausible, since the reduction of nickel was already seen at 466°C in case of iso-octane cracking [18]. Since in the current work the cracking of n-heptane is studied, this could decrease this reduction temperature during the cracking reaction.

Lewis and Brønsted acid site concentration for CBV500 with and without impregnated metal can be seen in table 12 for fresh catalyst and after 1.5 min of TOS of pure n-heptane cracking. It should be noticed that the reduction of Lewis acid site concentration for 0.5% nickel (40%), as compared to the reference (24%), is relatively high already from early on in the cracking reaction. This could be the result of the interaction of the nickel hydroxyls with coke molecules that makes them unable to adsorb pyridine.

Table 12 - Lewis and Brønsted acid site concentration for metal impregnated- and reference CBV500, for fresh samples and after 1.5 min of TOS of pure n-heptane cracking reaction

	Lewis acid site concentration (µmol/gr)			**Brønsted acid site concentration (µmol/gr)**		
	CBV500	*0.5% Ni*	*0.5% V*	*CBV500*	*0.5% Ni*	*0.5% V*
fresh	442	682	498	816	744	796
pure n-heptane	335	407	404	672	624	615
	-24%	-40%	-19%	-18%	-16%	-23%

The change of microporous volume with changing nickel and vanadium content can be seen in figure 43 for fresh sample and sample after 1.5 min of TOS of pure n-heptane cracking. A slightly higher decrease in microporous volume can be seen for n-heptane cracking over 0.5% nickel impregnated sample (15.8%) and 0.5% vanadium impregnated sample (14.7%) as compared to the catalyst without metal impregnation (12.4%). Increasing the metal content does not have a significant effect on the microporous volume, since the decrease of microporous volume for catalyst impregnated with 2% nickel (15.9%) and 2% vanadium (14.4%) are very similar to the values obtained for 0.5% metal content.

Mesoporous volume and external surface area for fresh catalysts and after pure n-heptane cracking can be seen in table 13 and 14, respectively. When comparing the fresh catalyst with the catalyst after pure n-heptane cracking, no significant change can be detected in the data. From this it can be

concluded that for all catalysts the coke is mostly deposited in the micropores of the zeolite structure, since a decrease in microporous volume was observed.

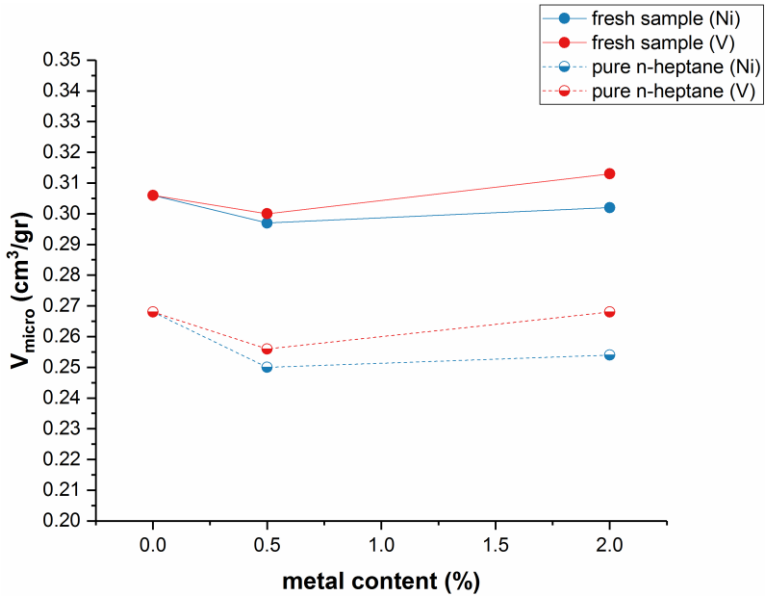

Figure 43 - Microporous volume as a function of nickel and vanadium content for fresh samples and samples after 1.5 min of TOS pure n-heptane cracking

Table 13 - Mesoporous volume of CBV500 with and without metal impregnation for fresh samples and after 1.5 min of TOS of pure n-heptane cracking

	V_{meso} (cm^3/gr)				
	CBV500	*0.5% Ni*	*2% Ni*	*0.5% V*	*2% V*
fresh	0.078	0.075	0.072	0.074	0.064
pure n-heptane	0.081	0.071	0.072	0.073	0.060
	4.4%	-5.2%	1.0%	-1.9%	-6.1%

Table 14 - External surface area of CBV500 with and without metal impregnation for fresh samples and after 1.5 min of TOS of pure n-heptane cracking

	S_{ext} (m^2/gr)				
	CBV500	*0.5% Ni*	*2% Ni*	*0.5% V*	*2% V*
fresh	52.5	47.1	51.5	49.6	39.3
pure n-heptane	55.4	41.4	51.6	47.8	42.8
	5.5%	-12.1%	0.3%	-3.6%	8.9%

4.3.2.2. Product distribution

4.3.2.2.1. Fresh catalyst

Product group selectivity at 35% iso-conversion, after 1.5 min of TOS during pure n-heptane cracking, is shown in figure 44 for the reference and samples with increasing nickel and vanadium content. It can be seen that the aromatics selectivity increases slightly when CBV500 is impregnated with nickel or vanadium, which could be the result of an increase in hydrogen transfer reactions with the introduction of metal species. For nickel it can be seen that the aromatics content slightly increases with increasing nickel content, while increasing the vanadium content from 0.5% to 2% seems to have no significant effect on the aromatics selectivity. Both 0.5% and 2% vanadium impregnation lead to an increase in aromatics selectivity that is more or less similar to the increase observed for 0.5% nickel impregnated sample. This result is in agreement with previous research, in which vanadium affects essentially the activity of the impregnated catalyst but not the selectivity [22].

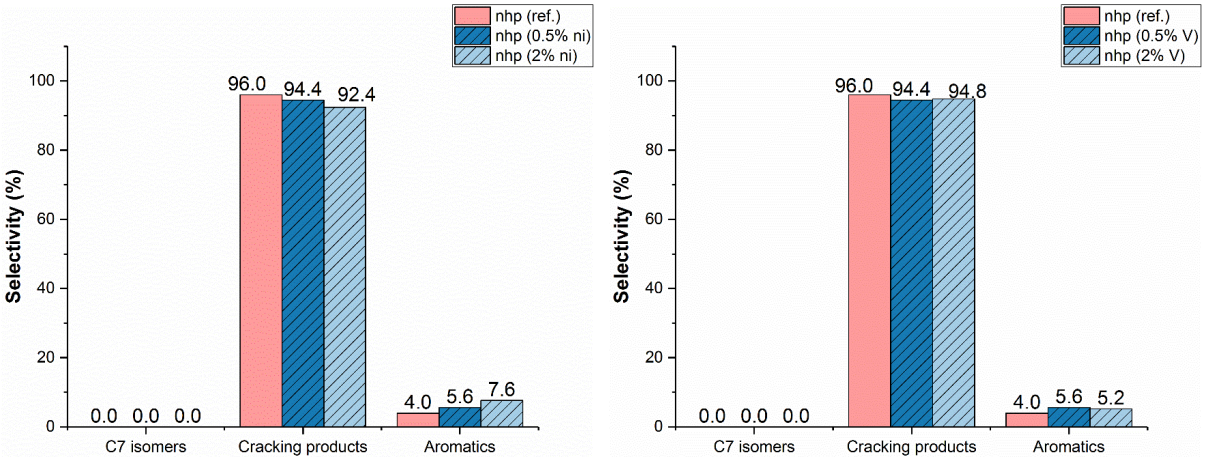

Figure 44 - Product group selectivity for pure n-heptane cracking for the reference and samples with increasing nickel (left) and vanadium (right) content

The product selectivity is shown in more detail in table 15 for cracking of pure n-heptane over CBV500 with increasing amounts of nickel and vanadium.

It can be seen that for both 0.5% and 2% nickel samples, the selectivity of C_1 and C_2 increases together with linear n-C_4. When looking again at the cracking mechanism (section 4.1) this can be explained by the increasing importance of the protolytic cracking mechanism. The observed increase in methane selectivity could also be the result of a hydrogenolysis reaction between nickel and the cracking reactants and/or products within the zeolite structure. At higher temperature (>400°C) excess methane is formed due to hydrogenolysis, i.e. terminal cracking, reaction that is catalyzed by reduced nickel in the metallic form. The reduction of nickel oxides and increased methane yield was observed in previous research when cracking paraffins over USY zeolite at temperatures above 400°C [18].

The increase in aromatic products with increasing nickel concentration can be seen in detail in the table below. Toluene selectivity increases with increasing nickel content, while xylenes selectivity show the same increase for both amounts of nickel loading. The increase in C_1, C_2 and aromatics selectivity with increasing nickel content is in line with expectation. Nickel deposited on the cracking catalyst causes nonselective cracking, which leads to increased coke, hydrogen and dry gas production at the expense of gasoline yield [18].

Table 15 - Detailed cracking products selectivity at iso-conversion (35%) at 1.5 min of TOS during pure n-heptane cracking for samples with varying amounts of nickel and vanadium impregnation

	Pure n-heptane				
	Reference	*Nickel content*		*Vanadium content*	
		0.5%	*2%*	*0.5%*	*2%*
C1	0.1	0.3	2.8	0.2	0.3
C2	1.4	1.6	4.5	1.4	1.2
C3	28.4	26.2	28.7	27.2	27.3
C3=	10.6	12.2	9.5	11.7	10.5
i-C4	34.4	31.3	28.2	32.2	32.8
n-C4	9.5	10.7	10.5	10.3	10.7
C4=	5.0	5.8	4.2	5.4	4.9
i-C5	4.2	4.0	2.8	4.0	4.0
n-C5	1.1	1.0	0.8	1.0	0.9
C5=	0.5	0.6	0.3	0.5	0.3
C6	0.7	0.6	0.1	0.6	0.6
C6=	0.1	0.2	0.1	0.1	0.1
toluene	2.2	2.6	4.6	2.9	2.3
m,p-xylene	1.5	2.4	2.4	2.2	1.7
o-xylene	0.3	0.5	0.6	0.4	1.1

No significant increase in C_1 and C_2 selectivity can be detected for 0.5% and 2% vanadium impregnated samples. Also it can be seen that C_4 selectivity does not exhibit a significant change when introducing vanadium in the Y zeolite. Product selectivity does not seem to change with the amount of vanadium, as opposed to nickel samples, for which the selectivity changes significantly with the amount of impregnated metal.

Iso-paraffin / n-paraffin ratio and paraffin / olefin ratio for increasing nickel and vanadium content can be seen in figure 45. For both nickel and vanadium samples, a decrease in iso-paraffin / n-paraffin can be seen with the introduction of metal in the zeolite. The decrease of the ratio is higher with increasing nickel content, as opposed to vanadium, for which the ratio is similar for 0.5% and 2% loading. Two situations could induce the decrease in iso-paraffin / n-paraffin ratio: i) The importance of the B-scission mechanism decreases relatively to the protolytic cracking reactions or ii) there are more spatial constraints to the branched molecules diffusion.

Since the methane and ethane selectivity increases with increasing nickel content the first option is very plausible for nickel impregnated samples. With the increased coke production observed there is also a decrease in space available for diffusion, which could induce spatial constraints for iso-paraffins. For both options i) and ii), this would explain why the decrease is more pronounced for 2% nickel content as compared to 0.5% nickel content.

Since the methane and ethane selectivity is not increasing with increasing vanadium content, as was the case with nickel impregnated samples, the first option is not very plausible. It can be assumed that only option ii), an increase in spatial constraints due to increased coke formation, can be the reason in the case of vanadium impregnation. Since there is no change is aromatics selectivity and the coke formation is more or less the same for 0.5% and 2% vanadium, this would explain why the ratio does not change from 0.5% to 2% vanadium.

The increase in paraffin / olefin ratio that is seen for 2% metal content, as compared to 0.5% metal content, can be explained by the increase in hydrogen transfer reactions and is in line with the decrease of propene, butene and pentene and the increase in aromatics selectivity [36]. Another explanation would be the increased hydrogenation of olefins catalyzed by nickel and vanadium particles.

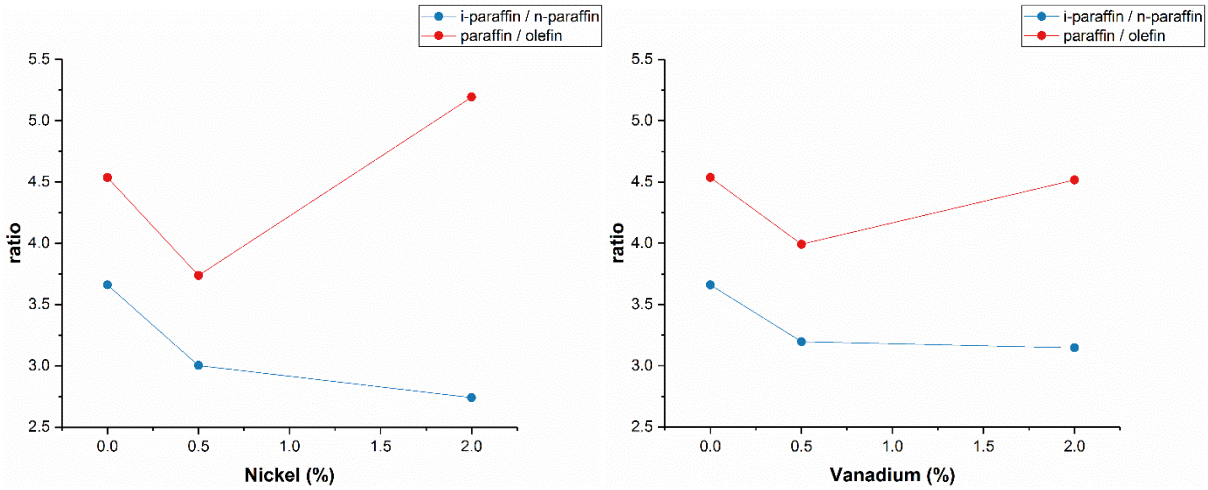

Figure 45 - Iso-paraffin / n-paraffin and paraffin / olefin ratio for pure n-heptane cracking reaction as a function of nickel (left) and vanadium (right) content

4.3.3. n-Heptane conversion – Influence of guaiacol poisoning

4.3.3.1. Deactivation

Figure 46 (left) shows n-heptane conversion as a function of time on stream for pure n-heptane cracking and in the case of cracking n-heptane + 1.2% guaiacol for catalysts with increasing impregnated nickel content. On the right side of figure 46 the residual activity, as compared to the initial activity of the catalyst at 1.5 min of TOS of pure n-heptane cracking, is illustrated for cracking with and without guaiacol.

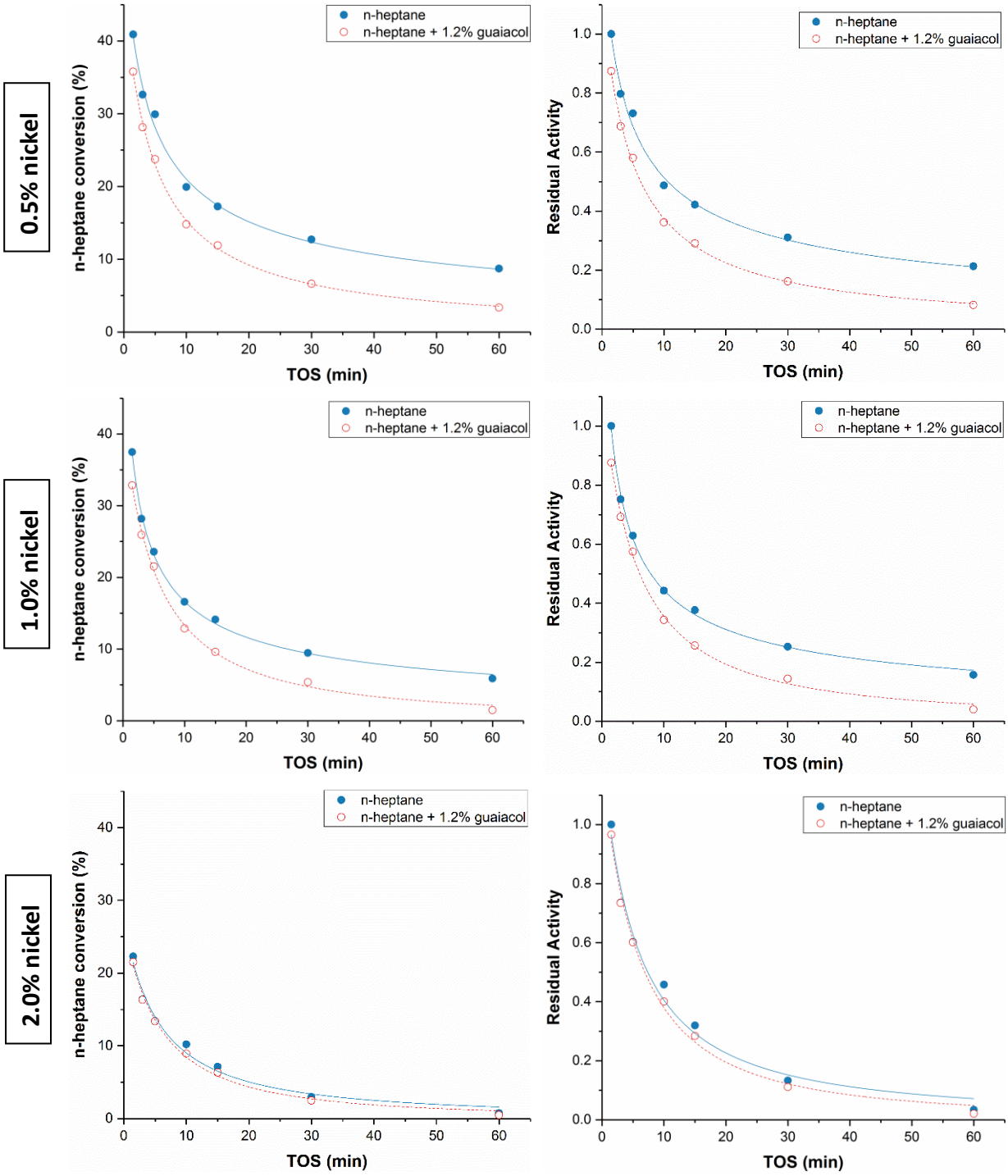

Figure 46 - n-heptane conversion and n-heptane + 1.2% guaiacol conversion (left) and residual activity (as compared to the initial activity of the sample for pure n-heptane conversion at 1.5 min of TOS) vs. time on stream for CBV500 samples with increasing nickel content.

It can immediately be seen that there is a decrease of n-heptane conversion when guaiacol is added to the reaction mixture. This decrease is lower with increasing nickel content as can be seen when the difference between n-heptane conversion with and without guaiacol for 0.5% nickel content is compared to 2% nickel content. Figure 47 (left) shows the n-heptane conversion as a function of nickel content for n-heptane cracking with and without guaiacol in the reaction mixture. It can be seen that

especially at the start of the reaction the decrease in n-heptane conversion when adding guaiacol to the reaction mixture is lower for increasing nickel content.

This phenomena can also be seen when looking at the residual activity on the right side of figure 47. At the start of the reaction, the decrease in residual activity when guaiacol is added to the mixture, is lower with increasing nickel content. It can be seen very well that, at 1.5 min of TOS in presence of guaiacol, the graph has a positive slope. This means that guaiacol seems to have a less poisonous effect with increasing nickel content.

It has been seen earlier that there is a big increase of Lewis acid sites when impregnating CBV500 with nickel or vanadium. Since guaiacol is binding to Lewis and Brønsted acid sites in an equilibrium reaction, it could very well be the case that more guaiacol is binding to Lewis acid sites when there are more Lewis acid sites available. This also means that less guaiacol is binding to Brønsted acid sites if more Lewis acid sites are available. This effect becomes more apparent with increasing nickel content, since this also increases the number of Lewis acid sites. Later in this section this theory will be discussed and checked with the available experimental data.

Even though the guaiacol is less poisonous for nickel impregnated samples as compared to reference CBV500, the n-heptane conversion is always lower when cracking n-heptane with or without guaiacol compared to the reference. This is probably the result of a decrease in Brønsted acid sites when CBV500 is impregnated with nickel as was seen from the pyridine absorption for fresh samples with and without nickel.

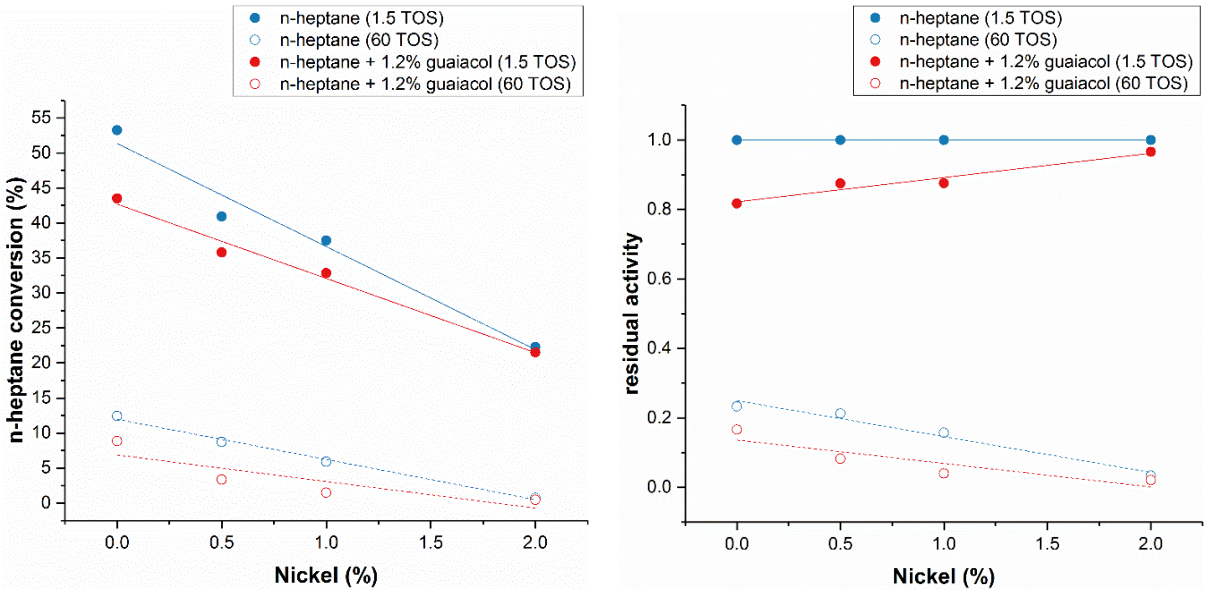

Figure 47 - n-heptane conversion (left) and residual activity (right) as a function of nickel content in case of pure n-heptane cracking and cracking n-heptane + 1.2% guaiacol

Figure 48 (left) shows n-heptane conversion as a function of time on stream for pure n-heptane cracking and in the case of cracking n-heptane + 1.2% guaiacol for catalysts with increasing impregnated vanadium content. On the right side of figure 48 the residual activity, as compared to the initial activity of the catalyst at 1.5 min of TOS of pure n-heptane cracking, is illustrated for cracking with and without guaiacol.

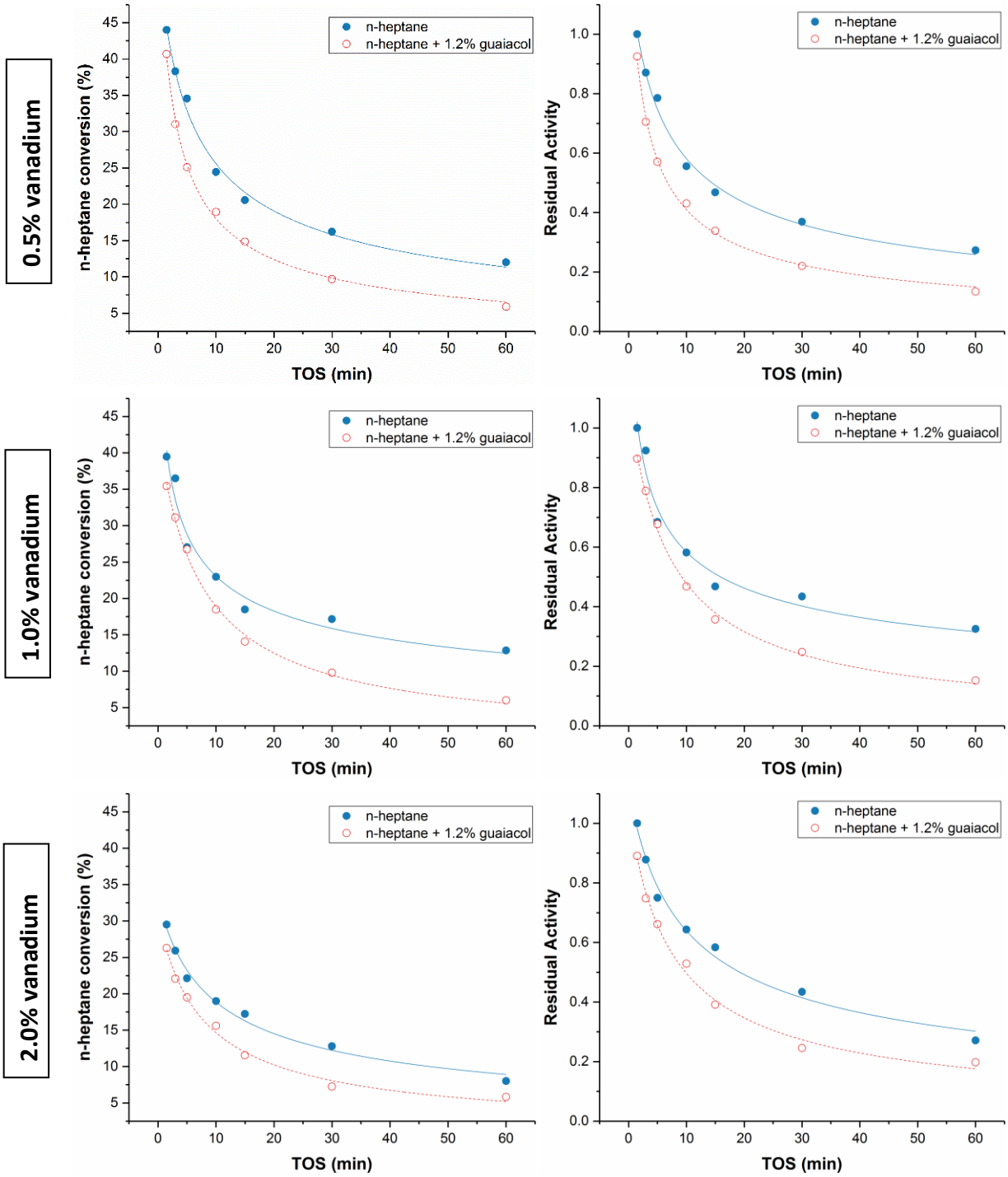

Figure 48 - n-heptane conversion and n-heptane + 1.2% guaiacol conversion (left) and residual activity (as compared to the initial activity of the sample for pure n-heptane conversion at 1.5 min of TOS) vs. time on stream for CBV500 samples with increasing vanadium content

It can immediately be seen that there are similarities between the activity data obtained from vanadium impregnated samples with the obtained data from nickel impregnated samples. A decrease of n-heptane conversion can be seen when guaiacol is added to the reaction mixture. The data is rearranged again to see the n-heptane conversion as a function of vanadium content on the left side of figure 49. At 1.5 min of TOS the n-heptane conversion for samples with higher content of vanadium show the same trend as the nickel impregnated samples with increasing metal content. This can be seen clearly on the right side of figure 49, where the data from 1.5 min of TOS shows a positive slope, which indicates that guaiacol poisoning is less severe for samples with higher vanadium content. This slope is, however, less steep as compared to the nickel data, which can be explained by the acid site distribution. The increase in Lewis acid site concentration is lower for vanadium as compared to nickel impregnation. Thus this would explain the same behavior as nickel impregnated samples, but to a lesser extent.

Another observation is the high n-heptane conversion in both cases of n-heptane cracking with and without 1.2% guaiacol, as compared to the data obtained from the nickel samples. One explanation is the less substantial decrease of Brønsted acid site concentration as compared to the Brønsted acid decrease in the case of nickel impregnation that was observed for the fresh 0.5% metal impregnated samples. There is still a decrease compared to the reference sample. Additionally when looking at the n-heptane conversion data of the reference sample and the metal impregnated samples, it can be seen that the vanadium samples are in the middle, which is consistent with the data.

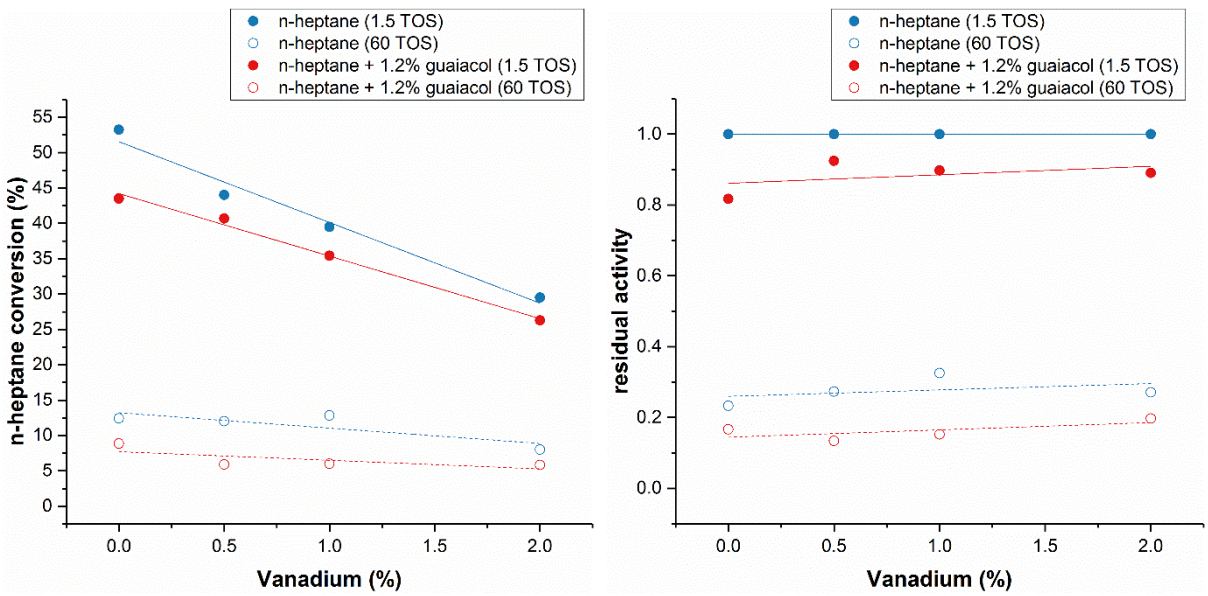

Figure 49 - n-heptane conversion (left) and residual activity (right) as a function of vanadium content in case of pure n-heptane cracking and cracking n-heptane + 1.2% guaiacol

Carbon content for the different catalysts after 1.5min of TOS of n-heptane cracking reaction with and without guaiacol can be seen in table 16. It can be seen that the carbon content for nickel impregnated samples is higher than the carbon content of reference and vanadium impregnated samples at both 1.5

and 60 min of TOS. This shows a direct relation between the deactivation of the catalyst and coke deposition. Especially the amount of carbon for 0.5% and 2% nickel impregnated catalyst after 60 min of TOS in presence of guaiacol (14.1% and 17.1%, respectively) explains the very low residual activity that could be seen for these catalysts at this time in the reaction as compared to the other catalysts.

Table 16 - Carbon content deposited on the zeolite after n-heptane cracking with and without 1.2% guaiacol for reference sample and CBV500 impregnated with increasing metal content, at 1.5 and 60 min of TOS

			CBV500	0.5% Ni	2.0% Ni	0.5% V	2.0% V
TOS (min)	1.5	*pure n-heptane*	1.7%	1.8%	1.5%	1.8%	1.7%
		n-heptane + 1.2% guaiacol	1.6%	1.9%	3.5%	1.5%	1.9%
	60	*pure n-heptane*	9.4%	10.6%	15.7%	8.9%	8.7%
		n-heptane + 1.2% guaiacol	10.4%	14.1%	17.1%	10.8%	10.4%

Both Brønsted and Lewis acid site concentration can be seen in figure 50 for the reference and 0.5% nickel and vanadium impregnated samples. It can be seen for both nickel and vanadium impregnated samples, that a smaller decrease in Lewis acid site concentration is observed when introducing guaiacol in the reaction mixture as compared to pure n-heptane cracking. This was not the case for the reference without metal impregnation, for which the Lewis acid site concentration showed a higher decrease when introducing guaiacol, as compared to pure n-heptane cracking.

The same can be observed for Brønsted acid site concentration. After 1.5 min of TOS of pure n-heptane cracking, the decrease in Brønsted acid sites is more or less similar for the samples with and without metal impregnation. However, when introducing guaiacol to the reaction mixture, this decrease is much lower for the metal impregnated samples. The decrease is 22.6%, 12.7% and 1.74% for reference, vanadium impregnated sample and nickel impregnated sample, respectively. This is an indication that the guaiacol being less poisonous for nickel and vanadium impregnated samples is due to a smaller decrease of the Brønsted acid sites. As discussed earlier, this is likely the result of the higher amount of Lewis acid sites (Ni > V > ref.), which makes that guaiacol bonds relatively more to Lewis acid sites than to Brønsted acid sites when introducing metal in CBV500, since the reaction is in equilibrium and thus can shift towards a side.

Microporous volume as a function of nickel and vanadium content is shown in figure 51 for the fresh samples and cracking of n-heptane with or without guaiacol at 1.5 min of TOS. The decrease in microporous volume for pure n-heptane cracking was discussed earlier and it could be seen that for both nickel and vanadium increasing the metal content from 0.5% to 2% did not have a negative effect on the decrease of the volume. Looking at the decrease of microporous volume when guaiacol is added to the reaction mixture, it can be seen that the microporous volume decreases with increasing nickel and

vanadium content. For the 0.5% nickel and 0.5% vanadium impregnated samples the decrease in microporous volume is more or less the same for n-heptane cracking with and without guaiacol. For the 2% metal impregnated samples, the microporous volume decreases as compared to pure n-heptane cracking, with the decrease being more pronounced for vanadium.

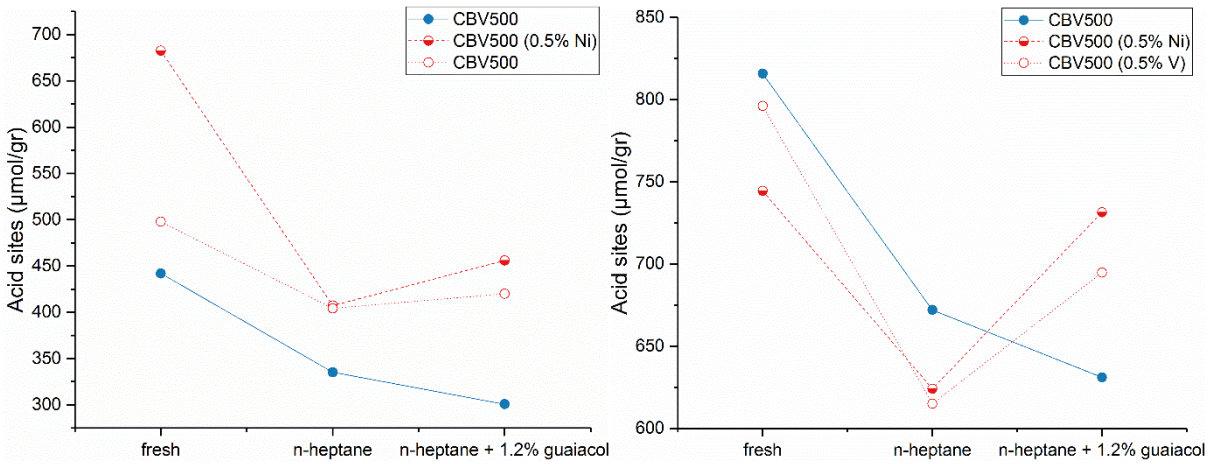

Figure 50 - Lewis (left) and Brønsted (right) acid site concentration for 0.5% nickel and vanadium impregnated CBV500 after 1.5 min of TOS cracking with and without guaiacol in the reaction mixture

The decrease in microporous volume is consistent with the increase in coke content, which would be an indication that the coke is deposited in the micropores of the zeolite where most of the active acid sites are located. For both nickel and vanadium, the amount of carbon increases significantly for the 2% impregnated samples and no significant increase was seen for the 0.5% impregnated samples.

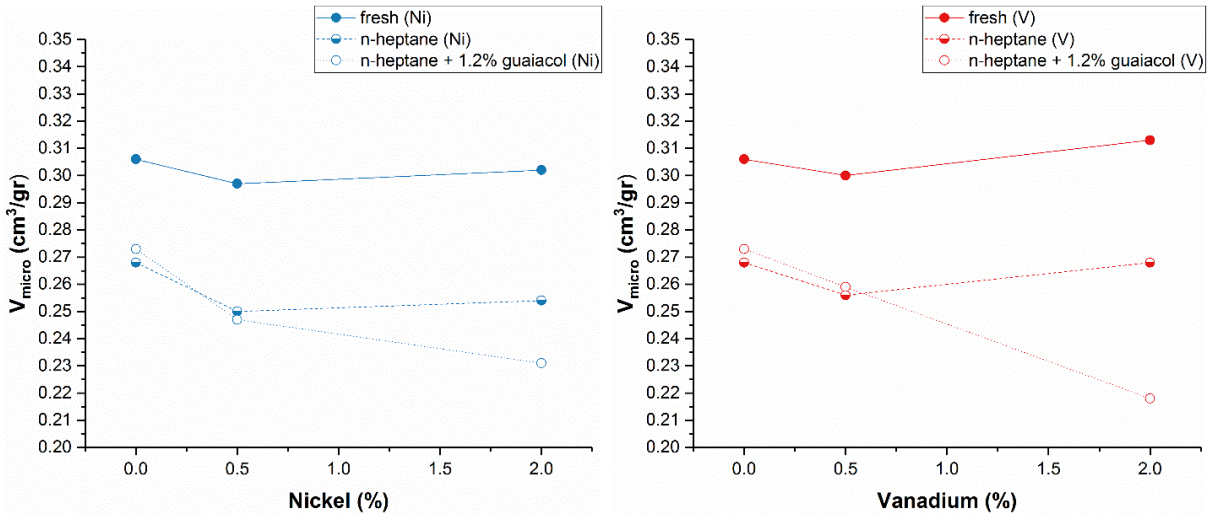

Figure 51 - Microporous volume as a function of nickel (left) and vanadium (right) content for fresh samples, pure n-heptane cracking and cracking of n-heptane + 1.2% guaiacol (1.5 min of TOS)

Mesoporous volume and external surface area for fresh catalysts and those after n-heptane cracking with and without guaiacol can be seen in table 17 and 18, respectively. For all catalysts, no significant change can be detected between the fresh and coked samples. In combination with the decrease in microporous volume, it can be concluded that coke is also mainly located in the micropores when guaiacol is added to the reaction mixture.

Table 17 - Mesoporous volume of CBV500 with and without metal impregnation for fresh samples and after 1.5 min of TOS of n-heptane cracking with and without guaiacol

	V_{meso} (cm^3/gr)				
	CBV500	*0.5% Ni*	*2% Ni*	*0.5% V*	*2% V*
fresh	0.078	0.075	0.072	0.074	0.064
pure n-heptane	0.081	0.071	0.072	0.073	0.060
n-heptane + 1.2% guaiacol	0.080	0.072	0.071	0.075	0.066

Table 18 - External surface area of CBV500 with and without metal impregnation for fresh samples and after 1.5 min of TOS of n-heptane cracking with and without guaiacol

	S_{ext} (m^2/gr)				
	CBV500	*0.5% Ni*	*2% Ni*	*0.5% V*	*2% V*
fresh	52.5	47.1	51.5	49.6	39.3
pure n-heptane	55.4	41.4	51.6	47.8	42.8
n-heptane + 1.2% guaiacol	54.3	43.5	50.5	51.4	45.6

4.3.3.2. Product distribution

4.3.3.2.1. Fresh catalyst

Product group selectivity at iso-conversion (35% n-heptane conversion) after 1.5 min of TOS during n-heptane cracking with and without guaiacol is shown in table 19 for the reference sample and samples with increasing nickel and vanadium content. The C_7 isomers selectivity is not shown, since no C_7 isomers were formed and therefore the selectivity is always 0%. From the table it can be seen that in general the aromatics selectivity slightly decreases and the cracking products selectivity increases when introducing guaiacol in the reactions over nickel and vanadium impregnated zeolites. A decrease in aromatics selectivity would be the logical result of guaiacol binding to metal particles. The increase of hydrogen transfer reactions and dehydrogenation reactions associated with the impregnated metal catalysts, would be reduced due to the binding of guaiacol to the metals.

The product selectivity is shown in more detail in table 20 and 21 for cracking of n-heptane with and without guaiacol over CBV500 with varying impregnated nickel and vanadium content, respectively. Compared to pure n-heptane cracking, no very significant changes can be detected in the product distribution when introducing guaiacol.

Table 19 - Product group selectivity for n-heptane with and without guaiacol for varying nickel content

	Pure n-heptane		**N-heptane + 1.2% guaiacol**	
Nickel content (%)	*Cracking products (C_1-C_6) selectivity (%)*	*Aromatics selectivity (%)*	*Cracking products (C_1-C_6) selectivity (%)*	*Aromatics selectivity (%)*
ref.	96.0	4.0	96.3	3.7
0.5	94.4	5.6	95.3	4.7
2	92.4	7.6	91.3	8.7
Vanadium content (%)	*Cracking products (C_1-C_6) selectivity (%)*	*Aromatics selectivity (%)*	*Cracking products (C_1-C_6) selectivity (%)*	*Aromatics selectivity (%)*
ref.	96.0	4.0	96.3	3.7
0.5	94.4	5.6	95.9	4.1
2	94.8	5.2	94.8	5.2

Table 20 - Detailed products from cracking at iso-conversion (35%) at 1.5 min of TOS for n-heptane cracking with and without guaiacol for samples with varying amount of nickel impregnation

	Pure n-heptane			**N-heptane + 1.2% guaiacol**		
	Nickel content			*Nickel content*		
	0%	*0.5%*	*2%*	*0%*	*0.5%*	*2%*
C1	0.1	0.3	2.8	0.1	0.3	2.1
C2	1.4	1.6	4.5	1.5	1.7	4.0
C3	28.4	26.2	28.7	28.5	27.3	26.9
C3=	10.6	12.2	9.5	10.6	11.5	10.2
i-C4	34.4	31.3	28.2	34.7	33.2	28.9
n-C4	9.5	10.7	10.5	9.6	9.9	10.1
C4=	5.0	5.8	4.2	4.7	5.1	4.4
i-C5	4.2	4.0	2.8	4.2	3.9	3.0
n-C5	1.1	1.0	0.8	1.0	1.0	0.8
C5=	0.5	0.6	0.3	0.5	0.5	0.3
C6	0.7	0.6	0.1	0.6	0.7	0.4
C6=	0.1	0.2	0.1	0.1	0.2	0.1
toluene	2.2	2.6	4.6	2.0	2.6	5.1
m,p-xylene	1.5	2.4	2.4	1.4	1.8	2.9
o-xylene	0.3	0.5	0.6	0.3	0.4	0.7

Table 21 - Detailed products from cracking at iso-conversion (35%) at 1.5 min of TOS for n-heptane cracking with and without guaiacol for samples with varying amount of vanadium impregnation

	Pure n-heptane			N-heptane + 1.2% guaiacol		
	Vanadium content			Vanadium content		
	0%	0.5%	2%	0%	0.5%	2%
C1	0.1	0.2	0.3	0.1	0.2	0.4
C2	1.4	1.4	1.2	1.5	1.5	1.7
C3	28.4	27.2	27.3	28.5	27.6	29.8
C3=	10.6	11.7	10.5	10.6	11.5	10.5
i-C4	34.4	32.2	32.8	34.7	33.1	33.7
n-C4	9.5	10.3	10.7	9.6	10.3	11.4
C4=	5.0	5.4	4.9	4.7	5.2	4.6
i-C5	4.2	4.0	4.0	4.2	4.0	3.9
n-C5	1.1	1.0	0.9	1.0	0.9	0.9
C5=	0.5	0.5	0.3	0.5	0.5	0.4
C6	0.7	0.6	0.6	0.6	0.7	0.5
C6=	0.1	0.1	0.1	0.1	0.2	0.1
toluene	2.2	2.9	2.3	2.0	2.2	2.6
m,p-xylene	1.5	2.2	1.7	1.4	1.6	1.9
o-xylene	0.3	0.4	1.1	0.3	0.4	0.9

The iso-paraffin / n-paraffin ratio that can be seen in figure 52 for varying nickel content and for cracking with and without guaiacol shows similar behavior as compared to cracking with and without guaiacol for the reference sample without nickel impregnation. The ratio is higher when guaiacol is added to the reaction mixture, which is the result of a decrease in spatial constraints due to guaiacol bonding to acid sites instead of bulky coke molecules. The data from the detailed product distribution (table 20) shows an increase in i-C_4 and i-C_5 and a decrease in n-C_4, which is in agreement with the conclusion above.

The decrease of iso-paraffin / n-paraffin is more pronounced in the case of nickel impregnated samples compared to the reference and vanadium impregnated samples. As was seen before, the Lewis acid site concentration and coke formation increases when nickel is introduced in the zeolite. From this it can be concluded that there is relatively more coke that could be replaced by guaiacol. The decrease in spatial constraints is therefore more pronounced in nickel impregnated samples.

For vanadium (figure 53) the iso-paraffin / n-paraffin ratio does not have clear increase when introducing guaiacol to the reaction mixture. The paraffin/olefin ratio for vanadium and nickel impregnated samples show a similar trend when introducing guaiacol to the reaction mixture as the reference CBV500.

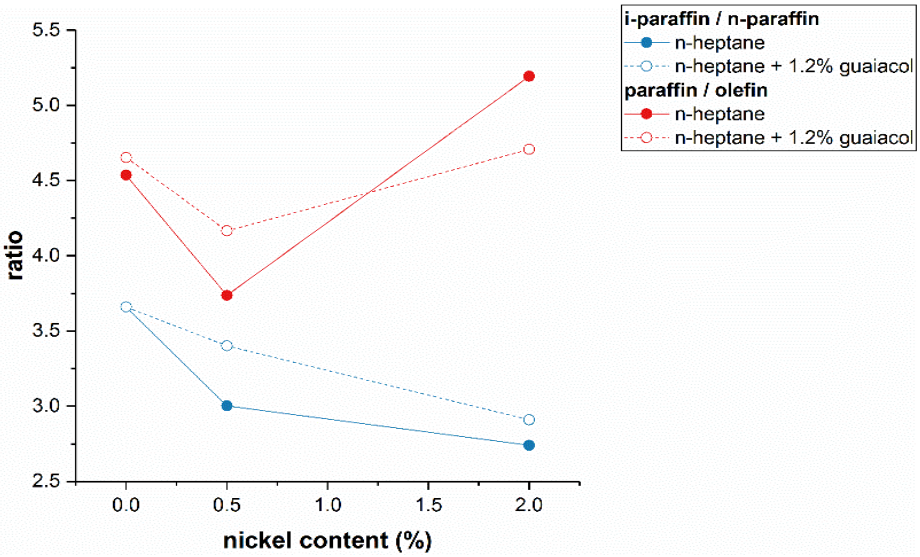

Figure 52 - i-paraffin / n-paraffin and paraffin / olefin ratio for n-heptane cracking reaction at 1.5 min of TOS at iso-conversion (35%) with and without guaiacol for varying impregnated nickel content

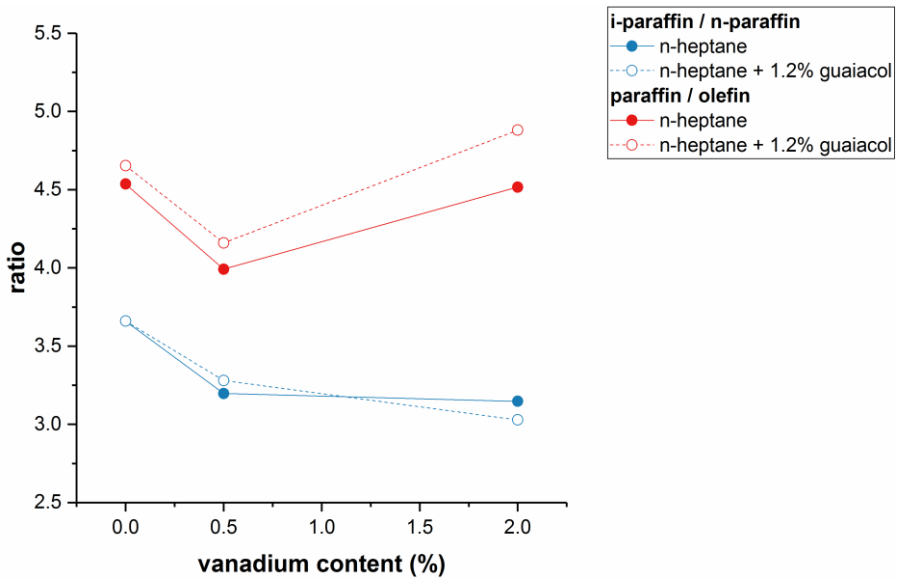

Figure 53 - i-paraffin / n-paraffin and paraffin / olefin ratio for n-heptane cracking reaction at 1.5 min of TOS at iso-conversion (35%) with and without guaiacol for varying impregnated vanadium content

4.4. References

[1] Kotrel, S., et al. "The Haag–Dessau mechanism of protolytic cracking of alkanes." Microporous and Mesoporous Materials, vol. 35-36, 2000, pp. 11-20.

[2] Graça, Inês. "Influence of Oxygenated Compounds on the Properties of FCC Catalysts." 2010. Instituto Superior Técnico, PhD Dissertation.

[3] "Zeolite Y (CBV500)." Zeolyst | Zeolyst International, www.zeolyst.com/our-products/standard-zeolite-powders/zeolite-y.html.

[4] Etim, U.J., et al. "Effect of vanadium contamination on the framework and micropore structure of ultra stable Y-zeolite." Journal of Colloid and Interface Science, vol. 463, 2016, pp. 188-198.

[5] Aizuddin M, Muhammad A., et al. "Analysis of the Textural Characteristics and Pore Size Distribution of a Commercial Zeolite using Various Adsorption Models." Journal of Applied Sciences, vol. 11, no. 21, 2011, pp. 3650-3654.

[6] Manuela, M., and L. Ribeiro Carrott. "Physisorption Of Gases By Solids: Fundamentals, Theories and Methods For The Textural Characterization Of Catalysts." Catalysis from Theory to Application,

[7] Barzetti, Tommy, et al. "Pyridine and ammonia as probes for FTIR analysis of solid acid catalysts." Journal of the Chemical Society, Faraday Transactions, vol. 92, no. 8, 1996, p. 1401.

[8] Lunsford, Jack H., et al. "Acid sites in zeolite Y: a solid-state NMR and infrared study using trimethylphosphine as a probe molecule." Journal of the American Chemical Society, vol. 107, no. 6, 1985, pp. 1540-1547.

[9] Yu, J. "Synthesis of Zeolites" Introduction to Zeolite Science and Practice (3rd edition), Elsevier, 2007, pp. 39-104

[10] Makarova, Marina A., and John Dwyer. "FTIR analysis of the hydroxyl region in US-Y zeolites." The Journal of Physical Chemistry, vol. 97, no. 24, 1993, pp. 6337-6338.

[11] Cerqueira, Henrique S., et al. "Influence of coke on the acid properties of a USHY zeolite." Microporous and Mesoporous Materials, vol. 38, no. 2-3, 2000, pp. 197-205.

[12] Corma, A., et al. "Extraction of extra-framework aluminium in ultrastable Y zeolites by (NH4)2SiF6 treatments." Applied Catalysis, vol. 59, no. 1, 1990, pp. 267-274.

[13] Wielers, A. "Relation between properties and performance of zeolites in paraffin cracking." Journal of Catalysis, vol. 127, no. 1, 1991, pp. 51-66.

[14] Corma, A. "The Role of Reaction Temperature and Cracking Catalyst Characteristics in Determining the Relative Rates of Protolytic Cracking, Chain Propagation, and Hydrogen Transfer." Journal of Catalysis, vol. 145, no. 1, 1994, pp. 171-180.

[15] Beirnaert, Hans C., et al. "A Fundamental Kinetic Model for the Catalytic Cracking of Alkanes on a USY Zeolite in the Presence of Coke Formation." Industrial & Engineering Chemistry Research, vol. 40, no. 5, 2001, pp. 1337-1347.

[16] Petranovskii, V., et al. "Formation of catalytically active copper and nickel nanoparticles in natural zeolites." Zeolites and related materials: Trends, targets and challenges, Proceedings of the 4th International FEZA Conference, 2008, pp. 513-516.

[17] Venkatathri, N. "Structural and Catalytic Properties of a Novel Vanadium Containing Solid Core Mesoporous Shell Silica Catalysts for Gas Phase Oxidation Reaction." The Open Catalysis Journal, vol. 5, no. 1, 2012, pp. 14-20.

[18] LongXiang, T., et al. "Characteristics of the poisoning effect of nickel deposited on USY zeolite." Applied Catalysis A: General, vol. 91, no. 2, 1992, pp. 67-80.

[19] Kefirov, Radoslav, et al. "FTIR Characterization of Fe3+–OH Groups in Fe–H–BEA Zeolite: Interaction with CO and NO." Catalysis Letters, vol. 125, no. 3-4, 2008, pp. 209-214.

[20] Wong, Syieluing, et al. "Catalytic Cracking of LDPE Dissolved in Benzene Using Nickel-Impregnated Zeolites." Industrial & Engineering Chemistry Research, vol. 55, no. 9, 2016, pp. 2543-2555.

[21] Escobar, Alyne S., et al. "Role of nickel and vanadium over USY and RE-USY coke formation." Applied Catalysis A: General, vol. 315, 2006, pp. 68-73.

[22] Torrealba, M., et al. "Influence of vanadium on the physicochemical and catalytic properties of USHY zeolite and FCC catalyst." Applied Catalysis A: General, vol. 90, no. 1, 1992, pp. 35-49.

[23] Yang, Shien-Jen, et al. "The interaction of vanadium and nickel in USY zeolite." Zeolites, vol. 15, no. 1, 1995, pp. 77-82.

[24] Cumming, K. A., and B. W. Wojciechowski. "Hydrogen Transfer, Coke Formation, and Catalyst Decay and Their Role in the Chain Mechanism of Catalytic Cracking." Catalysis Reviews, vol. 38, no. 1, 1996, pp. 101-157.

5. Conclusion

CBV500, a US-Y zeolite, was impregnated with varying amount of nickel and vanadium to resemble the metal deposition on the catalysts used in the FCC process during the cracking reaction of crude oil. The catalysts have been used in a model compound study in which the transformation of pure n-heptane and n-heptane with 1.2% guaiacol was under study. From the acquired data is was possible to evaluate the influence of nickel and vanadium on the deactivating effect of oxygenated compounds on the FCC catalysts.

Nickel and Vanadium impregnation

It was possible to determine the type of nickel and vanadium species after impregnation with UV-vis spectroscopy. Nickel species exist mainly as $Ni(H_2O)_6^{2+}$ species, but also a band corresponding to NiO species could be seen. In the case of vanadium, the species were partly tetrahedral coordinated species that form vanadium monomer and oligomer and partly octahedral coordinated species that form vanadium oligomers. From XRD measurements, it was concluded that crystallinity did not change upon nickel or vanadium impregnation.

A small decrease in the mesoporous volume and external surface area could be seen for nickel and vanadium impregnated samples, which indicates that the metal is enriched on the external surface layer of the zeolite crystallite and to a minor extent in the mesopores of the zeolite. Acid sites concentration was highly influenced by nickel, which resulted in a high increase of 54.5% in Lewis acid sites concentration and a decrease of 8.7% in Brønsted acid sites concentration, as compared to the USHY zeolite without metal impregnation. In the case of vanadium impregnation, Lewis acid sites concentration increased about 12.6% and Brønsted acid sites concentration was similar. The significant increase in Lewis acid sites observed for nickel is due to the introduced nickel particles that can act as Lewis acid sites. The decrease in Brønsted acidity can be the result of a reaction between NiO species and stronger Brønsted acid sites or the replacements of protons by Ni^{2+} through ion exchange.

Pure n-heptane conversion - Activity

In the transformation of pure n-heptane over nickel and vanadium impregnated samples, a clear decrease in n-heptane conversion was observed for both metal catalysts. For nickel the decrease was more pronounced with increasing nickel content and was observed for fresh and deactivated catalyst (1.5 – 60 min of TOS). For vanadium the decrease was also more pronounced with increasing metal content, but the decrease was lower than in the case of nickel impregnated samples and could only be seen for early times on stream (1.5 – 15 min of TOS). Interaction of the metals with the Brønsted acid sites in the zeolite

is assumed to be the reason for the decrease in initial activity. Higher carbon content was seen for deactivated nickel impregnated catalyst, which is consistent with the decrease in activity as compared to the reference sample. The increase in coke formation is due to (i) the increase in hydrogen transfer reaction that is favored by impregnated metals and (ii) reduced nickel that has a higher tendency to form coke as compared to cationic nickel species. During the cracking reaction only nickel impregnated catalysts showed a relatively high decrease of Lewis acid sites as compared to the reference and vanadium impregnated samples. A possible explanation would be the interaction of nickel hydroxyls with coke molecules, which makes them unable to adsorb pyridine. From nitrogen adsorption experiments, it was concluded that coke is mostly located in the micropores of the zeolite for all studied catalysts.

Pure n-heptane conversion - Products selectivity

It can be seen that the aromatics selectivity increases slightly when CBV500 is impregnated with nickel or vanadium, which could be the result of an increase in hydrogen transfer reactions with the introduction of metal species. From the detailed products selectivities, an increasing importance of the protolytic cracking mechanism was observed in the case of nickel impregnated catalyst. Nickel deposited on the cracking catalyst causes non selective cracking, which leads to increased coke and hydrogen production. For vanadium no significant change was detected in the products selectivities. A clear decrease in iso-paraffin / n-paraffin ratio was seen for both metals. Two situations could induce the decrease in iso-paraffin / n-paraffin ratio: i) The importance of the β-scission mechanism decreases relatively to the protolytic cracking reactions or ii) there are more spatial constraints to the branched molecules diffusion. It is plausible that both explanations are relevant for nickel impregnated samples, while only the latter is relevant for vanadium impregnated samples.

Guaiacol poisoning - Activity

For both nickel and vanadium impregnated samples there is a decrease in n-heptane conversion when guaiacol is added to the reaction mixture, as compared to pure n-heptane conversion. However, from the residual activity is can be seen that the deactivation is lower with increasing metal content. From this it can be concluded that guaiacol has a less poisonous effect with increasing metal content. This effect is more pronounced for nickel than for vanadium and that is consistent with the higher increase in Lewis acid sites for nickel. Additional Lewis acid sites can protect the Brønsted acid sites from the poisoning of guaiacol that bonds to both Lewis and Brønsted acid sites. Carbon content is higher at 1.5 and 60 min of TOS for nickel as compared to the reference and vanadium impregnated samples. Especially high coke deposition for nickel samples at 60 min of TOS is the reason for the very low activity of coked nickel impregnated catalyst. Lewis and Brønsted acid site concentrations after coking are consistent with the conclusion presented. Also for the cracking reaction in presence of guaiacol, the coke is mostly located in the micropores of the zeolites.

Guaiacol poisoning – Products selectivity

A slight decrease in aromatics selectivity is seen in the case of guaiacol poisoning for both metals. A possible explanation would be the binding of guaiacol to metal species, thus reducing the importance of hydrogen transfer and dehydrogenation reaction associated with the impregnated metal catalysts. Compared to pure n-heptane cracking, no very significant changes can be detected in the detailed product distribution when introducing guaiacol. As opposed to the reference and vanadium impregnated samples, an increase in iso-paraffin / n-paraffin ratio was seen for nickel impregnated catalyst when introducing guaiacol to the reaction mixture. This is consistent with the increase in coke deposition and Lewis acid sites concentration upon nickel impregnation, which results in more potential places for guaiacol to replace coke molecules. This leads to a reduction in spatial constraints, and thus an increase in iso-paraffin selectivity.

Industrial point of view

From the industrial point of view it is most important to look at the results at 1.5 min of TOS, since the time spent in the riser is only a couple of seconds. From previous research of I. Graca it was seen that a small amount of guaiacol did not show a significant deactivating effect in ECAT. Since the ECAT contains nickel and vanadium, this can be explained by the decreasing poisonous effect of guaiacol when these metals are present.

Future research

- For vanadium impregnated samples the decrease in activity observed was low, as compared to results obtained in previous research efforts. This is mostly due to the fact that the deactivating effect of vanadium is more pronounced after steaming treatment, which could also have an influence on the product distribution. For that reason it would be interesting to perform a streaming treatment after impregnation to have a better resemblance of the industrial FCC catalyst.
- It was observed that guaiacol is adsorbed on both Lewis and Brønsted acid sites. Lewis acid sites can protect Brønsted acid sites from guaiacol poisoning. Alumina possesses only Lewis acid sites and could therefore give protection to the cracking catalyst. It would be interesting to mix HY zeolite with alumina to observe if a decrease in deactivating effect of guaiacol can be observed.
- RE introduced in the cracking zeolite can protect the catalyst from deactivation by vanadium through a process called *metal trapping*. It would be of interest to study the influence of solely RE content or together with vanadium.

Annex

Annex 1

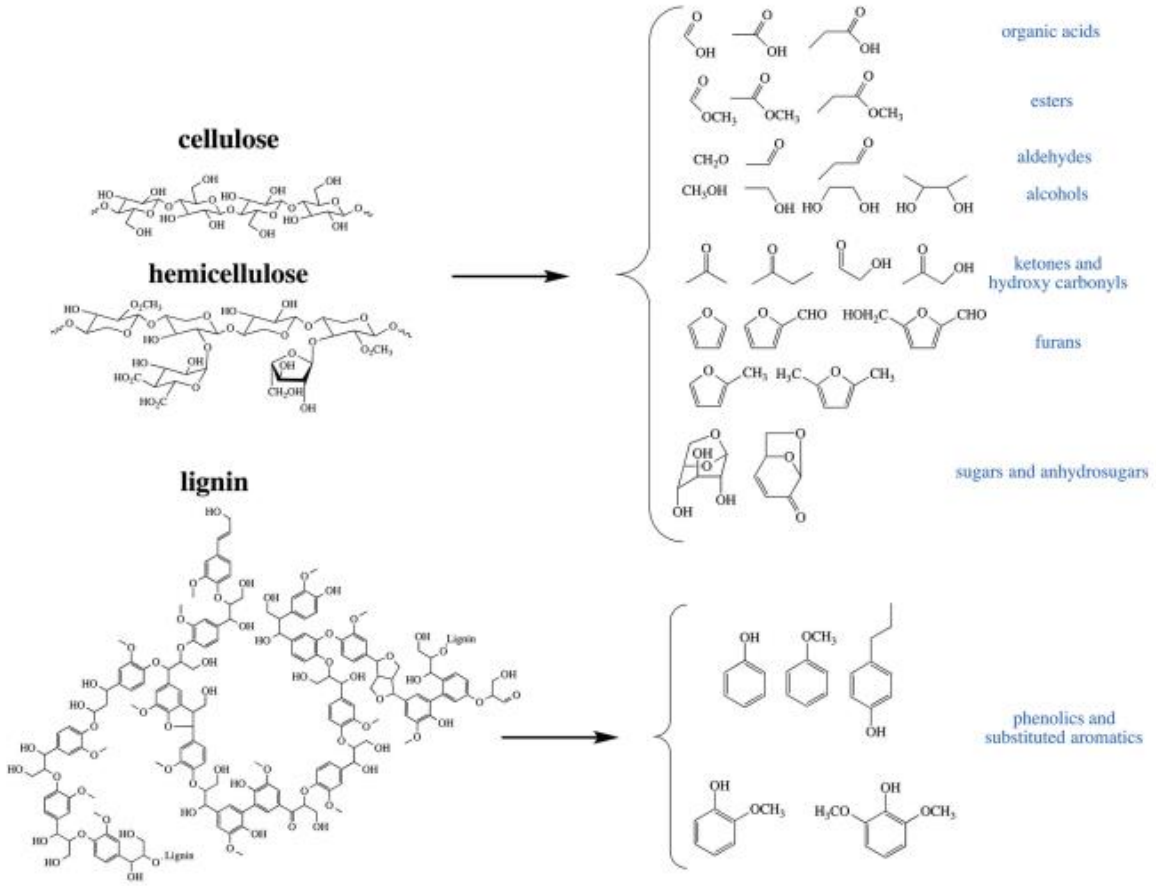

Figure 1 - Typical products from the biopolymers of biomass during pyrolysis [8]

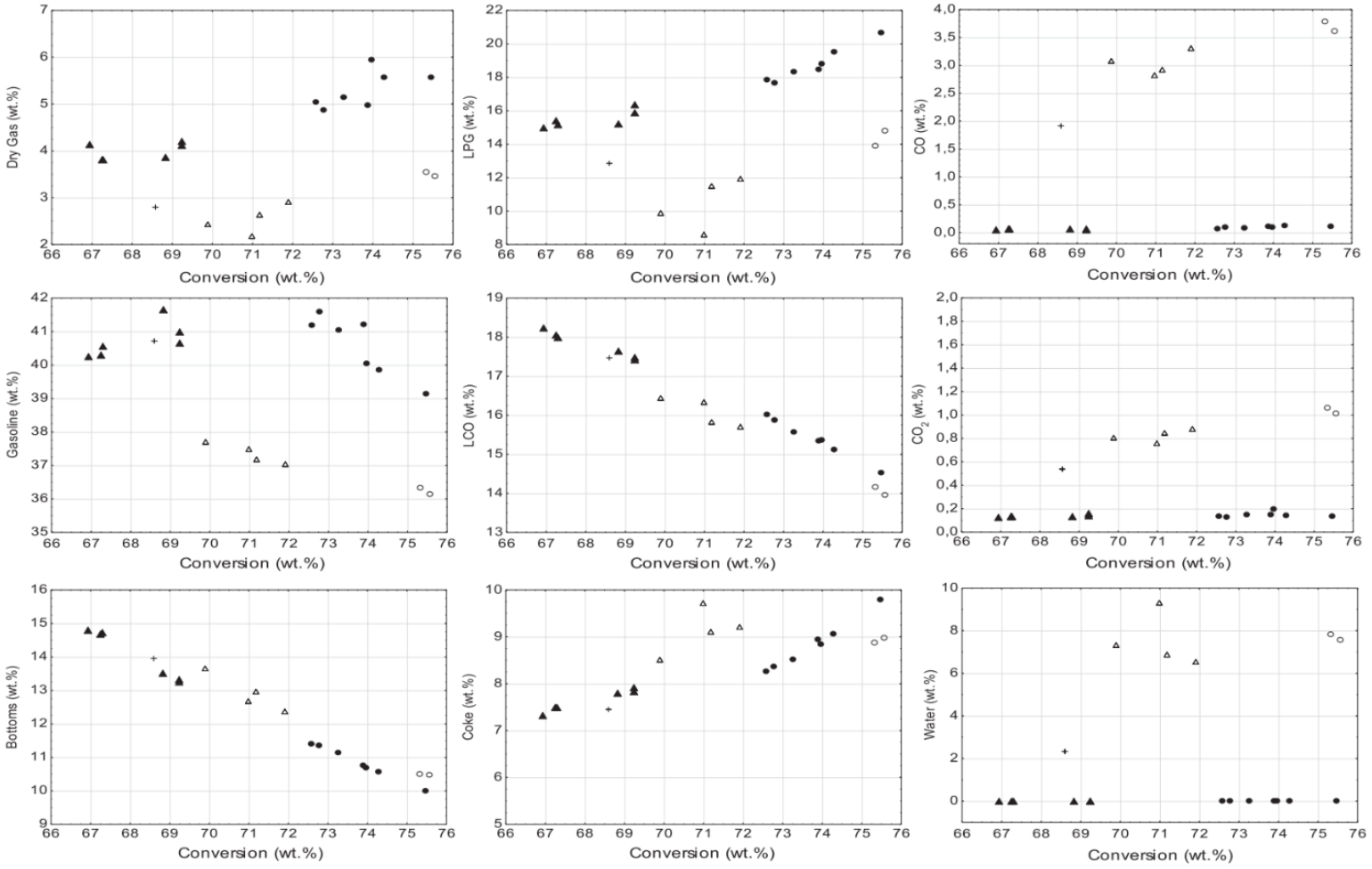

Figure 2 - Effect of the feed on the yields at different conversion levels: VGO cracking at 540 °C (▲),VGO cracking at 560 °C (●), VGO/bio-oil cracking 90/10 at 540 °C (+), VGO/bio-oil 80/20 cracking at 540 °C (Δ), VGO/bio-oil 80/20 cracking at 560 °C (○) [23]

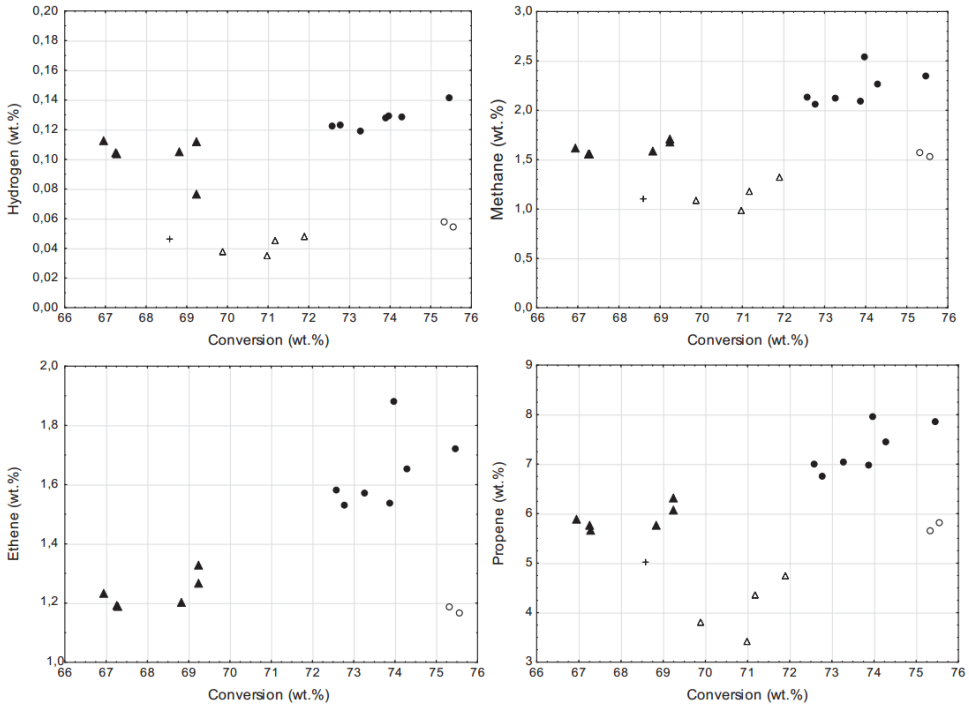

Figure 3 - Gas phase yields at different conversion levels: VGO cracking at 540 °C (▲),VGO cracking at 560 °C (●), VGO/bio-oil cracking 90/10 at 540 °C (+), VGO/bio-oil 80/20 cracking at 540 °C (Δ), and VGO/bio-oil 80/20 cracking at 560 °C (○) [23]

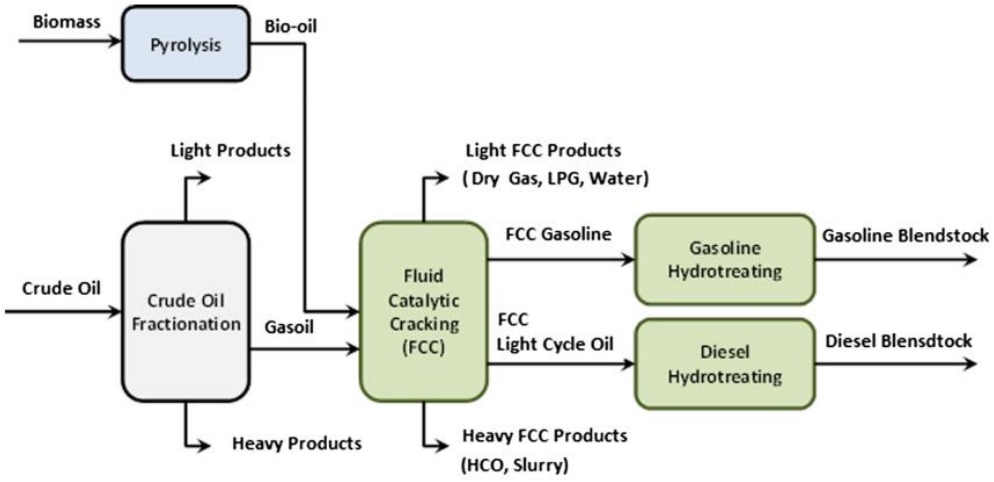

Figure 4 - Refining scheme for the co-processing of bio-oil with conventional hydrocarbon feedstock [19]

Annex 2

Table 1 - Cracking products selectivity at 35% iso-conversion of n-heptane with and without guaiacol over fresh CBV500 at 1.5 min of TOS

	Pure n-heptane	N-heptane + 1.2% guaiacol
C1	0.1	0.1
C2	1.4	1.5
C3	28.4	28.5
C3=	10.6	10.6
i-C4	34.4	34.7
n-C4	9.5	9.6
C4=	5.0	4.7
i-C5	4.2	4.2
n-C5	1.1	1.0
C5=	0.5	0.5
C6	0.7	0.6
C6=	0.1	0.1
toluene	2.2	2.0
m,p-xylene	1.5	1.4
o-xylene	0.3	0.3

Annex 3

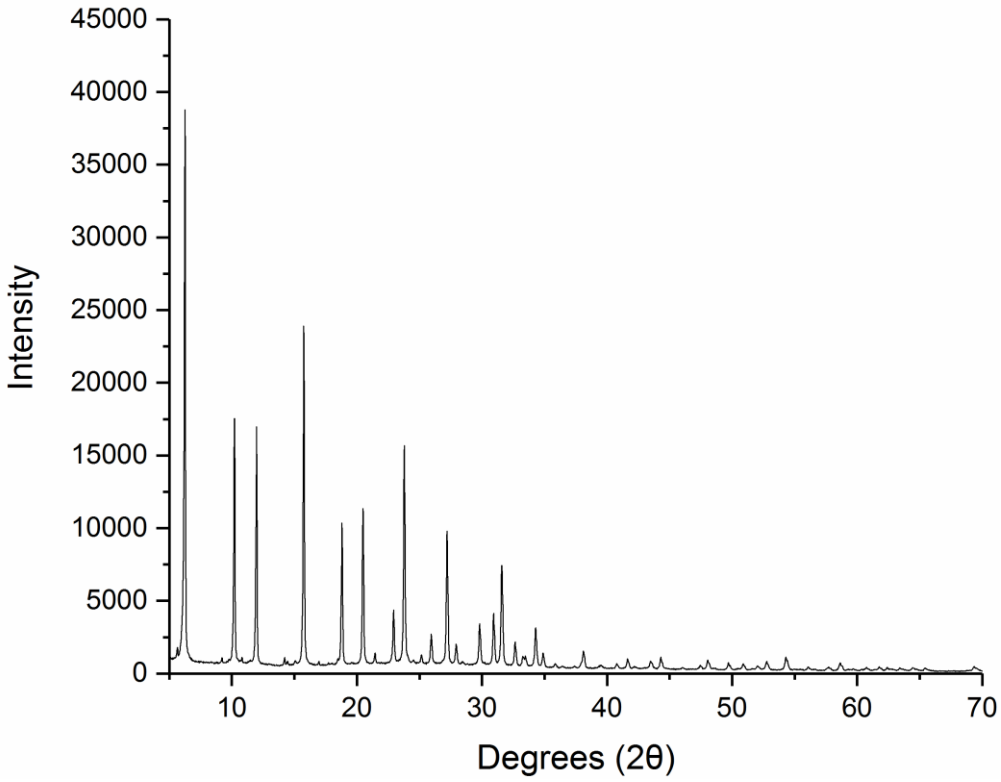

Figure 5 - XRD spectrum of CBV500

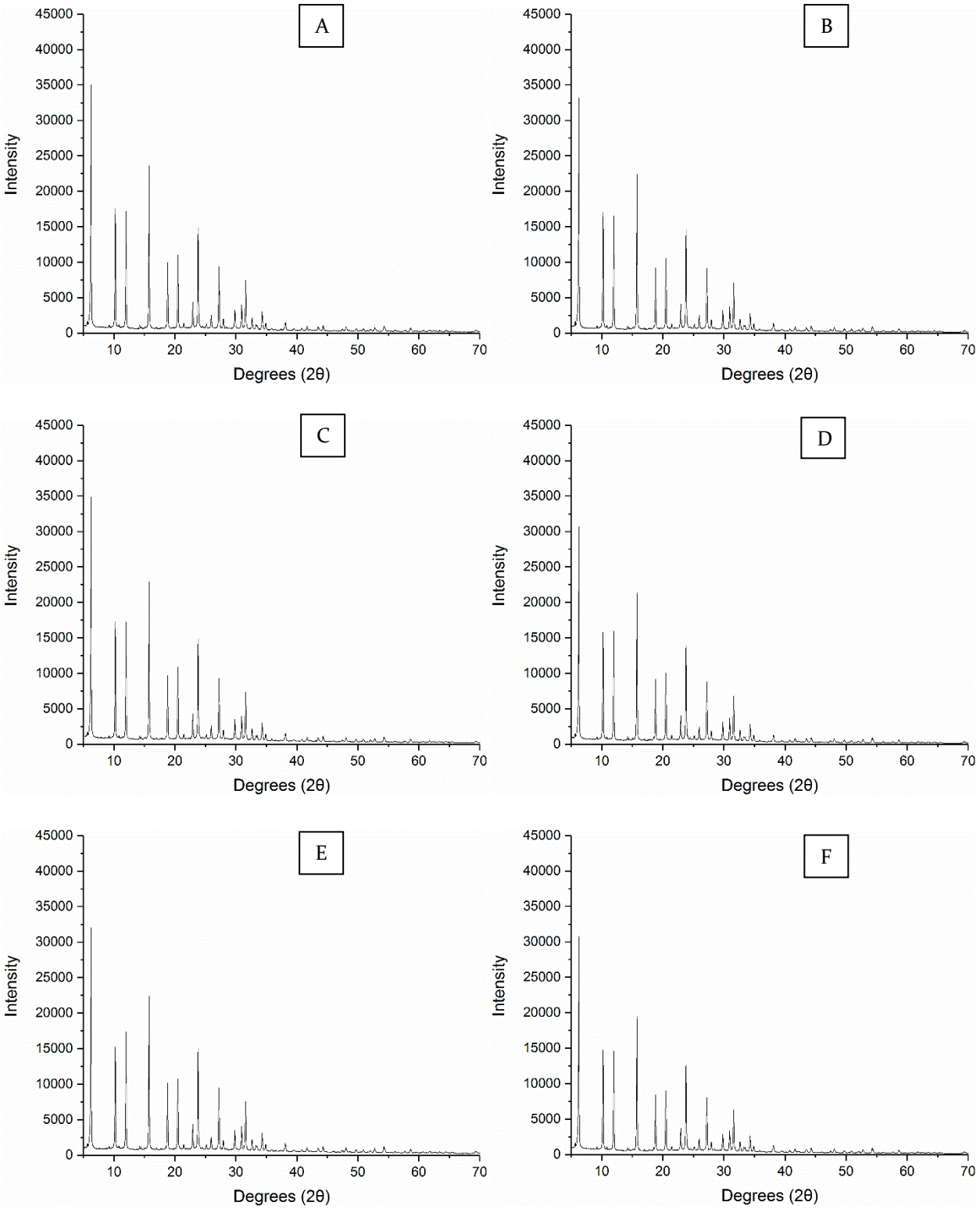

Figure 6 - XRD spectra ofCBV500 impregnated with 0.5% Ni (A) and V (B), 1.0% Ni (C) and V (D) and 2.0% Ni (E) and V (F)